INVESTIGATION INTO THE SUSCEPTIBILITY OF CORROSION RESISTANT ALLOYS TO BIOCORROSION

Dr. Clive R. Clayton
Department of Materials Science and Engineering
State University of New York at Stony Brook
Stony Brook, NY 11794-2275

Final Report
Contract No. N0001492J4089

Prepared for: **Office of Naval Research**
Department of the Navy
Arlington, VA 22217

State University of New York at StonyBrook

Department of Materials Science and Engineering

INVESTIGATION INTO THE SUSCEPTIBILITY OF CORROSION RESISTANT ALLOYS TO BIOCORROSION

Dr. Clive R. Clayton
Department of Materials Science and Engineering
State University of New York at Stony Brook
Stony Brook, NY 11794-2275

Final Report
Contract No. N0001492J4089

Prepared for: **Office of Naval Research**
Department of the Navy
Arlington, VA 22217

INVESTIGATION INTO THE SUSCEPTIBILITY OF CORROSION RESISTANT ALLOYS TO BIOCORROSION

Dr. Clive R. Clayton
Department of Materials Science and Engineering
State University of New York at Stony Brook
Stony Brook, NY 11794-2275

Final Report
Contract No. N0001492J4089

Prepared for: **Office of Naval Research**
Department of the Navy
Arlington, VA 22217

URITY CLASSIFICATION OF THIS PAGE

REPORT DOCUMENTATION PAGE

Form Approved OMB No. 0704-0188

REPORT SECURITY CLASSIFICATION: Unclassified	1b. RESTRICTIVE MARKINGS: None
SECURITY CLASSIFICATION AUTHORITY	3. DISTRIBUTION/AVAILABILITY OF REPORT: Unrestricted
DECLASSIFICATION/DOWNGRADING SCHEDULE	
PERFORMING ORGANIZATION REPORT NUMBER(S)	5. MONITORING ORGANIZATION REPORT NUMBER(S)
NAME OF PERFORMING ORGANIZATION: State University of New York at Stony Brook. / 6b. OFFICE SYMBOL (If applicable):	7a. NAME OF MONITORING ORGANIZATION
ADDRESS (City, State, and ZIP Code): epartment of Materials Sci.& Engg., tate University of New York at Stony Brook, tony Brook ,NY 11794	7b. ADDRESS (City, State, and ZIP Code)
NAME OF FUNDING/SPONSORING ORGANIZATION: Office of Naval Research / 8b. OFFICE SYMBOL (If applicable): Code	9. PROCUREMENT INSTRUMENT IDENTIFICATION NUMBER
ADDRESS (City, State, and ZIP Code): 300 North Quincy St. Arlington, VA 22217-5000	10. SOURCE OF FUNDING NUMBERS: PROGRAM ELEMENT NO. / PROJECT NO. / TASK NO. / WORK UNIT ACCESSION NO.

TITLE (Include Security Classification)
Investigation into the Susceptibility of Corrosion Resistant Alloys to Biocorrosion

PERSONAL AUTHOR(S)
Clive R. Clayton

a. TYPE OF REPORT	13b. TIME COVERED	14. DATE OF REPORT (Year, Month, Day)	15. PAGE COUNT
Technical	FROM 9/91 TO 10/95	96/2/2	

SUPPLEMENTARY NOTATION

17. COSATI CODES			18. SUBJECT TERMS (Continue on reverse if necessary and identify by block number)
FIELD	GROUP	SUB-GROUP	Microbiologically Influenced Corrosion (MIC), sulfate reducing bacteria (SRB), X-ray photoelectron spectroscopy (XPS)

19. ABSTRACT (Continue on reverse if necessary and identify by block number)

The influence of sulfate-reducing bacteria (SRB) on the passivity of type 304 and 317L stainless steels (SS) was investigated by x-ray photoelectron spectroscopy (XPS), microbiological and electrochemical tests. Samples were exposed to SRB, and then the resultant surfaces were analyzed by XPS and the corrosion resistance by potentiodynamic polarization in deaerated 0.1 M HCl. To further understand their passivity, the SRB-exposed samples were also analyzed by XPS after potentiostatic polarization at a passive potential in the hydrochloric solution. Comparisons were made with control samples immersed in uninoculated medium. SRB caused a severe loss of the passivity of 304 SS through sulfide formation and possible additional activation to form Cr^{6+} species. The sulfides included FeS, FeS_2, Cr_2S_3, NiS and possibly $Fe_{1-x}S$. The nonuniform interaction resulted in undercutting of the passive film.The existence of the Cr^{6+} species was magnified by the subsequent potentiostatic polarization. In contrast, 317L SS exhibited a limited passivity: The sulfides were formed mainly in the outer surface layers. Although the Cr^{6+} species were found after the exposure, they were dissolved upon polarization. Since these two steels mainly differs in the Mo content, the interaction of SRB with Mo was studied. It was observed that molybdate could be retained on the surfaces of Mo coupons. In the presence of SRB, however, a large portion of the molybdate interacted with sulfur-containing proteins, forming Mo(V)-S complexes and reduced bacterial growth and sulfate reduction. Additionally, the interactions of SRB with Cr and Ni were studied.

20. DISTRIBUTION/AVAILABILITY OF ABSTRACT	21. ABSTRACT SECURITY CLASSIFICATION
☒ UNCLASSIFIED/UNLIMITED ☐ SAME AS RPT. ☐ DTIC USERS	

22a. NAME OF RESPONSIBLE INDIVIDUAL	22b. TELEPHONE (Include Area Code)	22c. OFFICE SYMBOL
Dr. Clive R.Clayton	(516) 632 9272	

DD Form 1473, JUN 86 — Previous editions are obsolete. — SECURITY CLASSIFICATION OF THIS PAGE

An XPS Study of the Passivity of Stainless Steels Influenced by Sulfate-Reducing Bacteria

A Dissertation Presented

by

Guocun Chen

to

The Graduate School in Partial Fulfillment of the Requirements for the

Degree of

Doctor of Philosophy

in

Materials Science and Engineering

State University of New York

at Stony Brook

May 1996

Abstract of the Dissertation

An XPS Study of the Passivity of Stainless Steels Influenced by Sulfate-Reducing Bacteria

By

Guocun Chen
Doctor of Philosophy

in

Materials Science and Engineering

State University of New York
at Stony Brook

1995

The influence of sulfate-reducing bacteria (SRB) on the passivity of Mo-bearing (type 317L) and low Mo content (type 304) austenitic stainless steels (SS) was investigated by x-ray photoelectron spectroscopy (XPS), microbiological and electrochemical techniques. Samples were exposed to SRB, and then the resulting surfaces were analyzed by XPS, and the corrosion resistance by potentiodynamic polarization in deaerated 0.1 M HCl. In order to further understand their passivity, the SRB-exposed samples were also analyzed by XPS after potentiostatic polarization at a passive potential in the

hydrochloric solution. The characterization was performed under two surface conditions: unrinsed and rinsed by deaerated alcohol and deionized water. Comparisons were made with control samples immersed in uninoculated medium and "as polished" coupons. SRB caused a severe loss of the passivity of 304 SS through sulfide formation and possible additional activation to form hexavalent chromium, although there was a possibility that the residual biomass retained a small amount of hexavalent chromium formed during polishing. The sulfides included FeS, FeS_2, Cr_2S_3, NiS and possibly $Fe_{1-x}S$. The interaction took place nonuniformly, resulting in undercutting of the passive film and the formation of a higher proportion of hydrated chromium (III) in the inner surface region. The influence of the biofilm on either the formation or retention of preexisting hexavalent chromium was magnified by subsequent potentiostatic polarization. In contrast, 317L SS exhibited a limited passivity. The sulfides were formed mainly in the outer surface layers. Although hexavalent chromium species were also retained during the exposure, they were dissolved upon polarization. Since a major difference between these two steels is the higher Mo content of 317L SS, its higher passivity was largely attributed to Mo which existed as molybdate on the surface and a Mo^{5+} compound in the biofilm that was insoluble in 0.1 M HCl. Consequently, the interaction of SRB with Mo was studied with pure Mo and low concentrations of molybdate. It was

observed that molybdate could be retained on the surfaces of Mo coupons by corrosion products. In the presence of SRB, however, a considerable portion of the molybdate interacted with the extracellular sulfur-containing proteins, forming Mo(V)-S complexes and thereafter reduced bacterial growth and sulfate reduction. The limited insolublity of the Mo(V)-S complex in 0.1 M HCl provided a certain protection so that the pitting potential of the SRB-exposed Mo coupons was not considerably decreased in the presence of the biofilm. The interaction of the extracellular proteins with Mo also provided mechanistic information about the adhesion of the biolfilm to Mo-bearing steels. Additionally, the interactions of SRB with other constituent alloying elements, Cr and Ni, were investigated.

Table of Contents

List of Figures.....xii

List of Tables.....xix

Acknowledgements.....xxi

Publications.....xxii

I. INTRODUCTION.....1

1. Dissimilatory sulfur metabolism of SRB.....1

2. The influence of SRB on the electrochemical process of MIC.....3

3. The passivity of steels under the influence of SRB.....6

4. The role of biofilm.....7

5. Remaining questions.....9

II. EXPERIMENTAL METHODS.....12

1. Experimental protocol.....12

2. Microbiological.....15

2. 1. Culture medium and bacterium.....15

2. 2. Addition of Mo, MoO_3 and $Cr(OH)_3$ powders to the culture...18

2. 3. Microbiological analysis.....19

3. Biotic and Abiotic simulations.....20

4. Sample preparation.....22

5. Electrochemical....24

5. 1. Fundamentals of DC techniques used in this study....24

5. 2. Procedures....27

6. X-ray photoelectron spectroscopy....29

6. 1. Spectra interpretation....29

6. 1. 1. Chemical shifts....29

6. 1. 2. Quantification....31

6. 1. 3. Variable angle XPS....32

6. 2. Equipment, parameters and procedure....37

III. RESULTS....39

1. Characterization of the passivity of 304 SS exposed to SRB....39

1. 1. Potentiodynamic polarization in deaerated 0.1 M HCl....39

1. 2. XPS analysis at different stages of the polarization test....40

1. 2. 1. Immediately after the exposure....40

1. 2. 2. After the potentiostatic polarization in deaerated 0.1 M HCl....44

1. 2. 2. 1. The rinsed samples....44

1. 2. 2. 2. The unrinsed samples....47

1. 2. 3. Variable angle XPS....49

2. Characterization of the passivity of 317L SS exposed to SRB 52

2. 1. Cyclic polarization in deaerated 0.1 M HCl 52

2. 2. XPS analysis at different stages of the polarization test.....54

2. 2. 1. Immediately after the exposure.....54

2. 2. 2. After the potentiostatic polarization in deaerated 0.1 M HCl.....57

2. 2. 2. 1. The rinsed samples.....57

2. 2. 2. 2. Variable XPS analysis.....60

2. 2. 2. 3. The role of the biofilm.....62

3. Biotic and abiotic simulations using anaerobic solutions of Na_2S and NH_4Cl with and without addition of cysteine.....64

3. 1. Potentiodynamic polarization of 304 SS in 0.1 M HCl subsequent to the exposure.....64

3. 2. XPS analysis at different stages of the polarization test 65

4. The interaction of SRB with the constituent alloying elements.....68

4. 1. The interaction of SRB with Mo.....69

4. 1. 1. Characterization of the Mo coupons exposed to SRB by DC polarization in deaerated 0.1 M HCl and XPS analysis...69

4. 1. 1. 1. Potentiodynamic polarization in 0.1 M HCl.....70

4. 1. 1. 2. XPS analysis..... 70

4. 1. 2. DC polarization of "as polished" Mo coupons in the stationary stage culture.....73

4. 1. 3. The interaction of SRB with the dissolved Mo during the exposure of sputter-deposited Mo thin films and pure Mo

powder....77

4. 1. 3. 1. Culture growth and sulfate reduction....77

4. 1. 3. 1. 1. During exposure of the Mo thin films and Mo powders....77

4. 1. 3. 1. 2. The culture growth in the presence of low concentrations of molybdate....80

4. 1. 3. 2. XPS analysis....81

4. 1. 3. 2. 1. Dissolved Mo from Mo thin films....81

4. 1. 3. 2. 2. Mo in the centrifuged biomass of the cultures containing low concentrations of molybdate..83

4. 1. 3. 3. UV absorption spectroscopic analysis of the Mo dissolution products....86

4. 2. The interaction of SRB with Cr....89

4. 2. 1. Characterization of the Cr coupons exposed to SRB by DC polarization in deaerated 0.1 M HCl and XPS analysis...89

4. 2. 1. 1. Potentiodynamic polarization in 0.1 M HCl....89

4. 2. 1. 2. XPS analysis....90

4. 2. 2. Potentiodynamic polarization of "as polished" Cr coupons in the stationary stage culture....93

4. 2. 3. Addition of $Cr(OH)_3$ to the growth medium....93

4. 3. The interaction of SRB with Ni....95

4. 3. 1. Characterization of the Ni coupons exposed to SRB by DC polarization in deaerated 0.1 M HCl and XPS analysis...95

4. 3. 1. 1. Potentiodynamic polarization in 0.1 M HCl.....96

4. 3. 1. 2. XPS analysis.....97

4. 3. 2. Potentiodynamic polarization of "as polished" Ni coupons in the stationary stage culture.....98

4. 4. Characterization of the Fe coupons exposed to SRB by DC polarization in deaerated 0.1 M HCl and XPS analysis.....99

4. 4. 1. Potentiodynamic polarization in 0.1 M HCl.....99

4. 4. 2. XPS analysis.....99

IV. DISCUSSION.....101

1. Passivity of the SRB-exposed steel samples characterized by the DC polarization tests in deaerated 0.1 M HCl and XPS analysis.....101

1. 1. 304 SS.....101

1. 2. 317L SS.....105

2. The interaction of SRB with the constituent alloying elements.....109

2. 1. The interaction of SRB with Mo.....109

2. 1. 1. Characterization of the SRB-exposed Mo coupons.....109

2. 1. 2. The interaction of SRB with Mo shown in potentiodynamic polarization in the stationary stage culture.....111

2. 1. 3. The interaction of SRB with the dissolved Mo from the Mo thin films and Mo powders.....112

2. 2. The interaction of SRB with Cr.....116

2. 2. 1. DC polarization tests and XPS analysis.....116

2. 2. 2. The potentiodynamic polarization of "as polished" Cr coupons in the stationary stage culture and the influence of $Cr(OH)_3$ on the culture growth....118

2. 3. The interaction of SRB with Ni....120

2. 4. The interaction of SRB with Fe....121

V. CONCLUSION....122

1. 304 SS....122

2. 317L SS....122

FUTURE WORK....123

REFERENCES....124

Appendix 1....131

Tables....150

Figures....164

List of Figures

Figure 1. A possible metabolic pathway of the sulfate reduction by SRB.

Figure 2a. Flow diagram of the experimental procedure for the exposure of metal samples to SRB and subsequent analyses by XPS and DC polarization in deaerated 0.1 M HCl, and for potentiodynamic polarization of the "as polished" metal coupons in stationary stage culture.

Figure 2b. Flow diagram for study of interaction of SRB with low concentrations of molybdate.

Figure 2c. Flow diagram for XPS and UV analyses of the interaction of SRB with Mo thin films and Mo powders.

Figure 3a. Potentiodynamic polarization diagrams of 304 SS in deaerated 0.1 M HCl following exposure to SRB for 5 days.

Figure 3b. Potentiodynamic polarization diagrams of the control samples of 304 SS in deaerated 0.1 M HCl.

Figure 4a. Potentiodynamic polarization diagrams of 317L SS in deaerated 0.1 M HCl following exposure to SRB for 5 days, unrinsed prior to the test.

Figure 4b. The role of biofilm in the passivation performance of the SRB-exposed 317L SS shown in the polarization diagrams in 0.1 M HCl.

Figure 5. An illustration of the electrochemical significance of the Stern-Geary equation.

Figure 6. A schematic of sampling depth vs. take-off angles of photoelectrons in XPS analysis.

Figure 7. Fe2p spectra from the surfaces of 304 SS, TOA: 20°. (a) In SRB for 5 days, rinsed; (b) A control sample; (c) "As polished".

Figure 8. S2p spectra from the surfaces of 304 SS, TOA: 20°. (a) In SRB for 5 days, rinsed; (b) A control sample.

Figure 9. Cr2p spectra from the surfaces of 304 SS, TOA: 20°. (a) In SRB for 5 days, rinsed; (b) A control sample; (c) "As polished".

Figure 10. Ni2p spectra from the surfaces of 304 SS, TOA: 20°. (a) In SRB for 5 days, rinsed; (b) A control sample; (c) "As polished".

Figure 11. Relative proportions of sulfides in the percentage of total metal content, formed on the surfaces of 304 and 317L SS coupons during the exposure to SRB.

Figure 12. Fe2p spectra on the surfaces of 304 SS after the potentiostatic polarization at -160 mV_{SCE} for 5 minutes in deaerated 0.1 M HCl, TOA: 20°. (a) Previously in SRB for 5 days, rinsed; (b) A control sample; (c) "As polished".

Figure 13. Cr2p spectra on the surfaces of 304 SS after the potentiostatic polarization at -160 mV_{SCE} for 5 minutes in deaerated 0.1 M HCl, TOA: 20°. (a) Previously in SRB for 5 days, rinsed; (b) A control sample; (c) "As polished".

Figure 14. Polarization current vs the resultant hexavalent chromium on the surfaces of 304 SS formed during the potentiostatic polarization at -160 mV_{SCE} in deaerated 0.1 M HCl for 5 minutes after the 5 day exposure to SRB, TOA: 20°. (a) I_{ps} = 20 μA; (b) I_{ps} = 80 μA; (c) I_{ps} = 450 μA.

Figure 15. Ni2p spectra on the surfaces of 304 SS after the potentiostatic polarization at -160 mV_{SCE} for 5 minutes in deaerated 0.1 M HCl, TOA: 20°. (a) Previously in SRB for 5 days, rinsed; (b) A control sample; (c) "As polished".

Figure 16. Fe2p spectra from the surfaces of 304 SS after the potentiostatic polarization at -160 mV_{SCE} for 5 minutes in deaerated 0.1 M HCl, TOA: 50°, Ar^+ etched for 5 seconds. (a) Previously in SRB for 5 days, unrinsed; (b) A control sample.

Figure 17. Cr2p spectra from the surfaces of 304 SS after the potentiostatic polarization at -160 mV_{SCE} for 5 minutes in deaerated 0.1 M HCl, TOA: 50°, Ar^+ etched for 5 seconds. (a) Previously in SRB for 5 days, unrinsed; (b) A control sample.

Figure 18. Ni2p spectra from the surfaces of 304 SS after the potentiostatic polarization at -160 mV_{SCE} for 5 minutes in deaerated 0.1 M HCl, TOA: 50°, Ar^+ etched for 5 seconds. (a) Previously in SRB for 5 days, unrinsed; (b) A control sample.

Figure 19. Relative proportions of sulfides on the surfaces of 304 SS in the percentage of total contents of the alloying elements.

Figure 20. The polarization current vs the ratios of the residual FeS in the inner region to the one in the outer region of the SRB-exposed 304 SS coupons determined by variable angle XPS after the potentiostatic polarization in the hydrochloric solution.

Figure 21. The ratios of the relative proportion of $Cr(OH)_3$ to Cr_2O_3 in the inner region to the one in the outer region vs the uneven sulfidation of SRB-exposed 304 SS coupons determined by variable angle XPS after the potentiostatic polarization in the hydrochloric solution.

Figure 22. Fe2p spectra from the surfaces of 317L SS, TOA: 20°. (a) In SRB for 5 days, rinsed; (b) A control sample; (c) "As polished".

Figure 23. Cr2p spectra from the surfaces of 317L SS, TOA: 20°. (a) In SRB for 5 days, rinsed; (b) A control sample; (c) "As polished".

Figure 24. Ni2p spectra from the surfaces of 317L SS, TOA: 20°. (a) In SRB for 5 days, rinsed; (b) A control sample; (c) "As polished".

Figure 25. Mo3d spectra from the surfaces of 317L SS, TOA: 20°. (a) In SRB for 5 days, rinsed; (b) A control sample; (c) "As polished".

Figure 26. Fe2p spectra on the surfaces of 317L SS after the potentiostatic polarization at -160 mV_{SCE} for 5 minutes in deaerated 0.1 M HCl, TOA: 20°. (a) Previously in SRB for 5 days, rinsed; (b) A control sample; (c) "As polished".

Figure 27. Cr2p spectra on the surfaces of 317L SS after the potentiostatic polarization at -160 mV_{SCE} for 5 minutes in deaerated 0.1 M HCl, TOA: 20°. (a) Previously in SRB for 5 days, rinsed; (b) A control sample; (c) "As polished".

Figure 28. Ni2p spectra on the surfaces of 317L SS after the potentiostatic polarization at -160 mV_{SCE} for 5 minutes in deaerated 0.1 M HCl, TOA: 20°. (a) Previously in SRB for 5 days, rinsed; (b) A control sample; (c) "As polished".

Figure 29. Mo3d spectra on the surfaces of 317L SS after the potentiostatic polarization at -160 mV_{SCE} for 5 minutes in deaerated 0.1 M HCl, TOA: 20°. (a) Previously in SRB for 5 days, rinsed; (b) A control sample; (c) "As polished".

Figure 30. Variable angle Fe2p spectra on the surface of 317L SS after the potentiostatic polarization at -160 mV_{SCE} for 5 minutes in deaerated 0.1 M HCl following the 5 day exposure to SRB, rinsed prior to the polarization. (a) TOA: 20°; (b) TOA: 50°.

Figure 31. Variable angle Mo3d spectra on the surface of 317L SS after the potentiostatic polarization at -160 mV_{SCE} for 5 minutes in deaerated 0.1 M HCl following the 5 day exposure to SRB, rinsed prior to the polarization. (a) TOA: 20°; (b) TOA: 50°.

Figure 32. Variable angle Fe2p spectra on the surface of 317L SS after the potentiostatic polarization at -160 mV_{SCE} for 5 minutes in deaerated 0.1 M HCl following the 5 day exposure to SRB, unrinsed prior to the polarization. (a) TOA: 20°; (b) TOA: 50°.

Figure 33. Variable angle Mo3d spectra on the surface of 317L SS after the potentiostatic polarization at -160 mV_{SCE} for 5 minutes in deaerated 0.1 M HCl following the 5 day exposure to SRB, unrinsed prior to the polarization. (a) TOA: 20°; (b) TOA: 50°.

Figure 34. Comparison of potentiodynamic polarization diagrams of 304 SS in 0.1 M HCl following exposure to the H_2S-containing synthetic solutions with those previously exposed to SRB. (a) polarization diagrams following the exposure to anaerobic 10 mM cysteine; (b) polarization diagrams following the exposure to anaerobic H_2S-containing solutions for 5 days.

Figure 35. Fe2p spectra of 304 SS samples subjected to the exposure to the anaerobic H_2S-containing solutions and subsequent anodic polarization at -160 mV_{SCE} in 0.1 M HCl for 5 minutes. (a) previously exposed to deaerated 10 mM

Na_2S + 1 g/l NH_4Cl for 5 days, not rinsed; (b) previously exposed to deaerated 10 mM Na_2S + 1 g/l NH_4Cl + 10 mM cysteine for 5 days, not rinsed.

Figure 36. Cr2p spectra of 304 SS samples subjected to the exposure to the anaerobic H_2S-containing solutions and subsequent anodic polarization at -160 mV_{SCE} in 0.1 M HCl for 5 minutes. (a) previously exposed to deaerated 10 mM Na_2S + 1 g/l NH_4Cl for 5 days, not rinsed; (b) previously exposed to deaerated 10 mM Na_2S + 1 g/l NH_4Cl + 10 mM cysteine for 5 days, not rinsed.

Figure 37. Potentiodynamic polarization diagrams of the SRB-exposed pure Mo coupons in deaerated 0.1 M HCl.

Figure 38. Mo3d spectra from the surfaces of Mo coupons, TOA: 10°. (a) In SRB for 5 days, rinsed; (b) In SRB for 5 days, rinsed and then polarized at -160 mV_{SCE} for 5 minutes in deaerated 0.1 M HCl; (c) A control sample corresponding to (a); (d) A control sample corresponding to (b).

Figure 39. Variable angle Mo3d spectra from the surfaces of Mo coupons. (a), (b) and (c) In SRB for 5 days, unrinsed and then polarized at -160 mV_{SCE} for 5 minutes in deaerated 0.1 M HCl; (d), (e) and (f) A control sample.

Figure 40. Potentiodynamic polarization diagram of the "as polished" Mo in a 7 day old culture.

Figure 41. A comparison of the cyclic polarization diagrams of the "as polished" Mo and Au in the 3 day old culture.

Figure 42. Mo3d spectra from the culture droplets dried on Au foil after the potentiodynamic polarization of the "as polished" Mo coupons in the 7 day old culture. (a) unfiltered; (b) filtered.

Figure 43. Inhibition of low concentrations of molybdate on the culture growth (assuming that the culture growing in the medium without molybdate reached 100% growth in 3 days, MoO_4^{2-} + SO_4^{2-} = 20 mM).

Figure 44. The relationship between the residual sulfate measured in ppm by the turbidimetric method, the culture growth (turbidity at 600 nm) and the sulfate added to the growth media.

Figure 45. Mo3d (a) and S2p (b) spectra from the culture droplet after the exposure of Mo thin film for 5 days.

Figure 46. Mo3d and S2p from the centrifuged biomass of the cultures growing in the media containing different concentrations of molybdate. (a) and (b) 5 mM MoO_4^{2-}; (c) and (d) 1 mM MoO_4^{2-}; (e) and (f) 0.1 mM MoO_4^{2-}.

Figure 47. A comparison of the UV absorption spectra of the dissolved Mo during the 12 hour exposure of Mo powder (1 g/l) to the 3 day old culture and its supernatant.

Figure 48. The UV absorbance of the dissolved Mo during the 12 hour exposure of Mo powder (1 g/l) to the supernatants of the cultures growing for different periods.

Figure 49. Potentiodynamic polarization diagrams of the SRB-exposed pure Cr coupons in deaerated 0.1 M HCl.

Figure 50. Cr2p spectra from the surfaces of the pure Cr coupons, TOA: 20°. (a) In SRB for 5 days, rinsed; (b) In SRB for 5 days, rinsed and then polarized at -160 mV_{SCE} in deaerated 0.1 M HCl for 5 minutes; (c) A control sample corresponding to (a); (d) A control sample corresponding to (b).

Figure 51. Variable angle Cr2p spectra from the rinsed surface of the SRB-exposed Cr coupon after the subsequent potentiostatic polarization at -160 mV_{SCE} in deaerated 0.1 M HCl for 5 minutes, (a) TOA: 20°; (b) TOA: 50°.

Figure 52. Variable angle Cr2p spectra from the unrinsed surface of the SRB-exposed Cr coupon after the subsequent potentiostatic polarization at -160 mV_{SCE} in deaerated 0.1 M HCl for 5 minutes, (a) TOA: 20°; (b) TOA: 50°.

Figure 53. Potentiodynamic polarization diagrams of the "as polished" Cr coupons in the 3 day old culture and in the uninoculated medium.

Figure 54. Cr2p from the centrifuged biomass of the cultures growing in the medium containing 0.21 g/l $Cr(OH)_3$, (a) biomass of 2 day old culture; (b) biomass of 5 day old culture; (c) S2p of biomass (a); (d) S2p of biomass (b).

Figure 55. Potentiodynamic polarization diagrams of SRB-exposed Ni coupons

in deaerated 0.1 M HCl.

Figure 56. Variable angle Ni2p spectra from the SRB exposed Ni samples. (a) and (b) In SRB for 5 days, rinsed; (c) and (d) In SRB for 5 days, rinsed and then potentiostatically polarized at -210 mV_{SCE} in 0.1 M HCl for 5 minutes.

Figure 57. Potentiodynamic polarization diagrams of the "as polished" Ni coupons in the 3 day old culture.

Figure 58. Potentiodynamic polarization diagrams of the SRB-exposed Fe samples in deaerated 0.1 M HCl.

Figure 59. Variable angle Fe2p spectra from the Fe coupons after the exposure. (a) and (b) in SRB for 5 days, rinsed; (c) and (d) In SRB for 5 days, unrinsed.

Figure 60. An illustrative schematic of the nonuniform interaction resulting from the exposure of 304 SS to SRB.

Figure 61. An illustrative schematic of the uniform interaction resulting from the exposure of 317L SS to SRB, and the protection effect of the biofilm.

List of Tables

Table 1. Different ratios of sulfate to molybdate added to the modified Postgate medium C (SO_4^{2-} + MoO_4^{2-} = 20 mM).

Table 2. Content of the organic salt mixtures simulating the organic salts in the stationary stage culture (mM).

Table 3. Contents of the constituent alloying elements of 304 and 317L SS used for this study.

Table 4. The empirical sensitivity factors of the main elements used in this study (F1s = 1.00).

Table 5. The inelastic mean free paths of the photoelectrons and the maximum sampling depth into the surfaces of 304 and 317L SS.

Table 6. Standard parameters used for the XPS spectrum deconvolution.

Table 7. The cathodic slopes and the open circuit potentials (OCP) of the SRB-exposed 304 and 317L SS coupons shown in potentiodynamic polarization diagrams in deaerated 0.1 M HCl.

Table 8. Atomic percentages of the constituent alloying elements on the surfaces of the same batch of SRB exposed 304 SS samples at different stages of the investigation.

Table 9. The fractional areas of iron sulfides and nickel sulfides remaining in the outer (TOA = 20°) and inner (TOA = 50°) surface regions of the same batch of the SRB-exposed samples after the potentiostatic polarization in deaerated 0.1 M HCl.

Table 10. Atomic percentages of the constituent alloying elements on the surfaces of the same batch of SRB exposed 317L SS samples at different stages of the investigation.

Table 11. The atomic percentage of Mo compounds on the surfaces of the pure Mo coupons at different stages of the investigation.

Table 12. The culture growth and sulfate reduction during the exposure of the Mo thin films and Mo powders.

Table 13. The culture growth and sulfate reduction in the medium containing 0.21 g/l $Cr(OH)_3$.

ACKNOWLEDGEMENT

The program was supported by the Office of Naval Research under the contract number N0001485K0437 (Dr. A. J. Sedriks). In addition, I would like to present my sincere gratitude to my advisor, Professor C. R. Clayton, for introducing me into this exciting area and his dedication to the scientific research, to Dr. A. J. Francis at the Brookhaven National Laboratory for his instructions and advice in conducting the program. Dr. Tim E. Ford at the Division of Applied Sciences of Harvard University provided the exopolymer samples and offered many ideas to help understand the microbiology and biofilms. Mr. J. R. Kearns[1] at the Technical Center of Allegheny Ludlum Steels Corp. provided part of the steel samples and offered critical comments at the early stage of this program. My coworkers and friends, Dr. Gary P. Halada, Dr. Dongil Kim, S. V. Kagwade, G. E. French and Manuel Monserrat at the Department of Materials Science and Engineering of State University of New York at Stony Brook, J. B. Gillow, C. Dodge and M. Giles at the Brookhaven National Laboratory made great contributions in the laboratory work and comprehension of the experimental data.

---

[1]Present address: ALCOA Technical Center, ALCOA, PA 15609.

Publications

1. G. Chen and S. Xu, A New Reaction Mechanism of Halide Flux in Liquid Metal Purification, Iron and Steel, Metals Society of China, Jan, 1990;

2. G. Chen and S. Xu, Kinetics of Halide Reaction in Liquid Metals, A Computer Model of Chemical Kinetics and Fluid Mechanics, Iron and Steel, Metals Society of China, March, 1990;

3. G. Chen, S. Kagwade, G. E. French, C. R. Clayton, T. E. Ford and R. Mitchell, Metal Ion and Exopolymer Interaction: A Surface Analysis Study, Corrosion/95, Paper No. 219, NACE, Houston, Texas, USA, 1995 (to be published on Corrosion, July 1996);

4. G. Chen, C. R. Clayton R. A. Sadowski, J. R. Kearns, G. B. Gillow and A. J. Francis, Influence of Sulfate-Reducing Bacteria on the Passive Film Formed on Austenitic Stainless Steel, AISI 304, Corrosion/95, NACE, Houston, Texas, USA, 1995, Paper No. 217;

5. G. Chen, C. R. Clayton and A. J. Francis, The Influence of Sulfate-Reducing Bacteria on the Passivity of Austenitic Stainless Steels, Part I: Type 304 SS, to be submitted;

6. G. Chen, C. R. Clayton and A. J. Francis, The Influence of Sulfate-Reducing Bacteria on the Passivity of Austenitic Stainless Steels, Part II: Type 317L SS, to be submitted;

7. G. Chen, C. R. Clayton and A. J. Francis, Interaction of Dissolved Mo with Sulfate-Reducing Bacteria during Exposure of Sputter-Deposited Mo Thin Films and Pure Mo Powders, to be submitted;

8. G. Chen, C. R. Clayton, A. J. Francis and T. E. Ford, Enhancing Effect of Sulfur-Containing Proteins on Dissolution of Mo Induced by Anaerobic Na2S Solutions, to be submitted;

9. G. Chen, C. R. Clayton, T. E. Ford and A. J. Francis, Reduction of Molybdate by Sulfur-Containing Amino Acid Following Molybdate Surface Treatment of Type 304 Stainless Steel, to be subsmitted.

I. Introduction

Microbiologically influenced corrosion (MIC) is a corrosion process occurring where the presence and activity of microorganisms change the localized conditions at or near the surfaces of metal substrata so that corrosion acceleration or inhibition takes place. The influences of microorganisms on the corrosion process include directly changing cathodic and anodic conditions, affecting protective surface films, and thereby creating corrosive conditions and producing deposits[1]. In microbiologically influenced corrosion, sulfate-reducing bacteria (SRB) is a group of bacteria most extensively investigated due to their wide existence in environments, such as seawater, industrial water, soil and oil field, causing severe damage to corrosion resistance of engineering alloys[1-3].

1. Dissimilatory sulfur metabolism of SRB

The sulfate-reducing bacteria conduct dissimilatory sulfate reduction and release sulfide out of the bacterial cells. The dissimilatory sulfur metabolism includes a series of enzymatic reactions[3-5]. Figure 1 shows a generally accepted possible cyclic pathway.

Due to their analogous structure to sulfate, Group VI oxyanions,

including chromate, molybdate, tungstate and selenate, inhibit sulfate reduction. Selenate inhibits sulfate reduction by preventing transport of sulfate into the bacterial cells and its inhibition is selectively effective only for sulfate. Whereas, the other oxyanions inhibit sulfur reduction by preventing enzymatic formation of adenosine 5'-phosphosulphate (APS) by extracellular adenosine 5'-triphosphate (ATP) and their inhibition is non-selectively effective for reduction of sulfate as well as sulfite and thiosulfate[3, 6-12].

$$ATP + Me(VI)O_4^{2-} \rightarrow AMP + PP \qquad (1)$$

The inhibition is of the order: $CrO_4^{2-} > MoO_4^{2-} = WO_4^{2-} > SeO_4^{2-}$ [8]. For *Desulfovibrio*, 20 mM molybdate may completely inhibit its growth[6, 8, 9]. The investigations were performed with relatively high concentrations of these oxyanions. However, the mechanism of interaction has not been well understood. At first, the investigation on ATP depletion by molybdate excludes the influence of other enzymes in SRB. Secondly, the information about the ending products is unclear. According to the mechanism, a lower concentration of molybdate can influence the bacterial sulfate reduction to a certain degree at the early stage of culture growth, and it should remain as molybdate at the end of the interaction. Contrarily, it is well known that molybdenum(V) is involved in the enzymes and cofactors of SRB[13, 14]. Bacterially induced chromate

reduction has also been found[15, 16]. Therefore, the interaction of SRB with low concentrations of the oxyanions is of great significance not only in SRB ecology but also in MIC because SRB is one of the groups of bacteria severely reducing the corrosion resistance of stainless steels for which the oxyanions are often used as corrosion inhibitors[17-20]. In particular, it is well known that molybdate formed on the surface of Mo-bearing stainless steels (SS) effectively enhances the pitting resistance in chloride-containing environment[19, 20]. Therefore, in the presence of SRB, a question arises regarding whether there are conditions for formation of a low concentration of molybdate on the steel surfaces, and if so, whether the molybdate will be consumed in the bacterial interaction or remain as a corrosion inhibitor.

2. The influence of SRB on the electrochemical process of MIC

SRB influences the electrochemical process of corrosion by releasing sulfides as metabolic products onto a metal substratum. Corrosion is accelerated by changes in surface conditions[21-25]. A conventional model of hydrogen cathodic depolarization attributes the accelerated corrosion to the consumption of cathodically accumulated hydrogen which otherwise reduces corrosion rate by cathodic polarization[21]:

$$Metal \rightarrow Metal^{n+} + ne \text{ (anodic reaction)} \quad (2)$$

$$H_2O \rightarrow H^+ + OH^- \text{ (water dissociation)} \quad (3)$$

$$H^+ + e^- \rightarrow H_{ads} \text{ (cathodic reaction)} \quad (4)$$

$$SO_4^{2-} + 8H \rightarrow S^{2-} + 4H_2O \text{ (bacterial metabolism)} \quad (5)$$

$$+) \quad Metal^{n+} + S^{2-} \rightarrow Metal\ sulfide \text{ (corrosion)} \quad (6)$$

$$Metal + SO_4^{2-} + H_2O \rightarrow Metal\ hydroxide + Metal\ sulfide \quad (7)$$

An alternate theory states that microbiologically formed H_2S will decompose and result in corrosion in a neutral solution where the hydrogen content is too low to cause cathodic polarization[26, 27]. Both of the theories imply that sulfide formation is dependent on the microbial activities (eqn 5). Supporting the hydrogen cathodic depolarization theory, investigations were conducted with various concentrations of ferrous ions in growth media, and it was observed that a large amount of ferrous sulfide precipitated during the bacterial sulfur metabolism resulted in severe cathodic depolarization on the surfaces of mild steels through both bacterial hydrogenase system and the solid ferrous sulfide itself[21, 28-32]. On the other hand, it was also found that the corrosion rate of mild steels was independent of the hydrogenase activity of the bacteria[33], which gave rise to a question regarding the validity of the bacterially induced hydrogen cathodic depolarization. The difference between the cathodic

hydrogen depolarization and decomposition of biotic H_2S is, in fact, the difference in estimation of the extent of MIC. In the cathodic hydrogen depolarization model, the influence of the biotic H_2S is ignored. However, the anodic process facilitated by H_2S adsorption has been recognized as the key feature leading to rapid pitting attack[22].

A common weakness in these two mechanisms described is that the influence of the microbial activity on the metal surface, in addition to sulfide production, is not considered. This prevented further understanding of the mechanism of MIC. In particular, the bacterially influenced processes are often thermodynamically unpredictable. Unfortunately, most investigations in this area are case studies yielding instances of microbially accelerated corrosion processes. It is not unusual to find an article in which hydrogen cathodic depolarization is claimed to be the operating mechanism without any rationale. However, it is difficult to verify the mechanism by laboratory study using growing culture because H_2S formed during culture growth can cause drastic anodic corrosion and overshadow the effect of bacterial sulfate reduction and hydrogenase, although there is a possibility that the pH may be greatly reduced by hydrolysis in a local area where sulfides reduce the stability of a metal substratum.

3. The passivity of steels under the influence of SRB

As discussed above, biogenic sulfides have been historically considered to be the only cause of passivity loss[22, 24, 25], and their influence has been confined to the general knowledge of the sulfides in corrosion processes. It is known that solid ferrous sulfide can cause cathodic depolarization in corrosion of mild steels in addition to the cathodic depolarization by bacterially induced hydrogen evolution[24, 29]. The sulfides are pitting initiators which result in an increased acidity in a local area through oxidation, promote pitting attack as weak points on the steel surface and enhance electron transfer due to their good conductivity[34]. Investigations on the effect of iron sulfide precipitates on the corrosion resistance of mild steels have indicated that the corrosion rate is increased with increased biogenic iron sulfide[22, 24, 28- 36].

By contrast, few investigations have been conducted on the corrosion resistance of stainless steels under the influence of SRB. In order to understand the mechanistic nature, Newman *et al* made a valuable contribution by analogy between SRB and inorganic sulfur compounds[22]. Considering the influence of the remote cathodic effect of oxygen and chloride, they concluded that pitting initiators such as chloride must be present and exceed the contents of other anions for pitting to take place. However, the investigation heavily relied on

inorganic sulfur simulation and underestimated the influence of the metabolic process of the bacteria on the metal surface. So far, the influence of SRB on the passivity of stainless steels has not been well understood or characterized.

4. The role of biofilm

It is implicitly assumed in the above discussion that microorganisms influence the corrosion process upon their colonization on a metal substratum. The sessile bacteria are found to be the major part in MIC in many cases[26, 37]. A bacterium adsorbs to a metal substratum, taking in nutrients and metal ions through its exopolymers which are the outermost extracellular polymeric envelope mainly comprised of polysaccharides and residual proteins[2, 38, 39]. The physical and chemical properties of the expolymers have been largely studied with regard to the interactions of polysaccharides with metal substrata. Nevertheless, the extracellular proteins and amino function groups have been found to contribute to the binding ability of the exopolymers to metal ions (appendix 1). In the bacteria utilizing sulfur in their metabolism, sulfur-containing proteins may widely exist as the extracellular substances, and their interactions with the substrata may determine the bonding mechanism of the biofilm to a metal substratuam[3, 12]. Regarding these aspects, a study on the

interaction of the exopolymer of a marine bacterium *Deleya marina* with molybdate by this group provided a good insight into the interaction of sulfur-containing proteins in SRB with the Mo-bearing steels (appendix 1).

The biogenic sulfides precipitating on a metal substratum will directly interact with the metal surface and accelerate the corrosion process. The influence of a microbial colony on a metal substratum includes its influence on mass transfer, on interfacial properties between the biofilm and metal substratum, and on the formation of local anodic and cathodic areas[2, 39, 40]. In practice, a biofilm may have two fold influences: it enhances the surface stability of a metal substratum by forming insoluble species and modifying the surface oxide layer[41, 42], or it reduces the surface stability by activating a passive surface and providing a conduit for electron transfer[34, 43]. It has been observed that ennoblement of type 316L SS took place after exposure to a river water, arising from an increase of surface Fe_2O_3[41]. Although further characterization is needed, the cathodic polarization of the fresh river water-exposed samples indicated a possibility of the increased insulation of the surface oxides due to the incorporated deposits[41]. A recent study of this group also found that the Mo-containing interaction products on the surface of SRB-exposed 317L SS remained insoluble in deaerated 0.1 M HCl, providing a

limited protection[42]. On the other hand, a biofilm may not possess any protection[43]. A biofilm is herewith defined as a microcolony that creates concentration cells, changes the interfacial energy and corrosion potential of a metal substratum, results in the differences in charge and metal binding ability and affects the corrosion rate. This definition differs from the traditional definition in microbiology: here the interfacial phenomena are emphasized instead of a whole cluster of biomass.

5. Remaining questions

As described, the major question in the study of MIC is the clarification of the corrosion mechanism. Secondly, the influences of the metabolic activities of microorganisms on the electrochemical process of cathodic and anodic interactions have not yet been paid sufficient attention. This is mainly due to the lack of correlation between the microbiology and electrochemistry of corrosion. Microbiological reactions and corrosion have been historically considered as independent processes that occur simultaneously or sequentially on metal substrata[2]. The separation hindered both understanding of the mechanistic nature of the interaction and providing an effective solution to enhance the performance of materials against MIC. The influence of biogenic

sulfides will not be differentiated from common inorganic sulfides until the influence of microbial metabolism on a substratum is properly characterized. In both of the mechanisms of hydrogen cathodic depolarization and biotic H_2S decomposition, MIC is evaluated as a purely electrochemical process. Abiotic simulations take into consideration various sulfur compounds and chloride as possible species in SRB-containing environment, but the influence of bacterial metabolism is neglected by ignoring the changes of a passive film by the bacteria and by the metabolic products[22, 35, 36]. In addition, little information is available regarding the effect of a specific alloy element on MIC resistance. Although it is known that some transition metals are involved in the metabolism of microorganisms[13-16, 44, 45], no investigations have yet been conducted to correlate the interactions to the corrosion resistance of an alloy bearing these elements. For instance, the discovery of the inhibition of sulfate reduction by high concentrations of Group VI oxyanions has not brought about an investigation on the passivation performance of stainless steels, particularly Mo bearing steels, the pitting resistance of which is greatly enhanced by the outer layer of molybdate salt[18, 19]. No investigations have quantified the loss of passivity due to SRB nor have they provided a plausible explanation for the passivity loss. The lack of correlation between the microbiology and corrosion processes makes it impossible to understand the mechanism of MIC.

Another question remaining in MIC is the role of biofilms. A whole cluster of biomass has often been considered, instead of the interfacial properties. Characterizations include measurement of electrical properties, scanning electron microscopy (SEM) and energy dispersive X-ray (EDX) spectroscopy which yield the information about final corrosion products[34]. In contrast, the interfacial properties and their contributions to the electrochemical process have not been well understood. It is speculated that a biofilm will increase the polarization resistance in electrochemical measurements. However, no quantifications have yet been conducted[46].

The questions remaining in the understanding of MIC are mainly due to the limitations of the conventional methods described[46]. A pure microbiological research are often conducted with soluble metal ions, which hardly provides much valuable information pertinent to a solid surface. On the other hand, the electrochemical measurements, SEM and EDX are able to provide information about final reactions only. Changes in surface chemistry and chemical states, interfacial properties and process of electron transfer may not be determined by these conventional methods. Up to now, the investigations on the mechanism of SRB-influenced corrosion are still confined to the theory of cathodic hydrogen depolarization, although opposing arguments often arise[22, 24, 26].

II. Experimental Methodology and Techniques

1. Experimental protocol

The objective of the present program was to understand the fundamental corrosion processes influenced by SRB. To do so, it was necessary to obtain information about the loss of passivity and to understand the passivation behavior of stainless steels influenced by the presence of SRB. The specific effects of the constituent alloying elements were also investigated. Further investigation included abiotic simulations and basic electrochemical aspects of the interaction of SRB with the alloying elements.

In this program, austenitic stainless steels, including Mo-bearing (type 317L) and low Mo content (type 304) steels, were selected. A sulfur-containing amino acid, cysteine, was employed to confirm the role of sulfur-containing extracellular proteins in the interaction. Biotic and abiotic simulations were performed using sulfur-containing amino acid, organic salts, inorganic sulfide and chloride to aid in understanding of the interactions. Since the major difference between these two steels is the Mo content, and Mo-bearing steels possess an enhanced passivity in chloride containing media contributed by the outer layer of molybdate salt[17-20], the interactions of SRB with pure Mo and

low concentrations of molybdate were studied. The interactions of SRB with Cr and Ni were also investigated. Furthermore, basic aspects of the interaction of SRB with these alloying elements were studied using stationary stage culture.

X-ray photoelectron spectroscopy (XPS), ultraviolet (UV) absorption spectroscopy, direct current (DC) polarization and microbiological analyses were applied in this study. As a nondestructive surface analysis technique, XPS has the unique advantages for study of surface chemical states and provides information about the process of electron exchange. UV spectroscopy was used for further information about the interaction products of Mo with SRB. DC polarization techniques were applied to characterize the interactions and the corrosion resistance of these metals, and microbiological analyses to determine the culture growth and sulfate reduction.

Figure 2a is a flow diagram showing the experimental procedure. *Desulfovibrio desulfuricans* (ATCC 7757), one of the commonly existing SRB, was chosen for this study. It was grown in a modified Postgate medium C[47]. The coupons of the steels were exposed to the bacteria. The resultant changes in the passivity were then determined by potentiodynamic polarization in deaerated 0.1 M HCl, a commonly used electrolyte for investigation of pitting resistance of stainless steels. In order to obtain the knowledge of the resultant

surface chemical states, XPS analysis was conducted immediately after exposure to SRB. In order to further understand the mechanism of the loss of passivity, the SRB-exposed coupons were analyzed by XPS after potentiostatic polarization at a passive potential in the hydrochloric acid solution. The coupons were characterized under two surface conditions after the exposure, (1) rinsed with alcohol and deionized water to remove the biofilm and, (2) not rinsed. Comparisons were made with control samples immersed in uninoculated medium and "as polished" coupons.

Additionally, an anaerobic H_2S-containing solution made by a mixture of 10 mM Na_2S and 1 g/l (19 mM) NH_4Cl was utilized for exposure of these two steels, simulating the anodic effect of H_2S on initiating pitting[25]. A sulfur-containing amino acid, cysteine, was added to the solution to reveal the role of intermediate sulfur-containing proteins in the interaction, whose influence was differentiated by exposure of the steels to an anaerobic cysteine solution. The steels exposed to the solutions were subsequently characterized by XPS and DC polarization tests following the same protocol as those exposed to SRB.

To study the interaction of SRB with pure Mo, Cr and Ni, these metal coupons were exposed to SRB and subsequently analyzed with XPS and DC polarization tests following the same protocol as described. Because Mo is

known to be involved in enzymatic interactions with extracellular proteins such as ATP[8, 9, 13, 14], further study proceeded with potentiodynamic polarization of Mo in the 3 day old culture, in comparison with polarization of pure Au exhibiting the interactions occurring within the culture itself. In addition, different ratios of sulfate to molybdate were added to the growth medium in order to study the interference of molybdate with culture growth using microbiological and XPS analyses (Figure 2b). The investigation was extended by exposing Mo thin films to SRB and by adding pure Mo powders (500 mesh) to the culture and to the supernatants of the cultures growing for sequential time periods and thereafter determining the culture growth and interaction products by microbiological analysis, XPS and UV spectroscopy (Figure 2c). The interactions of SRB with Cr and Ni were also characterized by potentiodynamic polarization in the 3 day old culture. To study the effect of possible dissolution of $Cr(OH)_3$ on the culture growth and the susceptibility to sulfidation, 0.21 g/l $Cr(OH)_3$ powder was added to the growth medium.

2. Microbiological

2. 1. Culture medium and bacterium

A modified Postgate medium C[47] was used for culture growth and

immersion of the steel and pure metal coupons. The contents of ingredients are (g/l): KH_2PO_4, 0.50; NH_4Cl, 1.00; $CaCl_2.2H_2O$, 0.06; $MgSO_4.7H_2O$, 0.06; $FeSO_4.7H_2O$, 0.002; Na_2SO_4, 2.26, Na-citrate, 0.30; yeast extract, 1.00; lactic acid (80%), 3 ml, with deionized water (18.2 MΩ) added to 1 liter. Modification included reduction of ferrous iron content by 50% in order to avoid formation of an excess amount of iron sulfide precipitates causing excessive cathodic depolarization[22, 24, 34] and thereby overshadowing the influence of bacterial metabolism. The sulfate content was also reduced by 50% in order to avoid interference of residual sulfate with the interaction.

To study the influence of molybdate on the growth of culture, the media containing different ratios of sulfate to molybdate (Na_2MoO_4) were prepared. The molybdate content was varied from 0.1 to 20 mM, while the sum of sulfate and molybdate was held at 20 mM and the contents of other ingredients remained the same as in the modified Postgate medium C (Table 1).

Before adding lactic acid, the media were deaerated by boiling and purging with ultra high purity nitrogen for at least 20 minutes and then cooled to room temperature. The media were placed in a nitrogen filled anaerobic glove box. Lactic acid was added and then pH adjusted to a proper level with NaOH so that its final value would reach approximately 7.0 after autoclaving.

The above media were dispensed to 5 categories of volumes for different experiments: (1) For immersion of these metal coupons subsequently analyzed by XPS, 10 ml of the modified Postgate medium C was dispensed into 20 ml serum bottles, leaving enough head space for gas production. The medium was then autoclaved at 121 ^{0}C and 20 psi for 20 minutes (Figure 2a). (2) For immersion of the samples previously mounted on sample holders for subsequent polarization tests in deaerated 0.1 M HCl, a larger volume of the modified Postgate medium C was used to ensure a complete coverage: 150 ml medium was dispensed into 250 ml sealed flasks and then autoclaved (Figure 2a). (3) For potentiodynamic polarization tests in the stationary stage culture, 200 ml of the modified Postgate medium C was dispensed into 250 ml serum bottles to meet the requirement for a large volume of electrolyte (800 ml) in a 1 liter Greene cell (Figure 2a). Multiple samples were studied in the above tests. (4) For the growth of culture in the media containing different ratios of sulfate to molybdate, 100 ml medium was dispensed into 160 ml serum bottles, with each aliquot containing a different ratio of sulfate to molybdate. The relatively large volume of medium was able to grow enough biomass for XPS analysis (Figure 2b). (5) For UV spectroscopic study of the interaction of Mo powders with the culture and supernatant, 36 ml of the modified Postgate medium C was dispensed into 60 ml serum bottles. The 36 ml medium was

also prepared for addition of MoO_3 in order to study the influence of partially soluble Mo oxide on the growth of culture (Figure 2c). For study of possible dissolution and sulfidation of $Cr(OH)_3$ in SRB, additional amount of the 36 ml medium was prepared. These experiments were at least duplicated.

Desulfovibrio desulfuricans (ATCC 7757) was chosen for this study. It is a vibroid rod bacterium, Gram negative and desulfoviridin positive. It produces acetate and propionate as metabolic byproducts when growing on lactate[48]. The content of the inoculum was 5%(v/v).

2. 2. Addition of Mo, MoO_3 and $Cr(OH)_3$ powders to the culture

To add Mo, MoO_3 and $Cr(OH)_3$ powders to the culture, 10 g/l Mo (99.94%wt, 500 mesh), 14.4 g/l MoO_3 (99.99%wt) and 2.1 g/l $Cr(OH)_3$ (99.9%wt) powder suspensions were first prepared in deaerated deionized water (filtered by 0.22 μm Millipore filter). 4 ml of the Mo powder (1 g/l), MoO_3 (1.44 g/l) and $Cr(OH)_3$ (0.21 g/l) suspensions were added to the uninoculated 36 ml medium respectively (Figure 2c). The medium was then inoculated and incubated. In addition, 1 g/l Mo powder was added to 2 day old culture and then incubated at the same time as the newly inoculated medium. The 2 day old culture was selected because it had reached a certain microbial activity and

there remained some residual sulfate so that Mo dissolution would be faster than adding Mo powders before inoculation. The culture growth and sulfate reduction were subsequently determined after 2 and 5 days. For UV absorption spectroscopy, 1 g/l Mo powder was added to 3 day old culture and equilibrated for 12 hours prior to the analysis. The absorbance was scanned after filtration (0.22 μm Millipore filter), and then compared with those by adding 1 g/l Mo powder to the supernatant of the 3 day old culture. In order to study the effect of the growth-dependent metabolic products, 1 g/l Mo powder was respectively added to the supernatants of 2 hour to 5 day old cultures and then equilibrated.

2. 3. Microbiological analysis

Microbiological analysis was conducted after the culture grew for 2 and 5 days respectively, unless specified. The growth of culture was measured by turbidity with a Bausch and Lomb Spectronic 20 spectrometer at 600 nm wavelength. Residual sulfate was analyzed by the turbidimetric method[50]. Lactate and acetate were analyzed by high performance liquid chromatography (HPLC) with a UV/VIS spectrophotometer (Spectra-Physics) after the culture was filtered through 0.22 μm Millipore filter[51]. UV absorption of the cultures and supernatants containing Mo products was scanned in quartz cells (cross

section, 1 x 1 cm^2) in the range of wavelength from 190 to 820 nm, using a diode array Hewlett Packard 8452A spectrometer controlled by HP 89532A UV/VIS data acquisition software. The pH was measured at each stage of medium preparation and culture growth.

For the cultures containing 0.21 g/l $Cr(OH)_3$, the biomass was collected by centrifuging at 12,000 rpm and 4 °C for 20 minutes after 2 and 5 day growth periods. For the cultures containing low concentrations of molybdate, the biomass was collected after 5 days. Both types of the biomass were dried in a desiccator in the glove box for XPS analysis, and the supernatant stored in clean serum bottles for analysis of residual sulfate and organic salts.

3. Biotic and abiotic simulations

In order to study the anodic effect of H_2S on the initiation of pitting, an anaerobic solution of 10 mM Na_2S and 1 g/l NH_4Cl was prepared (pH 9.35), knowing the reaction:

$$Na_2S + 2NH_4Cl \rightarrow H_2S + 2\ NH_3 + 2NaCl \qquad (8)$$

where the content of sulfide was based on the rate of the sulfate reduction in the stationary stage culture[52]. 10 mM L-cysteine (molecular weight 121.16,

$[\alpha]_{546}^{20}$ + 9.5 ± 0.5°, $[\alpha]_{D}^{20}$ + 7.6 ± 0.5°, c = 5 in 5N HCl) was added to the solution (pH 8.65) to demonstrate the role of intermediate sulfur-containing proteins in the interaction. The high pH avoided possible cathodic hydrogen depolarization. An anearobic 10 mM cysteine (pH 5.00) was also prepared in order to exhibit the influence of cysteine only. These solutions were dispensed by 10 ml and 150 ml volumes for exposure of the steel coupons to be analyzed by subsequent XPS and DC polarization tests in the anaerobic glove box.

The interaction of Mo with intermediate sulfur-containing proteins, such as APS and residual cysteine, was simulated using L-cysteine by adding 10 mM molybdate to deaerated 10 mM cysteine (pH 5.00, and 6.60 after adding 10 mM Na_2MoO_4), which is known to form a binuclear dioxobridged Mo(V)-S complex, di-μ-oxo-bis[oxo(L-cysteinato)molybdate(V)][49]. In addition, the interactions with the organic salts in the culture, such as acetate, propionate and lactate, were studied by adding 10 mM molybdate to each of the 10 mM deaerated salt solutions and their mixtures in a proportion comparable to the contents in a stationary stage culture, with and without the presence of sulfur compounds (2 mM sulfite, Table 2). The interactions with the inorganic products, such as H_2S, chloride and ammonium, were simulated by adding 1 g/l Mo powder to a deaerated solution of 10 mM Na_2S and 1 g/l NH_4Cl. The

surface chemical states of the Mo powders were previously analyzed by XPS, and it was observed that the Mo powders were completely covered by MoO_3. However, the amount of the surface MoO_3 was not sufficient to affect the results, because the absorption was negligible in UV analysis 12 hours after 1 g/l Mo powder was added to 10 mM cysteine.

4. Sample preparation

For immersion tests, 1 mm thick 304 and 317L SS (composition listed in Table 3) and pure Mo foils (99.994%) were cut into 1 cm^2 coupons. 1 mm thick Cr and Ni discs were cut from 0.65 cm diameter Cr and 1 cm diameter Ni rods (99.99%). The steel coupons were stabilized by water quenching after annealing in vacuum at 1080 °C for 1 hour. They were subsequently polished to a 6 μm diamond finish and ultrasonically degreased in acetone. The pure Mo, Cr and Ni coupons were also polished to 6 μm diamond finish and then ultrasonically degreased.

In addition to the bulk Mo coupons, Mo thin films were used in the exposure tests for a greater degree of interaction because the thin films are structurally inferior to bulk Mo metal. The Mo thin films were produced by radio frequency (RF) sputter deposition on 1 cm^2 pieces of Si wafers in a US'

Gun II™ deposition system. The Si wafers had been previously cleaned in a 5% HF solution for 5 minutes and then thoroughly rinsed in deionized water. The Mo source was Ar^+ sputter-etched for 15 minutes before deposition in order to remove the surface oxides. 1.5 to 2 μm thick Mo films were produced in a period of 60 minutes with the processing parameters: output powder of 75 watts, Ar pressure of 3×10^{-2} torr and the base pressure of 2×10^{-6} torr.

Immersion of all of these metal coupons and Mo thin films was performed in the anaerobic glove box. They were sterilized with alcohol and filtered deaerated deionized water and then individually placed in the 10 ml autoclaved medium The medium was then inoculated and incubated at 30 °C for 5 days. After incubation, the coupons were collected in the glove box. They were rinsed with deaerated alcohol and deaerated deionized water to remove the biofilm, individually placed in 10 ml clean serum bottles and then dried in a desiccator in the glove box. For comparison, control samples were prepared. The steel coupons were also exposed to the anaerobic solutions described.

For immersion followed by DC polarization tests in deaerated 0.1 M HCl, all of the polished coupons were rinsed and mounted on $1.5 \times 2 \times 0.5$ cm^3 plexiglass sample holders with epoxy resin. Connection from the coupon to the potentiostat was provided by a copper wire previously placed between the

coupon and the plexiglass block through an 8 mm outer diameter glass tube. The electrodes were sterilized and then placed in the 150 ml medium. Control samples were also prepared. Biotic and abiotic simulations were conducted by exposure of the steel electrodes to the simulation solutions described.

For potentiodynamic polarization tests of the pure metals in the 3 day old culture, the metal coupons were polished to 6 μm diamond finish and then mounted on the plexiglass sample holders. Gold electrode (0.5 mm x 1 cm^2) was also polarized in the culture in order to distinguish the interaction of Mo with the culture from those occurring within the culture itself. The gold foils were rinsed in concentrated HCl before being mounted onto the sample holders.

5. Electrochemical

5. 1. Fundamentals of DC techniques used in this study

Potentiodynamic and potentiostatic polarization tests and open circuit potential measurement were performed for this study. Potentiodynamic polarization is a method to determine the overall corrosion resistance of a metal. During the polarization test, the potential of a working electrode (specimen) is slowly swept over a wide range. The working electrode thus

undergoes different electrochemical reactions, and resultant cathodic and anodic currents may be presented in separate (cathodic and anodic) regions in the polarization diagram (Figures 3 and 4). The corrosion rate may be estimated by relating the current flow to mass transfer using the Faraday's Law:

$$Q_s = nFM_s \tag{9}$$

for species S in: $S \rightarrow S^{n+} + ne^-$, where Q_s is the resultant charge in coulombs, n is the number of electrons transferred, F is the Faraday's constant (96,486.7 coulombs/mole) and M_s is the number of moles of species S reacting.

Introducing the concept of equivalent weight (EW, the mass of a species reacting with one Faraday of charge), the mass of the species S that has reacted can be calculated by:

$$W_s = EW_s\ Q_s / F \tag{10}$$

and the corrosion rate in mils per year[53]:

$$R_{corr}\ (mpy) = 0.1288\ I\ (\mu A/cm^2)\ EW\ (g) / \rho\ (g/cm^3) \tag{11}$$

where I is the reaction current density and ρ is the density of the species.

Assuming that the rates of cathodic and anodic reactions are controlled

by the kinetics of the electron transfer reaction at the sample surface, the electrochemical reaction obeys the Tafel equation[54]:

$$(E - E^\circ) = \pm \beta \ln (I / I^\circ) \qquad (12)$$

where E° is the equilibrium potential in volt, I° is the exchange current in amperes, and β is the Tafel slope in volts/decade. Therefore, in a corrosion system, the anodic and cathodic reactions can be combined:

$$I = I_{corr} \{\exp[(E - E_{corr}) / \beta_a] - \exp[(E - E_{corr}) / \beta_c]\} \qquad (13)$$

From a Tafel diagram (E - log I), I_{corr} may be derived with the first two terms of a power expansion ($e^x = 1 + x + x^2 / 2 + ...$)[55]:

$$I_{corr} = (1 / R_p) [\beta_a\beta_c / 2.303 (\beta_a + \beta_c)] \qquad (14)$$

where I_{corr} is the corrosion current in amperes indicating the beginning of dominant anodic dissolution, E_{corr} is the corrosion potential in volts, β_a and β_c are anodic and cathodic Tafel slopes, and R_p is the polarization resistance. The electrochemical significance of above terms are illustrated in Figure 5.

Potentiostatic polarization can be used to study the formation or breakdown of a passive film, to measure pitting and to electrochemically

pretreat a sample by applying a certain over (or under) potential. In this study, it was used to analyze the changes in the passivity of the SRB-exposed samples by pausing at a passive potential.

5. 2. Procedures

An EG & G Versastat controlled by M352 data acquisition software, and a Gamry CMS100 potentiostat were utilized for the experiment. A saturated calomel electrode (SCE) was the reference electrode. The counter electrodes were made of 1 mm diameter Pt wires. The experiments were performed using a 1 liter conventional Greene cell in the glove box at room temperature.

For the coupons exposed to SRB for 5 days, deaerated 0.1 M HCl was chosen as the test electrolyte representing typical pitting conditions. The samples were polarized under two surface conditions: unrinsed and rinsed with deaerated alcohol and deaerated deionized water to remove the biofilm. No cathodic surface treatment was performed before polarization. Potentiodynamic polarization tests were conducted with a sweep rate of 0.2 mV/sec from -0.2 V below open circuit potential (OCP) up to 1.0 V above (Figure 3). In cyclic polarization tests, the potential of working electrode was also swept at 0.2

mV/sec up to 1.0 V above the OCP and then reversed. Hysteresis of the diagram indicated crevice formation when the reversed E-log i curve entered the active to passive transition where the increase of the current density arose from the exposure of relatively larger areas of substrate, while pitting formation was indicated by reversed polarization into the passive range associated with a smaller increase of the current density (Figure 4). Potentiostatic polarization treatments of SRB-exposed samples were conducted for 5 minutes at -0.16 mV_{SCE}, a potential in the beginning of passivation of 304 and 317L SS in the hydrochloric solution (Figure 3 and 4). Nickel coupons were polarized at -0.21 mV_{SCE} because of the limited passivity in the hydrochloric solution. For subsequent XPS analysis, the samples were then taken out of the Greene cell with the potential applied in case that the surface products would return to the open circuit conditions if the potential was disconnected earlier. The samples were rinsed with deaerated deionized water and removed from the sample holders. They were then dried by blowing nitrogen, individually sealed in 10 ml clean serum bottles in the glove box and immediately transported into the XPS chamber. Comparisons were made with control samples and the "as polished" coupons. The steel coupons exposed to the anaerobic solutions of Na_2S and NH_4Cl were also analyzed by the polarization tests under the surface conditions of being rinsed and not rinsed.

In order to obtain further knowledge about the interaction of SRB with Mo, Cr and Ni, potentiodynamic polarization tests were performed in stationary stage culture using "as polished" coupons. The 3 day old culture was used for the experiment unless specified. In order to differentiate the interactions within the culture itself from those with Mo, potentiodynamic polarization of Au was conducted in the culture and the polarization diagram was compared with that of Mo, assuming that Au did not interact with SRB. After the potentiodynamic polarization, the culture was collected in clean serum bottles for XPS analysis in the forms: (1) not filtered, (2) filtered (0.22 μm Millipore filter).

6. X-ray Photoelectron Spectroscopy

6. 1. Spectra interpretation

6. 1. 1. Chemical shifts

XPS is a well established method to determine the surface composition and chemical states. A beam of low energy X-ray photons excites core level electrons to emerge out of the surface with specific kinetic energies from which the binding energies of the photoelectrons are determined by[57]:

$$B.\,E. = h\nu - K.\,E. - \phi \qquad (15)$$

where B. E. is the binding energy of the photoelectrons characteristic of an element, hν is the energy of the incident X-ray photon, K. E. is the kinetic energy of the photoelectrons, and ϕ is the work function of a spectrometer.

Shifts in binding energy from that obtained from a pure element indicate changes of valence states which provide information about the electron exchange of an interaction. The fundamental physics may be described as follows. The energy of an electron in a tightly bound core level is determined by the attractive potential of the nucleus and repulsive Coulomb force to all the other electrons. Changes in the chemical states or molecular environments of an atom involve a spatial rearrangement of the valence charges of this atom and a different potential created by the nuclear and electronic charges on all the other atoms in the compound. The binding energy difference of core levels of an atom in two compounds A and B may be calculated using the charge potential model[57, 58]:

$$\Delta E_c(A, B) = K_c(q^A - q^B) + (V^A - V^B) \qquad (16)$$

where $\Delta E_c(A, B)$ is the binding energy difference of the core levels of the atom in compounds A and B, K_c is the coupling constant, q^A and q^B are the valence charges, and V^A and V^B are the summation of potential at the atom in

compounds A and B due to "point charges" on surrounding atoms.

The charge potential model includes a number of simplifications. A major simplification is that the relaxation effect is ignored. The energies involved in the drastic rearrangement of the system upon ionization of an atom are not considered. There are two ways to correctly calculate the chemical shifts: (1) the hole state has to be calculated in addition to the ground state[59-61], or (2) relaxation energies are included in the right hand side of equation 16[62].

6. 1. 2. Quantification

The quantitative information about the relative concentration of surface composition may be obtained by measuring normalized peak areas in terms of unit time and scan number. For a sample homogeneous in an analysis volume, the intensity of photoelectrons in a specific peak area in unit time[56, 63]:

$$I = nF\sigma\theta y\lambda AT, \text{ and } n = I/F\sigma\theta y\lambda AT \qquad (17)$$

where n is the number of atoms in unit volume, F is the flux of X-ray photon in unit area and unit time, σ is the photoelectric cross section in unit area per atom, θ is the instrumental angular efficiency factor based on the angle between the paths of the incident photon and emerging electron, y is the

efficiency of production of photoelectrons having normal energy, λ is the inelastic mean free path of the photoelectron (imfp), A is the sampling area, and T is the efficiency of detection of photoelectrons.

For a given photoelectron transition in a sample, the constants in equation (17) may be defined as the atomic sensitivity:

$$S = \sigma\theta y\lambda AT \qquad (18)$$

The empirical sensitivity factors used in this study are given in Table 4. Thus, the atomic concentration of an element is given by:

$$C_x = n_x / \Sigma\, n_i = (I_x / S_x) / \Sigma (I_i / S_i) \qquad (19)$$

6. 1. 3. Variable angle XPS

In XPS analysis, the vertical distribution of the constituents in the surface film may be evaluated by varying photoelectron take-off angles (TOA) with respect to the sample surface (Figure 6). The depth from which the photoelectrons emerge is a function of the inelastic mean free path of the photoelectrons and their take-off angle (α)[64]:

$$d = 3\lambda \sin\alpha \qquad (20)$$

In the case of a substrate (s) is covered by a fractional monolayer F_a of species A, the signal from the substrate (s) may be determined by[64]:

$$I_s = I_s^{\infty}.\{1 - F_a + F_a \exp[-d_a/\lambda_a \sin\alpha]\}.\exp[-d_c/\lambda_c \sin\alpha] \qquad (21)$$

and the signals of the species A:

$$I_a = F_a.I_a^{\infty}.\exp\{1 - \exp[-d_a/\lambda_a \sin\alpha]\}.\exp[-d_c/\lambda_c \sin\alpha] \qquad (22)$$

where I_i^{∞} is the signal from a pure material i, the last exponential term on the right sides of the above formulae represents the attenuation by the hydrocarbon contamination overlayer if diffusion pumps are employed to generate the ultrahigh vacuum (UVH) of a spectrometer.

For this study, multiple components existed on the sample surface, including iron, chromium and nickel compounds, as well as biospecies formed during the exposure. Considerations are herewith only given to the rinsed samples, and it is assumed that the surface biospecies have been completely removed by rinsing. In addition, it is assumed that each type of detectable metallic signals from the substrate is only attenuated by one type of the metal compounds. For example, the species shown in the Fe2p spectra from the SRB-exposed surface of 304 SS included Fe, Fe^{2+}, Fe^{3+}, FeS, FeS_2, and $Fe_{1-x}S$[43].

Assuming that each compound has a uniform thickness and the overlapped monolayers of different types of compounds add to a thickness greater than the inelastic mean free path of the photoelectrons of metallic iron, the equations are derived as follows:

$$I_{Fe} = I_{Fe}^{\infty} \{1 - F_{FeS} - F_{FeS_2} - F_{Fe_{1-x}S} - F_{Fe^{2+}} - F_{Fe^{3+}} + F_{FeS}.\exp[- d_{FeS}/\lambda_{FeS}\sin\alpha] + + F_{FeS_2}.\exp[- d_{FeS_2}/\lambda_{FeS_2}\sin\alpha] + F_{Fe_{1-x}S}.\exp[- d_{Fe_{1-x}S}/\lambda_{Fe_{1-x}S}.\sin\alpha] + + F_{Fe^{2+}}.\exp[- d_{Fe^{2+}}/\lambda_{Fe^{2+}}\sin\alpha] + F_{Fe^{3+}}.\exp[-d_{Fe^{3+}}/\lambda_{Fe^{3+}}\sin\alpha]\}. \exp[-d_c/\lambda_c\sin\alpha] \quad (23)$$

$$I_{FeS} = F_{FeS}I_{FeS}^{\infty} \{1 - \exp[- d_{FeS}/\lambda_{FeS}\sin\alpha]\}.\exp[-d_c/\lambda_c\sin\alpha] \quad (24)$$

$$I_{FeS_2} = F_{FeS_2}I_{FeS_2}^{\infty} \{1 - \exp[- d_{FeS_2}/\lambda_{FeS_2}\sin\alpha]\}.\exp[-d_c/\lambda_c\sin\alpha] \quad (25)$$

$$I_{Fe_{1-x}S} = F_{Fe_{1-x}S}I_{Fe_{1-x}S}^{\infty} \{1 - \exp[- d_{Fe_{1-x}S}/\lambda_{Fe_{1-x}S}\sin\alpha]\}.\exp[-d_c/\lambda_c\sin\alpha] \quad (26)$$

$$I_{Fe^{2+}} = F_{Fe^{2+}}I_{Fe^{2+}}^{\infty} \{1 - \exp[- d_{Fe^{2+}}/\lambda_{Fe^{2+}}\sin\alpha]\}.\exp[-d_c/\lambda_c\sin\alpha] \quad (27)$$

$$\text{and } I_{Fe^{3+}} = F_{Fe^{3+}}I_{Fe^{3+}}^{\infty} \{1 - \exp[- d_{Fe^{3+}}/\lambda_{Fe^{3+}}\sin\alpha]\}.\exp[-d_c/\lambda_c\sin\alpha] \quad (28)$$

Thus, the fractional area of FeS may be determined by:

$$F_{FeS} = \frac{1}{\left[1 + \frac{I_{Fe}I_{FeS}^{\infty}}{I_{FeS}I_{Fe}^{\infty}} + \frac{I_{FeS_2}I_{FeS}^{\infty}}{I_{FeS}I_{FeS_2}^{\infty}} + \frac{I_{Fe_{1-x}S}I_{FeS}^{\infty}}{I_{FeS}I_{Fe_{1-x}S}^{\infty}} + \frac{I_{Fe^{2+}}I_{FeS}^{\infty}}{I_{FeS}I_{Fe^{2+}}^{\infty}} + \frac{I_{Fe^{3+}}I_{FeS}^{\infty}}{I_{FeS}I_{Fe^{3+}}^{\infty}}\right]} \times 1/[1-\exp(-d_{FeS}/\lambda_{FeS}\sin\alpha)] \quad (29)$$

$$F_{FeS} = \frac{1}{\left[1 + \frac{I_{Fe}(N\lambda)_{FeS}}{I_{FeS}(N\lambda)_{Fe}} + \frac{I_{FeS_2}(N\lambda)_{FeS}}{I_{FeS}(N\lambda)_{FeS_2}} + \frac{I_{Fe_{1-x}S}(N\lambda)_{FeS}}{I_{FeS}(N\lambda)_{Fe_{1-x}S}} + \frac{I_{Fe^{2+}}(N\lambda)_{FeS}}{I_{FeS}(N\lambda)_{Fe^{2+}}} + \frac{I_{Fe^{3+}}(N\lambda)_{FeS}}{I_{FeS}(N\lambda)_{Fe^{3+}}}\right]} \times 1/[1-\exp(-d_{FeS}/\lambda_{FeS}\sin\alpha)] \quad (30)$$

and the depth of iron sulfide:

$$d_{FeS} = -\lambda_{FeS}\sin\alpha . \ln\left\{1 - \frac{1}{F_{FeS}\left[1 + \frac{I_{Fe}(N\lambda)_{FeS}}{I_{FeS}(N\lambda)_{Fe}} + \frac{I_{FeS_2}(N\lambda)_{FeS}}{I_{FeS}(N\lambda)_{FeS_2}} + \frac{I_{Fe_{1-x}S}(N\lambda)_{FeS}}{I_{FeS}(N\lambda)_{Fe_{1-x}S}} + \frac{I_{Fe^{2+}}(N\lambda)_{FeS}}{I_{FeS}(N\lambda)_{Fe^{2+}}} + \frac{I_{Fe^{3+}}(N\lambda)_{FeS}}{I_{FeS}(N\lambda)_{Fe^{3+}}}\right]}\right\} \quad (31)$$

where $(N\lambda)_i$ is the product of atomic density (N) multiplied by the inelastic mean free path (λ) of component i.

The inelastic mean free path of a photoelectron is a function of its kinetic energy, the density and molecular weight of a species through which the photoelectrons travel, and the nature of the species. Using the empirical data, Seah and Dench derived the equations for the inelastic mean free path[66]. For an element, the inelastic mean free path is given by:

$$\lambda_{elem} = 538 / E_k^2 + 0.41 (aE_k)^{1/2} \text{ monolayers} \quad (32)$$

For an inorganic compound:

$$\lambda_{inorg} = 2170 / E_k^2 + 0.72 (aE_k)^{1/2} \text{ monolayers} \quad (33)$$

For an organic compound:

$$\lambda_{orga} = 49 E_k^2 + 0.11 (aE_k)^{1/2} \text{ monolayers} \quad (34)$$

and the monolayer thickness a is given by:

$$a = [A \times 10^{24} / (\rho n N_A)]^{1/3} \text{ nanometers} \quad (35)$$

where A is the molecular weight of the substance, ρ is its density in kg/m^3, n is the number of atoms in the molecule, and N_A is the Avogadro's number. The inelastic mean free paths of the photoelectrons in the major species and the maximum sampling depth are calculated (Table 5).

Based on the above derivations, the fractional area of iron sulfide may be estimated if the range of the sulfide thickness is known. The assumptions made for these derivations would bring about a certain degree of variation in estimation of sulfide thickness or area ratio, since nonuniform thickness of the interaction products would more likely result from the exposure and the photoelectrons from the underlayer can contribute to the count of intensity. However, these assumptions should be reasonable because the estimation of the fractional areas or depth of the sulfide is possible only when the metallic signals are detectable which otherwise may be completely attenuated if several monolayers overlap and render a thickness greater than the inelastic mean free paths of the photoelectrons. This is different from the general understanding of the relatively uniform passive film formed in abiotic corrosion.

6. 2. The equipment, parameters and procedure

A VG Scientific ESCA 3 Mark II spectrometer was used, which was controlled by VGX900 data acquisition system. The entrance and exit slit widths for the hemispherical analyzer were set at 4 mm. The analyzer energy for wide survey scans was 100 eV, and 20 eV for narrow region scans. Al K_α (1486.6 eV, 400 watts) X-ray radiation was used, providing a full width at half maximum (FWHM) of 1.35 eV for $Au4f_{7/2}$ singlet at 83.8 eV. Charge shifting was corrected with the adventitious carbon 1s line at 284.6 eV. The take-off angle was varied from 20° to 50° except the Mo coupons for which the take-off angle was varied from 10°, 20° to 50°. During spectra analysis, nonlinear least square curve fitting was performed, with the parameters including the constant tail ratio, Gaussian/Lorentzian ratio, constant/exponential tail mixing ratio and exponential tail slope. Background subtraction was conducted using the Shirley method[67]. When necessary, curve smoothing was conducted with the smallest intervals using the Savitsky and Golay method[68, 69]. Peak subtraction and secondary differentiation were carried out to aid in peak identification[69-71]. The peak parameters used as standards were obtained from pure elements and compounds using the same spectrometer settings (Table 6).

The vacuum was maintained below 3×10^{-9} torr during the experiment.

The samples sealed in the serum bottles were transported into the spectrometer through Ar purged glove bags. The centrifuged biomass was pressed onto In foil, and the droplets of culture and supernatant were dried on Au foil in the glove box. Liquid nitrogen cooling was provided to avoid decomposition and evaporation under x-ray radiation (~ -50 °C). Occasionally, Ar^+ etching was performed for the unrinsed samples to remove the top layer of biospecies, with an energy of 2.5 kV and the partial pressure of 5×10^{-7} torr for 5 seconds unless specified.

III. Results

1. Characterization of the passivity of 304 SS exposed to SRB

1. 1. Potentiodynamic polarization in deaerated 0.1 M HCl

The potentiodynamic polarization diagrams of the 304 SS coupons in deaerated 0.1 M HCl, following exposure to the inoculated and uninoculated media, are shown in Figures 3a and b. A polarization diagram of the "as polished" coupon is given in both Figures 3a and b to aid in comparison. The cathodic slope and open circuit potential are listed in Table 7.

It was seen that prior exposure to SRB resulted in a considerable loss of passivity (Figure 3a). Compared with the "as polished" coupons, the open circuit potential was decreased by 200 ± 75 mV, indicating a decrease of the surface stability. Both cathodic reduction and anodic dissolution were accelerated. The rate of the interaction was increased by 0.5 to 2 orders of magnitude, of which the cathodic slope was on average increased by 50 mV/decade. The presence of biofilm did not result in obvious difference in the range of cathodic reduction to active anodic dissolution. Associated with a greater decrease of the OCP, fast anodic dissolution indicated a serious loss of the passivity. Some of the samples remained a limited surface stability shown

by a smaller decrease of the OCP and a less accelerated anodic interaction, whereas the others were severely degraded by the exposure. Interestingly, for all the SRB-exposed samples, the rapid anodic dissolution started to decrease at an overpotential approximately equal to the active to passive transition potential of the "as polished" coupons. At the potential where the interaction was increased again, the polarization diagrams of the unrinsed samples exhibited a limited diffusion barrier effect of the biofilm, but not protective. In contrast, the control samples remained their passivity (Figure 3b).

1. 2. XPS analysis at different stages of the polarization tests

XPS analysis was performed at two stages of the polarization tests: (1) immediately after the exposure, exhibiting the surface changes as the initial states before the polarization and, (2) after potentiostatic polarization at -160 mV_{SCE}, providing further information about the loss of passivity.

1. 2. 1. Immediately after the exposure

The spectra of Fe2p, S2p, Cr2p and Ni2p from the surfaces of the SRB-exposed 304 SS coupons are shown in Figures 7, 8, 9 and 10 respectively. They were taken at TOA of 20° from the rinsed samples. No spectra of these

metal elements could be obtained from the unrinsed samples without removing the outer layer of biospecies by Ar^+ etching. The surface states of the control samples are included in these figures to demonstrate the microbial influence. The surface states of the "as polished" coupons are also given to aid in comparison. The atomic percentages of these alloying elements on the surfaces are calculated (Table 8).

A significant amount of iron sulfides was detected, including FeS, FeS_2 and possibly $Fe_{1-x}S$ (Figure 7a). $Fe_{1-x}S$ was arbitrarily fitted in Figure 7a because the standard was not available. The assignment of its binding energy position was according to the spectrum of the control sample, in which metallic Fe and Fe^{2+} were clearly separated (Figure 7b). In addition, the S2p spectrum indicated the possible existence of the non-stoichiometric sulfide because the peak was much wider than the one composed of FeS, Cr_2S_3 and NiS only (Figure 8). Because the S2p binding energies of FeS, Cr_2S_3 and NiS were very close, they were fitted into one peak, while FeS_2 and $Fe_{1-x}S$ were separated. In addition to the formation of these sulfides, the relative proportions of metallic Fe, Fe^{2+} and Fe^{3+} were greatly reduced in the presence of SRB, indicating dissolution of iron during the exposure. This is consistent with the atomic percentage of the total surface iron estimated by XPS analysis. In contrast,

large quantities of FeO and Fe^{3+} were seen on the surfaces of the control samples, and a high proportion of hydrated ferric oxide indicated a smaller degree of dissolution without the influence of SRB.

As usually seen in abiotic corrosion, surface enrichment of Cr took place during the exposure (Table 8). A small amount of chromium sulfide was visible in the Cr2p spectra, indicating a possibility of sulfidation of the passive film. A stronger hydration of trivalent chromium took place, associated with formation of a certain proportion of hexavalent chromium including CrO_3 and CrO_4^{2-} (Figure 9a). This spectrum indicated a vulnerability of the passive film to microbial influence, since the main kinetic barrier in abiotic corrosion, Cr_2O_3, was greatly reduced. On the other hand, the surface chromium of the control samples was far less hydrated, and the hexavalent chromium was negligible. Therefore, the greater proportion of $Cr(OH)_3$, together with the appearance of the hexavalent chromium species, indicated an additional bacterial influence other than sulfide formation. At this stage of the investigation, it appears to be doubtful to assign these high binding energy peaks to the hexavalent chromium, CrO_3 and CrO_4^{2-} in Figure 9a, because it is known that CrO_4^{2-} can be reduced to $Cr(OH)_3$ in the presence of SRB[72, 73]. The reduction of hexavalent chromium by X-ray radiation is also well known[74]. Its

stability in the present investigation could be due to the influence of surface hydrocarbons inhibiting photochemical reduction by the ready release of oxygen from the surface. Despite the controversy, the spectra indicate a difference from the abiotic interactions.

The atomic percentage of Ni on the surfaces of SRB-exposed samples was slightly higher than that on the control samples because of a stronger dissolution of iron into the culture (Table 8). Nickel sulfide became dominant in the Ni2p spectra, while metallic Ni and Ni^{2+} were also detected (Figure 10a). The nickel sulfide remained stable during the analysis, even without liquid nitrogen cooling. To illustrate, Ni2p spectra in Figure 10a was chosen from a sample which had been under X-ray radiation for at least 8 hours at room temperature. This indicated a possible complex of NiS with other sulfides, because, generally, a pure NiS needs liquid nitrogen cooling to prevent decomposition[75]. The presence of metallic Ni in the outer surface region showed a difference from the abiotic corrosion where the metallic Ni was usually in the interface between the passive film and the steel substrate. This indicated several phenomena associated with the exposure to SRB: (1) The rinsing method was able to remove most of the biospecies from the surface; (2) The passive film influenced by SRB was so thin that the interfacial metallic Ni

was detectable; (3) The bacterial uptake of Ni enhanced its transfer from the interface to the outer surface and; (4) the interaction was possibly nonuniform so that a severe dissolution of the interaction products resulted in exposure of substrate in certain local areas.

The vertical distribution of sulfide in surface film was determined by variable angle XPS analysis. The spectra were normalized, and the atomic percentages of the sulfides in total metal content determined (Figure 11). It was noted that the sulfides proceeded into the sublayer, indicated by the data at TOA of 50°. More FeS was detected from the sublayer, exhibiting a nonuniform interaction, but $Fe_{1-x}S$ and NiS were less depth-dependent. Further analysis will be addressed separately.

1. 2. 2. After the potentiostatic polarization in deaerated 0.1 M HCl

1. 2. 2. 1. The rinsed samples

XPS analysis was performed on the samples anodically polarized for 5 minutes at -160 mV_{SCE} in deaerated 0.1 M HCl following the exposure. For the samples rinsed prior to the polarization treatment, the spectra of Fe2p, Cr2p, Cr2p vs the polarization current and Ni2p at TOA of 20° are given in Figures

12, 13, 14 and 15 respectively, with the spectra from the surfaces of the control samples and "as polished" coupons included .

By comparing Figure 7a with 12a, it may be seen that a considerable dissolution of the iron sulfides, particularly FeS, took place during the anodic polarization in the hydrochloric solution. The relative proportion of Fe^{2+}, a sign of active dissolution rather than passivity[76], became dominant. This result explained the fast anodic interaction shown in the potentiodynamic polarization diagrams. By comparing multiple samples at this stage, we found that the polarization current was proportional to the relative proportion of the resultant ferrous iron and dissolution of the iron sulfides. In contrast, a high proportion of Fe^{3+} existed on the surfaces of the control samples at this stage, indicating a better passivity. The Cr2p spectra consistently revealed the passivity difference between biotic and abiotic interactions as indicated by an increased proportion of the hexavalent chromium (Figures 9a and 13a). The spectra did not indicate an obvious dissolution of Cr_2S_3. The relative proportions of the high binding energy species fitted as hexavalent chromium were significantly higher than those immediately after the exposure. By this stage, the determination of these hexavalent chromium species became convincing, and there were two reasons: At first, anodic polarization of 304 SS at -160 mV_{SCE} in the hydrochloric

solution should not produce the hexavalent chromium under abiotic conditions (Figures 13b and c)[77]. Secondly, the proportion of the hexavalent chromium increased after the polarization. The proportion would not have been increased if the high binding energy species were simply certain products of the bacterial interaction or were mistakenly fitted in the spectra due to the peak widening by differential charging of the residual biomass. Thus, the increased amount of the hexavalent chromium was formed during the anodic polarization after the surface had been activated by the bacterial interaction. In this study, the degree of the loss of passivity was found to be proportional to the resultant relative proportions of the hexavalent chromium species formed during the polarization (Figure 14). The Ni2p spectra at this stage provided further evidence of the bacterial influence additional to sulfidation, which was indicated by the absence of the passive $Ni(OH)_2$ and metallic Ni observed in the abiotic situation, while NiS remained dominant (Figures 15). In addition, it was also noted that the Ni^{2+} did not show any charge shifting, indicating a dissolution of some of the exposure products.

The relative proportions of the alloying elements at this stage are calculated (Table 8). The cleanliness of the surface could have been influenced by degradation of epoxy used for mounting the samples, because there was a

higher relative proportion of iron in the outer layer. However, the relative proportions of nickel and chromium provided some insights. Surface enrichment of Ni became much stronger than immediately after the exposure, indicating a possibility of a less dissolution of the bacterially uptaken Ni compounds during the polarization. On the other hand, depletion of chromium exhibited dissolution of the soluble chromium compounds.

1. 2. 2. 2. The unrinsed samples

In order to determine the influence of the biofilm on the interaction, the unrinsed samples were also anodically polarized at -160 mV (SCE) in 0.1 M HCl and then analyzed by XPS. Ar^+ etching was occasionally performed to obtain the signals of the alloying elements since the surface was covered with the constituents, mainly carbon and oxygen, of the biofilm, and the spectra of Fe2p, Cr2p and Ni2p were obtained at TOA of 50° (Figures 16, 17 and 18). The spectra at the TOA of 20° were not fitted concerning the possible ambiguity of low intensity. The relative proportions of the alloying elements are given in Table 8. The normalized atomic percentages of the sulfides remaining on the surfaces are shown in Figure 19.

It was seen that more iron was retained by the biofilm, whereas the

atomic percentages of chromium and nickel were markedly lower (Table 8). Compared with the rinsed sample, the relative proportions of these iron sulfides and nickel sulfide were much lower while the proportion of chromium sulfide was comparable (Figure 19). This indicated that the Cr2p signal was mainly from the substratum while iron and nickel were from the compounds arising from the bacterial uptake. The spectra of Fe2p showed that Fe^{2+} remained as a dominant valence state while ferric iron could also exist in the biofilm. In particular, the relative proportions of the iron sulfides in the residual biofilm was much lower than those from the rinsed samples suggesting that sulfidation took place on the steel substratum (Figure 16). In the Cr2p spectra, more hexavalent chromium was observed, indicating the possible forms of the bacterial removal of chromium from a solid metal surface. Whereas, the proportion of chromium (III) hydroxide was much lower than those on the rinsed samples, indicating a nonuniform interaction (Figure 17). The high Cr_2O_3 peak was from the steel surface. For the nickel compounds in the biofilm, Ni^{2+} other than NiS became a dominant species (Figure 18). It was also noted that no considerable charge shifting was seen in the spectra, indicating the conductivity contributed by the sulfide complexes in the biofilm, particularly after the dissolution of soluble exposure products during the polarization.

1. 2. 3. Variable angle XPS analysis

The variable angle XPS (VAXPS) analysis was conducted for depth variation of the exposure products. Because the interaction appeared to have proceeded nonuniformly, the analysis was only performed for the rinsed samples utilizing the spectra obtained at the TOA's of 20° and 50° so that the assumptions for derivation of fractional area of the products were applicable. At these two stages of the investigation, the atomic percentages of the sulfides in the total surface components are estimated in Figure 19, and their fractional areas in Table 9. In particular, the spectra obtained after the potentiostatic polarization were analyzed, because they provided the information directly related to the polarization current, a measurement of the loss of passivity. The extent of the variable distribution of the sulfides with the depth was estimated by the ratios of the atomic percentages of FeS in the total components of the alloying elements in the inner surface region (TOA = 50°) to the atomic percentages in the outer region (TOA = 20°), and subsequently correlated to the polarization current of the potentiostatic polarization (Figure 20). The sulfide distribution estimated by XPS analysis immediately after the exposure was not utilized for the correlation because it was not possible to remove the samples out of the XPS chamber and mount them on the sample holders for the

polarization tests without exposing to air. In addition, a higher proportion of FeS remained on the sample surface could be a result of less dissolution during the polarization treatment. The ratio of the FeS percentage in the inner region to that in the outer region after the polarization treatment, however, is able to demonstrate the variable distribution of FeS with the depth. The extent of surface hydration was evaluated by the ratios of the relative proportions of chromium (III) hydroxide to oxide in the inner region to their proportions in the outer region. The ratios greater than unity represented a preferential hydration in the inner region, i. e. undercutting of the passive film or oxide kinetic barriers. The degree of the nonuniform sulfidation with depth was thereafter correlated to the degree of the surface hydration (Figure 21). These evaluations, together with the fractional areas of the iron sulfides in Table 9, exhibited the nonuniform interaction.

Immediately after the exposure, the relative proportions of the sulfides changed with the depth, depending on the specific type (Figure 19). More FeS was detected in the inner region, whereas more FeS_2 and Cr_2S_3 remained in the outer region. In contrast, the proportions of $Fe_{1-x}S$ and NiS were less depth-dependent. Upon the potentiostatic polarization in the hydrochloric solution, the sulfides in the outer region, mainly FeS and FeS_2, were dissolved, but most of

the sulfides in the inner region remained. The relative proportions of NiS and Cr_2S_3, increased to a certain extent. The estimated fractional areas of FeS and NiS were consistent with the atomic percentages, indicating the relevance of the assumptions for deriving equations 30 and 31. With the fast anodic dissolution shown in Figure 3a, the result indicated that the formation of these sulfides proceeded into a certain depth of the surface. It was noted that the polarization current was proportional to the preferential sulfidation in the inner region, as the ratios of the atomic percentage of FeS in the inner region to its percentage in the outer region increased (Figure 20). Significant loss of the passivity began when the ratio was greater than unity, and the initiation of pitting was indicated by a fluctuation of polarization current in a range of ± 10 μA when its average value reached 80 μA. The polarization current drastically increased with a further increase of the proportion of FeS in the inner region. Furthermore, the extent of hydration of the passive film, measured by the ratios of the relative proportion of $Cr(OH)_3$ to Cr_2O_3 in the inner region to the proportion in the outer region, was closely related to the nonuniform distribution of FeS (Figure 21). This indicated that the formation of FeS was followed by hydration. No doubt, the existence of sulfides enhanced the transport of ingressing anions.

2. Characterization of the passivity of 317L SS exposed to SRB

2. 1. Cyclic polarization in deaerated 0.1 M HCl

Figure 4a is the cyclic polarization diagram of a 317L SS sample in 0.1 M HCl, not rinsed after the 5 day exposure to SRB. The E-log i curve of an "as polished" coupon is provided for comparison. Figure 4b is the polarization diagram of the rinsed sample, with the polarization diagram of the unrinsed sample included to demonstrate the influence of the biofilm.

It may be seen that the exposure to SRB caused a certain degree of the loss of passivity, but far less than the loss of passivity suffered by the 304 SS samples (Figure 4). Shown in the polarization diagrams, the open circuit potential was decreased by about 200 mV. Compared with 304 SS, the anodic dissolution was slower, and both the samples with and without the biofilm exhibited a limited passivity. For the samples tested by the polarization tests, the current density in the limited passive range never exceeded 10 μA, and was lower in the presence of the biofilm. The cathodic slopes of the SRB-exposed 304 and 317L SS are compared in Table 7. It was noted that the cathodic slopes were about 15 mV/decade lower than that of the "as polished" coupons, indicating an influence of the surface products on cathodic hydrogen evolution.

The anodic dissolution was more significant for the rinsed samples, but to a smaller extent than the "as polished" coupons. For the unrinsed samples, the polarization current in the passive region was close to that of the "as polished" coupons, lower than those of the rinsed samples, indicating a limited insolubility of the biofilm in the hydrochloric solution. On the other hand, the pitting potential was almost equal for both the rinsed and unrinsed samples, suggesting that the limited protection of the biofilm could be damaged by the dissolution of trapped soluble salts. The hystereses of the polarization diagrams of the rinsed and unrinsed samples represented different mechanisms of the breakdown of the passive film: in the presence of the biofilm, crevice formation was indicated by the reversed E-log i curve entering the active to passive transition region, whereas, without the biofilm, pitting was indicated by the reversed polarization into the passive region (Figure 4b). This result indicated that the dissolution of soluble salts trapped in the biofilm could have caused exposure of the steel substratum and consequent formation of concentration cells so that the passivity breakdown took place in local areas relatively larger than on the surfaces of the rinsed samples. In contrast, control samples maintained their passivity. The polarization diagrams are omitted now that the surface stability of the less corrosion resistant 304 SS control samples has been given (Figure 3b).

2. 2. XPS analysis at different stages of the polarization test

As the 304 SS samples, XPS analysis of the SRB-exposed 317L SS samples was conducted at two stages of the polarization test, immediately after the exposure and following the potentiostatic polarization at -160 mV_{SCE} in 0.1 M HCl for 5 minutes.

2. 2. 1. Immediately after the exposure

The XPS spectra of Fe2p, Cr2p, Ni2p and Mo3d were obtained from the rinsed sample surfaces immediately after the exposure. Figures 22, 23, 24 and 25 are the respective spectra at TOA of 20°. Their atomic percentages were evaluated according to the XPS analysis at TOA's of 20° and 50° (Table 10), and the proportions of the sulfides compared with those on the surfaces of 304 SS samples (Figure 11).

The amount of iron sulfides formed on the surface of 317L SS was considerably less than that on the surface of 304 SS (Figures 11 and 22), particularly in the sublayer. In the spectra, metallic iron became the highest component peak after the 5 day exposure, indicating a smaller degree of the interaction. The atomic percentage of the iron compounds in the total surface

components of the alloying elements was higher than that on the surfaces of 304 SS samples, suggesting a less dissolution into the bacteria (Table 10). In a strong contrast, a greater degree of surface depletion of iron was observed on the control samples, indicating different mechanisms in the biotic and abiotic interactions. In the Fe2p spectra from the control sample surfaces, ferric oxide had the highest relative proportion, contributing to the passivity (Figure 22b).

The smaller degree of the interaction is also shown in the Cr2p spectra. The amount of chromium sulfide was lower than those on the 304 SS samples, indicating less sulfidation (Figure 11). The atomic percentage of surface chromium was lower compared with the control samples and the SRB-exposed 304 SS samples, because a higher percentage of iron was retained. In the spectra from the SRB-exposed samples, a higher proportion of chromium (III) hydroxide existed, associated with the hexavalent chromium species (Figure 23). In contrast, the control samples were far less hydrated. The limited sulfidation and hydration of the passive film provided an explanation for the higher polarization current in the passive range when the rinsed samples were tested by the polarization following the exposure. The relative proportions of the hexavalent chromium appeared to be higher than those from the 304 SS samples, probably because the smaller degree of the interaction did not result in

a marked dissolution while the presence of other compounds enhanced its adsorption to the surface, such as ferrous molybdate[79].

The Ni2p spectra did not show significant differences from those on the surfaces of the 304 SS samples at TOA of 20°: the relative proportions of nickel sulfide were comparable, and the metallic Ni indicated a thin passive film (Figures 10a, 11 and 24a). However, far less NiS was detected in the sublayer, suggesting a better corrosion resistance than 304 SS and the interaction mainly taking place in the outer layer.

The Mo3d spectra showed a sharp contrast between the biotic and abiotic interactions (Table 10 and Figure 25). The surface depletion of Mo was caused by the exposure to SRB, whereas surface enrichment of Mo was observed on the control samples. Together with the higher proportion of iron compounds on the surface, this indicated a preferential dissolution of Mo into the culture, an evidence of the bacterial uptake of Mo. The counts of intensity of Mo3d appeared even lower in Figure 25a because it was overshadowed by the S2s peaks. It was determined by curve deconvolution that the outer layer of Mo species consisted of a Mo^{5+} species and molybdate. In contrast, a high peak of metastable Mo^{5+} existed on the surface of the control sample, whose formation could be due to the deaeration of the medium. Smaller amounts of

Mo^{4+} (as MoO_2) and molybdate were also seen, contributing to the passivity.

2. 2. 2. After the potentiostatic polarization in deaerated 0.1M HCl

Corresponding to the beginning of passivation in the hydrochloric solution, the SRB-exposed 317L SS samples were anodically polarized at this overpotential (-160 mV_{SCE}) for 5 minutes and then analyzed by XPS under the surface conditions of being rinsed before the polarization and not rinsed.

2. 2. 2. 1. The rinsed samples

The respective spectra of Fe2p, Cr2p, Ni2p and Mo3d are shown in Figures 26, 27, 28, and 29, at TOA of 20°. The spectra from the control samples and "as polished" coupons polarized at this stage are included.

First of all, the Fe2p spectra exhibited the better passivity of 317L SS (Figure 26a). Dissolution of the iron sulfides appeared to take place uniformly as demonstrated by the overall reduction of the peaks of the sulfides. Although more ferrous iron compounds were formed, including ferrous oxide, chloride and molybdate, metallic iron was still visible, indicating a smaller degree of the interaction. Because the spectra more emphasized the outer surface, the existence of the metallic iron at this stage also indicated a thin passive film.

Formation of ferrous oxide and chloride may have increased the interaction, but the existence of molybdate counteracted the ingressing chloride so that a limited passivity was retained. For multiple samples tested at this stage, the polarization current never exceeded 10 μA, consistent with the slow anodic dissolution shown in the cyclic polarization diagrams (Figure 4b).

The Cr2p spectra consistently demonstrated the limited passivity. After the potentiostatic polarization, more chromium hydroxide was found on the SRB-exposed samples, but no further formation of the hexavalent chromium took place after the exposure-induced hexavalent chromium was dissolved in the hydrochloric solution (Figure 27). This was a significant difference from the SRB-exposed 304 SS samples where more hexavalent chromium was formed at this stage. Namely, the limited interaction mainly took place in the outer surface region during the exposure to SRB so that the integrity of the passive film was less affected. In order to demonstrate the possible sulfidation of the passive film, a small chromium sulfide peak was fitted in the spectra despite the insignificant count of intensity. On the other hand, the Cr compounds on the control samples were comprised of almost equal amount of chromium (III) hydroxide and oxide, in addition to the metallic Cr from the substrate.

The involvement of nickel compounds in the interaction is shown in the

Ni2p spectra (Figure 28). It was noted that the relative proportion of NiS was markedly reduced upon the polarization, indicating a consistency of the limited interaction within the outer surface region. This became more convincing when indicated in the Ni2p spectra because the current was so low that the dissolution of surface compounds was not considerable during the potentiostatic polarization. In addition, the better passivity was also indicated by the existence of a considerable proportion of nickel hydroxide in the spectra, although the species unable to contribute to the passivity, Ni^{2+}, were also observed. In contrast, a low peak of metallic nickel was detected from the surface of the control sample, originating from the interface (Figure 28b).

The better passivity of 317L SS was ascribed to the Mo content, which was explained by the Mo3d spectra (Figure 29). The dissolution of the sulfides during the polarization greatly reduced the shadowing effect of S2s on the Mo3d signal so that the Mo3d spectra became more pronounced than immediately after the exposure. The surface Mo compounds consisted of metallic Mo, Mo^{4+} (including MoO_2 and MoS_2), Mo^{5+}, and molybdate. MoO_2 and MoS_2 were not separated in curve fitting since their binding energy values were very close (Table 6). The existence of the Mo^{5+} on the sample surface after the potentiostatic polarization exhibited its insolubility in the hydrochloric

solution. This would provide a protection in addition to molybdate. Whereas, the metallic Mo indicated that the passive film was very thin. On the other hand, Mo^{5+} was greatly reduced, and molybdate became dominant on the surfaces of the control samples. Thus, the biotic Mo^{5+} differed from the abiotic one in its stability in the hydrochloric solution. The absence of metallic Mo on the control samples suggested that the passive film formed without the prior exposure to SRB would be thicker.

2. 2. 2. 2. Variable angle XPS analysis

In order to evaluate the depth-dependence of the interaction, variable angle XPS analysis was conducted at TOA's of 20° and 50° on the rinsed SRB-exposed samples which were subsequently polarized at -160 mV_{SCE} in the hydrochloric solution. The atomic percentages of the constituent alloying elements were evaluated (Table 10), and the representative information about the vertical variation of the interaction is provided in the Fe2p and Mo3d spectra (Figures 30 and 31 respectively).

Comparing the Fe2p spectra at different take-off angles, it was seen that sulfidation mainly took place in the outer surface region, rendering a thin passive film (Figure 30). Upon subsequent potentiostatic polarization in the

hydrochloric solution, the iron sulfides began to dissolve, and the surface iron compounds were more comprised of ferrous species, as indicated by the increased formation of ferrous oxide and appearance of ferrous chloride and molybdate (Figure 30a). In comparison, the inner surface region contained a far less amount of the sulfides, clearly revealing a uniform dissolution of the sulfides during the potentiostatic polarization. In the inner region, ferrous molybdate had a higher relative proportion than ferrous chloride, indicating a protection against the ingressing chloride[19]. As a result, the relative proportion of metallic Fe became the highest in the spectra, and the unstable compound, FeO, was greatly reduced (Figure 30b). The distribution of the multiple Mo species with the depth provided further information. While the Mo compounds in the outer region were largely composed of the Mo^{5+} species, the inner region contained more molybdate (Figure 31). Because the relative proportion of the Mo^{5+} species was much lower in the inner surface region, its stability in the outer region provided the evidence of its formation via interaction with SRB. Formation of molybdic acid, on the other hand, could be due to the low pH of the hydrochloric solution. Additionally, the evidence of the limited interaction in the outer surface region was also well shown in Cr2p and Ni2p spectra. While the chromium species in the outer region were dominated by $Cr(OH)_3$, the relative proportion of Cr_2O_3 was considerably higher in the inner region,

and metallic Cr was also visible. Ni2p spectra exhibited a very small amount of NiS formed in the the inner layers which was far less attacked by chloride.

2. 2. 2. 3. The role of the biofilm

XPS analysis of the SRB-exposed samples subsequently polarized with the biofilm explained its protective effect. This information is particularly useful because the resulting surface states immediately after the exposure was difficult to evaluate by XPS in the presence of the biofilm. Upon polarization in the hydrochloric solution, soluble species including organic and inorganic salts were dissolved so that the spectra of the constituent alloying elements became detectable. The representative information is summarized in the Fe2p and Mo3d spectra (Figures 32 and 33).

The Fe2p spectra in Figure 32 showed that the outer region contained more ferrous iron, including FeO, $FeCl_2$, and the iron sulfides, but no molybdate could be observed. The dominant proportion of the ferrous oxide revealed its origination from the interaction with SRB, consistent with the XPS analysis of the rinsed samples at a lower TOA. In contrast, the inner region was comprised of the metallic iron having the highest relative proportion. This indicated a protective effect of the biofilm. Such a high proportion of metallic

Fe in the inner region became visible because of the dissolution of soluble species in the biofilm. In addition, a considerable amount of ferrous molybdate in the inner surface region also provided a protection against the ingressing chloride[17-20]. Therefore, the passivity of the samples with the biofilm was less affected (Figure 4). The protection provided by the thin biofilm was consistently shown in the Mo3d spectra (Figure 33). In the outer surface region where the spectrum more emphasized the constituents of the biofilm, a dominant proportion of the Mo^{5+} species covered the steel substratum, exhibiting its insolubility in 0.1 M HCl, while a smaller amount of Mo^{4+} including MoS_2 was also observed. In contrast, the Mo3d spectrum from the inner region provided the information about the steel surface. Although the Mo^{5+} species had the highest relative proportion, a considerable amount of molybdate was also seen, and a smaller proportion of metallic Mo indicated that the biofilm was very thin. Furthermore, the S2s spectra next to the Mo3d revealed the resulting sulfur compounds in the interaction. In the biofilm, sulfur was largely associated with the organic molecules in addition to a small amount of sulfide, evidently demonstrating an incomplete sulfur reduction on the surface of 317L SS. In addition to the Fe2p and Mo3d spectra, chromium (III) hydroxide was detectable because the biofilm was very thin. Various types of nickel species, as shown on the surface of the rinsed sample, could be observed

in the inner region while the nickel entering the biofilm was totally sulfidized.

3. Biotic and abiotic simulations using anaerobic solutions of Na_2S and NH_4Cl with and without addition of sulfur-containing amino acid

The loss of passivity of these two types of steels during the exposure to SRB raised interesting issues regarding the active species which were able to reduce their surface stability. In this study, particular attention was paid to H_2S because of its well known anodic effect on initiating pitting[25]. H_2S was generated in the anaerobic solution of Na_2S and NH_4Cl so that the effect of chloride was also included. L-cysteine was added to the solution to demonstrate the role of intermediate sulfur-containing proteins in the interaction. In this part of the investigation, type 304 SS was studied regarding the interesting phenomena observed during the exposure to SRB, such as the severe loss of passivity and formation of the hexavalent chromium species.

3. 1. Potentiodynamic polarization of 304 SS in 0.1 M HCl subsequent to the exposure

Figure 34a shows the polarization diagrams of type 304 SS in deaerated 0.1 M HCl subsequent to the exposure to the anaerobic 10 mM cysteine only, and 34b are the polarization diagrams following the exposure to the solutions

containing H_2S compared with the those of the SRB-exposed 304 SS.

It was found that the exposure to the cysteine solution resulted in a slight ennoblement, associated with a decrease of the pitting potential in the hydrochloric solution. These results, in particular the decrease of the pitting potential, indicated an oxidation of the steel surface. On the other hand, the presence of H_2S in an anaerobic solution was able to severely damage the surface integrity of 304 SS, regardless of the existence of cysteine. Contrary to the diffusion barrier effect of the biofilm, the presence of the exposure products resulted in higher anodic dissolution. By combining cysteine with H_2S, the decrease of the open circuit potential was less and the both the rates of the cathodic and anodic interactions were slightly slower. The slight ennoblement was consistent with the oxidation observed in the cysteine solution only. However, the deterioration by H_2S was overwhelming so that the normal passivity no longer existed. The good approximation of the polarization diagrams to those obtained with the SRB-exposed samples exhibited that the loss of passivity arising from the exposure to SRB was mainly due to H_2S.

3. 2. XPS analysis at different stages of the polarization test

Corresponding to the polarization test, XPS analysis was conducted on

the 304 SS samples immediately after the exposure to the cysteine and H_2S-containing solutions and after potentiostatic polarization at -160 mV_{SCE} in the hydrochloric solution subsequent to the exposure. The samples immediately after the exposure to the cysteine-containing and non cysteine-containing solutions differed in the atomic percentages of the alloying elements on their surfaces: The samples exposed to the cysteine-containing solutions exhibited a strong surface enrichment of Cr and depletion of iron simulating the exposure to the bacterial culture, whereas the exposure to the non cysteine-containing solution resulted in formation of FeS and $Fe_{1-x}S$ covering the sample surfaces so that the atomic percentages of Cr and Ni were very low. This explained the higher interaction rate of these samples in the hydrochloric solution. The Cr2p spectra exhibited hydration of the passive film and formation of the hexavalent chromium induced by H_2S, which were enhanced by cysteine, and Ni2p spectra showed only NiS on the sample surfaces.

The variable angle XPS spectra of Fe2p and Cr2p from the samples subjected to the potentiostatic polarization provided further information (Figures 35 and 36). These spectra were chosen from the unrinsed samples since the presence of the exposure products resulted in a higher rate of the interaction. For the samples exposed to the non cysteine-containing solution, the Fe2p

spectra showed that a considerable amount of FeS and $Fe_{1-x}S$ remained on the surfaces after the subsequent potentiostatic polarization (Figure 35a). The surface iron compounds included a dominant proportion of ferrous oxide, and some ferrous chloride and ferric oxide in addition to the iron sulfides. The ferrous chloride was much more than that immediately after the exposure, indicating an enhancement of these sulfides on transfer of ingressing chloride during the polarization. The relative proportions of FeS and ferrous chloride was higher in the inner region, suggesting a possibility of nonuniform interaction. In addition, metallic Fe was also observed, indicating that the layer of the remaining exposure products was thin. The appearance of the dominant ferrous iron was consistent with the results of the SRB-exposed samples at this stage (Figure 12a). The result also differed from the observations made with the SRB- exposed samples in the appearance of the ferrous chloride which was not detected on the SRB-exposed samples. This was probably because the rate of the interaction was lower for the samples exposed to the synthetic solution so that the chloride was not completed dissolved. In the presence of cysteine, however, the nonstoichiometric $Fe_{1-x}S$ was not observed, suggesting that the formation of the $Fe_{1-x}S$ during the exposure to SRB was more dependent upon H_2S than the intermediate sulfur-containing proteins (Figure 35b). The higher relative proportion of FeS remaining in the inner region also indicated the

nonuniform interaction, whereas, more metallic iron was detected, exhibiting a thinner layer of the remaining exposure products.

The Cr2p spectra from the surfaces of these two types of samples provided further detail (Figure 36). Without the presence of cysteine, a smaller degree of hydration took place in the outer layer and the hexavalent chromium species were largely dissolved during the polarization. Addition of cysteine to the solution, however, greatly enhanced hydration of Cr and formation of the hexavalent chromium so that they remained remarkable after the polarization. Together with the ennoblement observed in the polarization diagrams, this explained the hydration and formation of the hexavalent chromium on the 304 SS samples during the exposure to SRB.

4. The interaction of SRB with the constituent alloying elements

The results of the interactions of SRB with these steels provided a general information about their passivation performance in SRB-containing environments. For further mechanistic details, the specific interactions of SRB with the constituent alloying elements were studied. Since Mo contributed to the passivity of 317L SS, it drew a particular attention.

4. 1. The interaction of SRB with Mo

Molybdenum is widely known for its involvement in the enzymes and cofactors[6-12, 49, 80]. Molybdate and other Group VI oxyanions including selenate, chromate and tungstate are also well known for their inhibitive effect on sulfate reduction by SRB[6- 12]. The better passivity of 317L SS than that of 304 SS revealed the importance of Mo. In particular, the interaction of Mo with SRB differed from its commonly known behavior, such as the surface depletion during the exposure, the formation of the Mo^{5+} species and their insolubility in the hydrochloric solution. These phenomena raised interesting issues about the interaction of SRB with Mo.

4. 1. 1. Characterization of the Mo coupons exposed to SRB by DC polarization in deaerated 0.1 M HCl and XPS analysis

The same test protocol was applied to the pure Mo coupons subjected to the 5 day exposure to SRB, as the steel coupons. Potentiodynamic polarization test was conducted in deaerated 0.1 M HCl following the exposure, and the surface chemical states determined by XPS after the exposure and after potentiostatic polarization in the passive range in the hydrochloric solution.

4. 1. 1. 1. Potentiodynamic polarization in 0.1 M HCl

Following the 5 day exposure to SRB, potentiodynamic polarization of the Mo coupons was conducted in deaerated 0.1 M HCl with and without the biofilm. The diagrams are compared with that of an "as polished" coupon (Figure 37). This result showed that the presence of the biofilm increased the surface stability so that both the rates of the cathodic reduction and anodic dissolution were reduced. In contrast to the rinsed samples, the polarization current in the passive range was reduced by one order of magnitude. On the other hand, the rinsed samples suffered from a certain degree of the loss of passivity, associated with the higher rates of both cathodic reduction and anodic dissolution. Although a limited passivity was retained, the pitting potential was reduced. It was also noted that the polarization currents of both types of the samples overlapped above the pitting potential, suggesting a limit of the protection of the biofilm.

4. 1. 1. 2. XPS analysis

XPS analysis was performed immediately after the exposure and after the anodic polarization at -160 mV_{SCE} in deaerated 0.1 M HCl. The surface states at these two stages are compared in Figures 38a and 38b, the Mo3d

spectra at TOA of 10°. The surfaces states of control samples at these two stages are provided in Figures 38c and 38d to aid in the comparison. The depth variation of the interaction was analyzed by variable angle XPS at TOA's of 10°, 20° and 50°. The depth distribution of various Mo compounds is given in Table 11. The Mo involved in the biofilm was analyzed after potentiostatic polarization of the unrinsed samples in the hydrochloric solution (Figure 39).

For the rinsed samples, formation of molybdate took place exclusively during the exposure to SRB (Figure 38). Compared with the control samples, it may be seen that the exposure to SRB resulted in a greater degree of the interaction so that the relative proportion of metallic Mo was obviously lower than those in the spectra from the control sample (Figure 38 and Table 11). The dominant proportion of the metallic Mo in the spectra indicated that the interaction layer was rather thin, but the bacterial sulfate reduction resulted in a considerable sulfidation into a deeper region so that the relative proportion of MoO_2 was greatly reduced. The determination of MoS_2 in the Mo3d spectra was based on the intensity of the S2p spectra and the sensitivity factors of the Mo3d and S2p photoelectrons (Table 4). Sulfidation and decrease of the passive MoO_2 on the Mo surface caused the loss of passivity, as shown in the potentiodynamic polarization diagrams (Figure 37). However, the surface

molybdate reduced the degree of the loss of passivity because of its repelling effect on ingressing chloride. As a result, a limited passivity was remained. In addition, the pentavalent Mo species were formed and developed into a certain depth during the exposure (Table 11). Upon the subsequent potentiostatic polarization in the hydrochloric solution, the products formed during the exposure began to dissolve so that the metallic Mo became more pronounced, and the relative proportion of MoO_2 increased (Figure 38b and Table 11). It was noted that a considerable amount of the pentavalent Mo remained on the surfaces of the Mo coupons, indicating a limited insolubility in the hydrochloric solution. In comparison, the surface of the control sample was far less affected, no molybdate could be seen, and the relative proportion of MoO_2 was much higher. Although a pentavalent Mo compound was observed after the immersion, it was limited within the outermost surface layers, and markedly dissolved during the subsequent potentiostatic polarization. Therefore, the formation of the abiotic pentavalent Mo was simply a result of oxidation during polishing and immersion in the oxygen deficient uninoculated medium.

In order to further understand the Mo products in the biofilm, variable angle XPS analysis was conducted after the potentiostatic polarization. In the outermost layer of the biofilm, no Mo signal was visible, but the sulfur signal

was pronounced, due to dissolution of soluble products (Figure 39a). However, the sulfur species in the remaining biofilm was not a sulfide but organic species. Compared with the organic sulfur on the surface of 317L SS, this S2s peak showed more than 1 eV charge shifting, indicating its insulating nature. This result indicated the ability of the Mo species of the biofilm to inhibit the sulfate reduction because otherwise sulfide should have been seen. With the increase of the take-off angle, the sampling depth increased and the Mo signal became detectable. At TOA of 20°, the pentavalent Mo species were clearly seen, with a relative proportion about 20% higher than that from the rinsed samples, and its relative proportion was not substantially decreased with the increase of sampling depth (Table 11). In addition, it was noted that MoS_2 became clearer as the take-off angle increased, indicating the sulfidation of the Mo coupons. Because of the limited insolubility of the biofilm, the unrinsed samples showed a better surface stability in the hydrochloric solution. By contrast, the control samples were cleaner, and the Mo species included MoO_2, Mo^{5+} and a small amount of MoO_4^{2-} (Figure 39b).

4. 1. 2. DC polarization of "as polished" Mo coupons in the stationary stage culture

In addition to the tests above, the interaction of SRB with Mo was

characterized by potentiodynamic polarization of the "as polished" coupons in the culture, and distinguished from the interactions within the culture itself by polarization of gold. In order to determine the dissolution products, XPS analysis was conducted on the filtered and nonfiltered culture droplets.

The interaction of Mo with the culture is shown in Figure 40, the potentiodynamic polarization diagram of the "as polished" Mo coupon in a 7 day old culture, with the E-log i diagram in the uninoculated medium included. The polarization diagram in the 7 day old culture was chosen because the interaction of Mo with the bacteria resulted in a considerable fluctuation of the polarization current and thus it was difficult to provide a smooth curve. In this test, the open circuit potential of Mo in a normally growing culture was usually about 200 mV higher than that in the uninoculated medium, indicating the influence of the bacteria on the Mo surfaces. Because the sulfate reduction was complete in the 7 day old culture, the cathodic slope did not show the effect of sulfate reduction which would contribute to it. The anodic interaction, on the other hand, was a summation of Mo dissolution, the interactions of the microorganisms and metabolic products and the interaction of the dissolved Mo with the microorganisms and metabolic products. In the polarization diagrams, there were no clear active to passive and passive to transpassive transitions.

Because of the higher open circuit potential, it appeared as if Mo were more noble in the presence of SRB. However, the rate of the interaction, measured by the rate of the current increase, was faster in the inoculated medium. As Mo dissolved in the culture, an orange coloration was generated while the dissolved Mo in the uninoculated medium resulted in a dark blue color indicating a mixture of polymolybdate and Mo^{5+}. The polarization diagrams in the inoculated and uninoculated media, in fact, represented two chemistries of the interaction, one containing the bacteria and metabolic products and the other essentially showing the interactions of Mo with low concentrations of the multiple ions in the uninoculated medium. In order to differentiate the interactions in the culture brought about by Mo, a cyclic polarization of Mo was conducted using the 3 day old culture in the range of potential of $\pm$ 200 mV around the OCP, and the result was compared with a polarization diagram using Au as the working electrode representing the interactions inside the culture itself (Figure 41). In the diagrams, the current is plotted in a linear relation to the potential to reduce the large fluctuation in the logarithm current. As shown in Figure 41, the surface activity of Mo was indicated by a lower OCP and a noticeably higher cathodic reaction rate representing an enhanced cathodic reduction resulting from the sulfide formation of Mo. The early stage of anodic reaction was also faster, dissolution of Mo and anodic corrosion

enhanced by the adsorbed H_2S took place. As more Mo was dissolved, the anodic reaction became slower than that without Mo, indicating the interference of the dissolved Mo with the interactions. As the polarization was reversed, a small hysteresis appeared. This indicated a decrease of the bacterial activity because the polarization potential was reasonably low.

XPS analysis of the culture droplets after the potentiodynamic polarization showed that the dissolved Mo primarily existed in the pentavalent state, associated with a small amount of hexavalent molybdenum (Figure 42). Figure 42a is a spectrum from the culture droplet directly dried on a piece of Au foil and Figure 42b is from its supernatant. The charge shifting was based on the N1s from the supernatant known as ammonium. The Mo^{5+} species was seen in both the spectra, but a considerable charge shifting was produced in the presence of the biocells, consistent with the charge shifting in the spectra from the biofilm on Mo coupons in Figure 39. The peak at the low binding energy side was not fitted concerning the possible differential charging by the biocells. In contrast, the low binding energy shoulder was tentatively fitted as a possible organic Mo peak in Figure 42b, which probably originated from a higher electron density surrounding Mo atom such as in carbonyl groups[81-83].

4. 1. 3. The interaction of SRB with the dissolved Mo during the exposure of sputter-deposited Mo thin films and pure Mo powder

The incomplete sulfate reduction on the surfaces of the Mo coupons during the exposure and the reduced microbial activity caused by the dissolved Mo during the cyclic polarization provided a partial explanation for the better passivity of the Mo-bearing stainless steel, 317L SS. For further information, the sputter-deposited Mo thin films and pure Mo powders were exposed to the culture. A greater degree of interaction was expected, because the Mo thin films were structurally more defective than bulk Mo metal and suffered from internal stress, and Mo powders had larger surface areas. To better understand the implications of the presence of molybdate on the surfaces of the 317L SS and Mo coupons, the culture growth and sulfate reduction in the medium containing low concentrations of molybdate were studied. XPS and UV spectroscopy were employed to characterize the interaction products.

4. 1. 3. 1. Culture growth and sulfate reduction

4. 1. 3. 1. 1. During exposure of the Mo thin films and Mo powders

The culture growth in the media containing the Mo thin films, 1 g/l Mo powder and 1.44 g/l MoO_3 is given in Table 12, measured by the turbidity at

600 nm, with the culture growth in the medium containing no Mo included for comparison. It was observed that sulfate reduction proceeded with the growth of culture. As a carbon source, lactate was oxidized to acetate as the culture grew. In a normal culture without Mo, less than 10% of sulfate remained after 2 days, and the sulfate was further reduced as the culture continued to grow. Considering the content of sulfate added, it was also noted that about 800 ppm sulfate had been converted into other types of sulfur compounds in uninoculated medium. Upon exposure of the Mo thin films to the culture, a significant delaying effect on the culture growth was observed and the culture became orange. In a two day period, the culture growth in the presence of the Mo thin films reached a certain turbidity, but reduction of sulfate was rather limited. After 5 days, the culture remained turbid, because the nutrients were still available although sulfate was greatly reduced. In contrast, the turbidity of the normal culture without Mo was markedly reduced after 5 days, because of the death of cells due to the consumption of the nutrients.

Addition of 1.44 g/l mM MoO_3 to the growth medium almost completely inhibited the culture growth and sulfate reduction. Associated with the inhibition, the pH was considerably reduced, indicating protonation. The culture also became orange. Addition of 1 g/l Mo powder at different stages of

culture growth led to different results: sulfate reduction was almost complete with an increase of turbidity after growing for 2 days when 1 g/l Mo powder was added before inoculation, whereas a limited inhibition was observed in the culture growing for 2 additional days after it had previously grown for 2 days and then 1 g/l Mo powder was added. Namely, the culture was able to dissolve Mo, and the dissolved Mo would be sufficient to counteract the culture growth when the microbial activity was high enough to cause considerable dissolution. In addition, the residual sulfate in the 2 day old culture containing no Mo was noticeably lower than that in the culture which had grown for 2 days before 1 g/l Mo powder was added, indicating a possibility of formation of larger molecular weight Mo-S compounds through interaction of dissolved Mo with the residual sulfate which yielded the higher reading when measured by weight ratio (ppm). This was probably also true for the residual sulfate measured during the exposure of Mo thin films, in which the residual sulfate should have been much lower if the rate of sulfate reduction was considered proportional to the rate of culture growth. Comparing the results of Mo thin film exposure tests with those of addition of Mo powders at different stages of culture growth, it may be deduced that dissolution of Mo from Mo thin films is a process dependent on the culture growth, and, on the other hand, also inhibitive when reaching a sufficient amount.

The results above gave rise to several questions regarding the interaction of Mo with SRB. First of all, the path of dissolution needs further study. Secondly, the possible formation of the large molecular weight Mo-S complex should be verified. Thirdly, no evidence of formation of the large molecular weight compounds was indicated by the residual sulfate analysis upon adding MoO_3 to the growth medium. The resulting orange color, consistent with those in the exposure of the Mo thin films and Mo powder to the culture, probably was an indication of the final products having the same functional Mo-S bonds. Finally, the minimum content of dissolved Mo to completely inhibit culture growth needs to be determined. For further study, different ratios of sulfate to molybdate were added to the growth medium.

4. 1. 3. 1. 2. The growth of culture in the presence of low concentrations of molybdate

A low concentration of molybdate was able to inhibit the culture growth markedly (Figure 43). The orange color became deeper in the range of molybdate concentration from 0.5 to 2 mM. pH decreased gradually as the molybdate content was reduced, but not significant compared with the culture containing no molybdate and uninoculated medium because the cultures showing noticeable growth contained a low content of molybdate. 0.1 mM

molybdate was apparently able to delay, and 5 mM molybdate completely inhibited the growth of culture. In addition, it is interesting to note that the residual sulfate, measured in ppm using the turbidimetric method, drastically increased with the culture growth and reduction of molybdate content, reaching a value several orders of magnitude higher than the initial contents added. A relationship among the residual sulfate measured in ppm, culture growth in turbidity and sulfate added is plotted in Figure 44. This demonstrated formation of the large molecular weight Mo-S complexes, whose molar concentrations should be consistent with the calibration method using a low molecular weight sulfate standard, Na_2SO_4. The result also revealed that the amount of the Mo-S complexes was proportional to the culture growth so that the orange color became deeper as the molybdate content was decreased and the culture able to grow. The necessity of characterization of the interaction products arose.

4. 1. 3. 2. XPS analysis

4. 1. 3. 2. 1. Dissolved Mo from Mo thin films

The culture showed a strong affinity for Mo. XPS analysis of the dried culture droplets following the exposure indicated that considerable dissolution of Mo took place when the Mo thin films were exposed to the culture, ranging

from 2 to 4 mM. This estimation was based on the extrapolation of the analysis of the dried droplets of various concentrations of molybdate solution, ranging from 10 to 100 mM, under the same spectrometer settings. The Mo3d spectra from the culture droplets showed that dominant amount of Mo existed as Mo^{5+}, with a smaller amount of molybdate and lower binding energy species, represented by Mo° and $Mo^{/}$. MoS_2 was also detected, as shown in the Mo3d and S2p spectra (Figure 45). The Mo^{5+} species were the Mo-S complexes that gave rise to an orange color of the culture, while the existence of molybdate indicated a pathway of Mo dissolution. Because the spectroscopic characteristics of the other related elements, such as C1s, O1s and N1s, were overshadowed by the major component peaks in their spectra, it was very difficult to derive further information about their molecular forms only by XPS analysis. The lower binding energy species in the spectra, Mo° and $Mo^{/}$, were distinguished from the S2s peaks because their binding energies were obviously higher than that of S2s of MoS_2. In addition, their sensitivity factors were also different from those of S2s[27]. Formation of these lower binding energy species suggested a possible involvement of Mo in the organic compounds other than the Mo(V) complexes. For example, Mo bound to carbonyl groups may have such low binding energies, and in particular, a negative shift of the binding energy occurs when the carbonyl groups are partially replaced by nitrogen or

phosphorus causing an increase of the electron density surrounding Mo[81-83]. Further verification was not conducted because of the limited quantity of the interaction products. In comparison, no dissolution of Mo was detected from the droplets of the uninoculated medium used for control test.

4. 1. 3. 2. 2. Mo in the centrifuged biomass of the cultures containing low concentrations of molybdate

The reduction to the pentavalent state took place when the molybdate content was not sufficient to inhibit culture growth. XPS analysis of the centrifuged biomass revealed that molybdate was increasingly reduced to the Mo(V) complexes when its initial content was below 5 mM (Figures 46a, c, and e). When the molybdate content was 0.1 mM, the Mo(V) complexes became dominant in the Mo3d spectrum although curve fitting was not performed considering the possible ambiguity arising from the low counts of intensity. Clearly, residual molybdate was very low in the spectrum, and the outstanding shoulder on the low binding energy side exhibited an increased proportion of MoS_2 resulting from the growth of culture. In addition, the Mo3d spectra showed considerable charge shifting. A higher charge shifting was seen before molybdate was reduced. In this study, we found that a Na_2MoO_4 standard usually caused about 4 eV charge shifting due to its insulating nature.

Upon reduction of molybdate, the charge shifting was reduced by about 0.5 eV, indicating a change in the constituents of the Mo compounds. Almost the same amount of charge shifting was shown in the spectra of the biomass of the cultures containing 1 and 0.1 mM molybdate. The charge shifting independent of molybdate content could be due to the poor conductivity of the biomass. The consistency of charge shifting in Figure 46c and 46e provided another evidence of the reduction of molybdate: there was little probability of spectrum widening by differential charging of the biomass, because, otherwise, the binding energies of the Mo(V) and MoS_2 in Figure 46c and 46e would vary if the spectra had been widened by differential charging.

The S2p spectra indicated an increased proportion of insoluble sulfur species with the increase of culture growth shown by the increasing counts of intensity of the S2p photoelectron (Figure 46b, d and f). The reduction of sulfate to thiosulfate was found in the uninoculated medium. Figure 46b was indeed much alike the S2p spectrum from a dried droplet of uninoculated medium. Curve fitting was not performed due to the low counts. It may be seen that sulfate reduction takes place via thiosulfate, finally yielding sulfides. In Figure 46d and f, Na_2S and MoS_2 were not separated because their binding energy values were very close. Multiple sulfur compounds were seen in the

biomass, including sulfate, thiosulfate, sulfite, organic sulfur and sulfides. As the culture growth continued, a higher proportion of sulfides appeared in the spectra, consistent with the shoulders on the low binding energy side of the Mo3d spectra in Figures 46c and 46e. The relative proportion of thiosulfate decreased. The existence of sulfite in the biomass indicated that the molybdate had interfered with the culture growth at a certain intermediate stage because sulfite was known as an intermediate product in sulfate reduction[3, 84]. The organic sulfur showed some evidence of involvement in the Mo(V) complexes, because its relative proportion decreased as molybdate content decreased from 1 to 0.1 mM. In particular, the constant charge shifting of the organic sulfur component peaks in Figures 46d and 46f differed from the variable charge shifting of the other sulfur compounds, suggesting a constant insulation of the complexes. This was consistent with the constant charge shifting in the Mo3d spectra in Figures 46c and 46e. In contrast, the charge shifting of the other sulfur compounds varied due to their distribution in the biomass.

The XPS analysis revealed the involvement of low concentrations of molybdate in culture growth. The result is different from the inhibition of high concentrations of molybdate which catalytically decomposes ATP into AMP[6-12]. Based on this analysis, a further UV spectroscopic analysis evolved .

4. 1. 3. 3. UV spectroscopic analysis of the Mo dissolution products

UV absorption spectroscopic analysis was conducted 12 hours after addition of 1 g/l Mo powder to the 3 day old culture and the supernatants of 2 hour to 5 day old cultures, respectively representing the interactions with bacterial cells and growth-dependent products. Because the dioxobridged Mo(V)-cysteine complex was known as a model for Mo-S enzymes[49], it was produced by adding molybdate to cysteine to aid in the interpretation of the UV spectroscopy. The effects of organic and inorganic products were simulated.

The absorption spectra of the interaction products of Mo with the 3 day old culture and its supernatant are compared in Figure 47, with the absorption of the Mo(V)-cysteine complex included. For both the culture and supernatant, absorption lines at 314, 396 and 468 nm were observed. The absorption at 314 nm was characteristic of the binuclear dioxobridged Mo(V)-S complex, the absorption at 396 nm characteristic of a Mo(VI) cofactor resulting from the interaction with nitrogenase, and the absorption at 468 nm characteristic of molybdenyl thiocyanate containing pentavalent molybdenum which has been utilized in colorimetric quantification of Mo[85, 86]. Theses absorption lines were neither observed without addition of Mo powder to the culture nor after addition of Mo powder to the uninoculated medium. Thus, it was deduced that

the Mo(V) complexes containing sulfur ligands resulted from the culture growth. Evidently, the presence of bacterial cells greatly increased the interaction, because the absorption lines were twice those in the supernatant. Since not all of the Mo powders in the culture was expected to interact with the bacteria, the value of absorption close to that of the interaction product of 10 mM molybdate with 10 mM cysteine raised a question regarding the quantity of Mo involved in the interaction. By XPS analysis, we determined that about one third of 10 mM molybdate was reduced to the Mo(V) by 10 mM cysteine. Therefore, the quantity of Mo involved in the interaction was about 3 to 4 mM, consistent with XPS analysis of the culture droplets following the Mo thin film exposure tests. It was also seen that the metabolic products in the supernatant of the 3 day old culture were able to lead to the interaction to a limited degree. This resulted in a further investigation of the influence of the growth-dependent metabolic products on the interaction. UV spectroscopic analysis was performed after 1 g/l Mo powder was added to the supernatants of 2 hour to 5 day old cultures and equilibrated for 12 hours. The absorption lines at 314, 396 and 468 nm are plotted versus the respective supernatants (Figure 48). It can be seen that the absorption increased with the period of culture growth during the first two days. Afterwards, the absorption decreased to the minima when the culture grew for 3 days, and slightly increased again as the

culture continued to grow. This clearly suggested that certain intermediate metabolic products enhanced the interaction, although further biochemical analysis was required in order to know the composition of these supernatants.

In this study, various organic salts existing in the culture, including lactate, acetate and propionate, were studied by adding 10 mM molybdate individually to each of the deaerated 10 mM salt solutions and the mixed solutions of them with and without the presence of 2 mM sulfite, in order to study the possible effect of organic salts on the interaction. The orange coloration (314 nm) was observed exclusively in the solution containing acetate and molybdate after cysteine was added. This result revealed that the organic salts were unable to bring about such interactions themselves even when Mo was dissolved. Considering the anodic effect of H_2S on inducing dissolution of Mo, another verification test was performed with a deaerated solution of 10 mM Na_2S and 1 g/l NH_4Cl known to form H_2S and NH_3. The absorption lines were observed 12 hours after addition of 1 g/l Mo powder, at the same wavelengths as those observed with the culture and the supernatants. The values of absorption were also close to those in the supernatants (Figure 48). Subsequent addition of cysteine in this solution, however, eliminated the absorption line at 396 nm, indicating a further reduction with an additional

amount of reducing agents provided. Because the supernatant would be saturated by NH_3 and H_2S as the culture grew and sulfate reduction continued, the Mo(V)-S products in the supernatants would result from the interaction of Mo with such products. The maxima of absorption lines seen in the supernatant of the 2 day old culture, on the other hand, clearly revealed the involvement of the intermediate products in the interaction.

4. 2 The interaction of SRB with Cr

As a major constituent element in the passive film, Cr was studied. Pure Cr coupons were exposed to SRB, and then the resultant surface changes were analyzed by XPS and DC polarizations in deaerated 0.1 M HCl. The "as polished" Cr coupons were also potentiodynamically polarized in the 3 day old culture. In addition, 0.21 g/l $Cr(OH)_3$ was added to the growth medium considering the hydration of the passive film during the exposure to SRB.

4. 2. 1. Characterization of the Cr coupons exposed to SRB by DC polarization in deaerated 0.1 M HCl and XPS analysis

4. 2. 1. 1. Potentiodynamic polarization in 0.1 M HCl

The exposure to SRB did not result in a considerable loss of the

corrosion resistance of Cr in deaerated 0.1 M HCl (Figure 49). Compared with the "as polished" coupons, the open circuit potential was decreased by about 150 ± 20 mV. There was no consistent difference in the decrease of the open circuit potential between the rinsed and unrinsed samples. Because none of these coupons was cathodically conditioned, the open circuit potential was considered the steady state of the surface oxide, Cr_2O_3, in the hydrochloric solution, and the decrease caused by the exposure was due to hydration[19]. The open circuit potential of the Cr coupons immersed in the uninoculated medium was also reduced by about 150 mV. This result indicated that sulfidation of the chromium surface was not significant. Comparing the polarization diagrams of the rinsed and unrinsed samples, it was noted that the biofilm on the unrinsed sample had a limited protective effect. The rate of the cathodic reduction was quickly reduced and the anodic interaction was also noticeably slower, whereas the rinsed samples usually showed a slightly higher rate of the interaction. However, the polarization current never exceeded 10 μA during the polarization test, indicating a good surface stability of pure Cr.

4. 2. 1. 2. XPS analysis

The Cr 2p spectra immediate after the exposure and after the

potentiostatic polarization subsequent to the exposure are given in Figures 50a and 50b respectively, obtained from the surfaces of the rinsed samples at TOA of 20°. The Cr2p spectra from the surfaces of the control samples at these two stages are given in Figures 50c and 50d to aid in comparison. The biospecies covered the surfaces of the unrinsed Cr coupons so that no Cr signals were detectable immediately after the exposure.

It was noted that a stronger degree of hydration took placed in the presence of the bacteria, associated with formation of a small amount of hexavalent chromium species (Figure 50a). As a result, the relative proportion of Cr_2O_3 was reduced, and metallic Cr in the substrate was barely visible. Sulfidation was negligible, consistent with the low polarization current in the potentiodynamic polarization diagrams. Upon the potentiostatic polarization, the outer layer of $Cr(OH)_3$ was dissolved in the hydrochloric solution to a limited extent so that the relative proportions of Cr_2O_3 and metallic Cr in the spectra were increased. The relative proportions of the hexavalent chromium species were also slightly increased, indicating a pathway of dissolution of $Cr(OH)_3$. In contrast, the surfaces of the control samples were far less hydrated so that a higher relative proportion of metallic Cr from the substrate was seen. The formation of the hexavalent chromium was negligible because their proportions

in the spectra were usually also seen on the "as polished" coupons. During the potentiostatic polarization, a limited dissolution of the thin $Cr(OH)_3$ layer resulted in a marked increase of the relative proportion of metallic Cr from the substrate while the hexavalent chromium became less. This formed a strong contrast to the bacterial activation of the hexavalent chromium.

By increasing the take-off angle of the photoelectrons, the information about the inner surface region is revealed. For the samples potentiostatically polarized subsequent to the exposure, it was noted that the limited dissolution of $Cr(OH)_3$ took place so that more metallic Cr was seen from the inner region, while a lower relative proportion of Cr_2O_3 in the inner region indicated a possibility of nonuniform hydration (Figure 51).

The XPS analysis of the potentiostatically polarized Cr coupons with the biofilm demonstrated that the outer region of the unrinsed sample surface contained more hexavalent chromium than the rinsed samples, and $Cr(OH)_3$ was the major Cr compound on the surface so that the relative proportions of Cr_2O_3 and metallic Cr were very low (Figure 52). A small amount of Cr_2S_3 was also detected, indicating that sulfidation could happen when the chromium compounds were activated into soluble species, such as activation of $Cr(OH)_3$ to the hexavalent chromium. Sulfidation of soluble chromium has been found

by this group[92]. In the inner layers, more metallic Cr appeared, while the proportion of $Cr(OH)_3$ was greatly decreased. This spectrum, on one hand, indicated a protection of the biofilm, consistent with the polarization diagram in Figure 49, on the other hand, it indicated a thin layer of hydrated chromium.

4. 2. 2. Potentiodynamic polarization of "as polished" Cr coupons in the stationary stage culture

Since the characterization of the resultant surface changes after the exposure did not provide adequate information about the interaction of SRB with Cr, potentiodynamic polarization of "as polished" Cr coupons was conducted in the 3 day old culture, and compared with the control test in the uninoculated medium (Figure 53). A decrease of the open circuit potential in the culture indicated the influence of bacterial sulfides on the surface stability. In addition, both of the cathodic and anodic interactions were accelerated compared with the control test, but the presence of the bacteria was unable to cause a marked decrease of the corrosion resistance.

4. 2. 3. Addition of $Cr(OH)_3$ to the growth medium

In order to confirm the bacterial activation of $Cr(OH)_3$ to hexavalent chromium and sulfidation, 0.21 g/l $Cr(OH)_3$ was added to the growth medium.

The culture growth and sulfate reduction were then determined, and the centrifuged biomass analyzed by XPS.

A limited inhibition on culture growth and sulfate reduction was observed upon adding $Cr(OH)_3$ to the growth medium (Table 13). Measured by the turbidity, the culture growth was found to have slightly delayed after incubation for 2 days, and hence the residual sulfate was at least 50 ppm more than that in the normal culture containing no Cr. After 5 days, the residual sulfate was further reduced but the turbidity was still slightly higher, indicating that the nutrients were not completely consumed because the initial growth was slower. However, this effect was not so strong as adding Mo compounds to the growth medium, because $Cr(OH)_3$ was more stable at neutral pH[76]. This experiment, however, demonstrated that formation of chromate was possible as an intermediate process of dissolution[86].

XPS analysis of the centrifuged biomass showed that multiple chromium compounds were formed in the culture, including Cr_2S_3, Cr_2O_3, $Cr(OH)_3$, CrO_3 and CrO_4^{2-} (Figure 54). In this analysis, it was observed that sulfidation of $Cr(OH)_3$ increased with the culture growth so that the relative proportion of Cr_2S_3 in the biomass of the 5 day old culture was markedly higher than that in the 2 day old culture. The relative proportion of Cr_2O_3 showed the same

tendency. However, the proportions of the hexavalent chromium species were almost equal. This indicated that the hexavalent chromium species were the intermediate product of dissolution which was subsequently sulfidized, and/or reduced to trivalent states, consistent with the general knowledge of the reduction of hexavalent chromium by SRB[71-73]. A consistency was shown by the S2p spectra in which the organic sulfur species associated with sulfur-containing proteins were dominant (Figure 54b).

4. 3. The interaction of SRB with Ni

The study of the interaction of SRB with Ni consisted of two parts: (1) the analysis of the surface changes of the Ni coupons following the exposure to SRB by XPS and DC polarization in deaerated 0.1 M HCl; (2) potentiodynamic polarization tests of the "as polished" Ni coupons in the 3 day old culture.

4. 3. 1. Characterization of the Ni coupons exposed to SRB by DC polarization in deaerated 0.1 M HCl and XPS analysis

In accordance with the other alloying elements, the surface changes of the Ni coupons after the 5 day exposure to SRB were determined by the potentiodynamic polarization tests in deaerated 0.1 M HCl and XPS analysis immediate after the exposure and at the passive range in the hydrochloric

solution. The overpotential for the potentiostatic polarization was decreased by 50 mV (-210 mV_{SCE}), because the passive range of Ni in the hydrochloric solution was narrow and the open circuit potential was lower.

4. 3. 1. 1. Potentiodynamic polarization in 0.1 M HCl

The potentiodynamic polarization diagrams of the SRB exposed Ni coupons with and without the biofilm are given in Figure 55, with the polarization diagrams of the control samples included. In this study, it was found that the open circuit potential of Ni in deaerated 0.1 M HCl was decreased by about 100 ± 10 mV. This was less than expected knowing that Ni was vulnerable to sulfidation, because NiS had largely decomposed before the polarization[75]. The open circuit potential of the control samples was slightly increased due to oxidation (Figure 55)[19]. The presence of biofilm did not show obvious influence on the potentiodynamic performance. In the polarization diagrams, it was noted that the corrosion potential of the SRB exposed samples was lower than the actual open circuit potential, because the cathodic reduction removed the outer layer of the surface products and decomposition of NiS prior to the polarization test reduced the contribution of H_2S to the current of cathodic hydrogen evolution. The anodic dissolution of the SRB-exposed

samples was faster, and gradually decreased. It was noted that the pitting potentials of both the SRB exposed and control samples were almost equal. This was because Ni was not passive in the hydrochloric solution. As a result, the potential of potentiostatic polarization was reduced to -210 mV_{SCE}, just below the transpassive transition.

4. 3. 1. 2. XPS analysis

The Ni2p spectra obtained immediately after the exposure to SRB and after the anodic polarization treatment are given in Figure 56, with the variable angle spectra showing the depth variation.

The Ni species on the surfaces of the SRB-exposed samples were mainly $Ni(OH)_2$, with a small amount of NiS. Because Ni is commonly known for its susceptibility to sulfidation, the extremely low proportion of NiS in the spectra indicates its instability as a pure compound. Upon the subsequent potentiostatic polarization, however, the outer layer of $Ni(OH)_2$ was dissolved, and then the underlying NiS was revealed. This explained the apparently lower corrosion potential than the open circuit potential in Figure 55. It was seen that the relative proportion of NiS in the outer surface region was approximate to that in the inner region, indicating a marked depth of sulfidation by the

bacterial sulfate reduction. In Figures 56c and d, the relative proportions of metallic Ni in the outer and inner region were very close, this indicated that the interaction with SRB was uneven on the sample surface.

4. 3. 2. Potentiodynamic polarization of "as polished" Ni coupons in the stationary stage culture

In addition to the analysis above, the interaction of Ni with SRB was determined by potentiodynamic polarization in the 3 day old culture using the "as polished" coupons (Figure 57). Compared with the control test in the uninoculated medium, the open circuit potential was decreased by about 300 mV, indicating the activity of Ni in the culture. The cathodic slope was also much higher, representing the additional contribution of the sulfides to the cathodic hydrogen evolution. The anodic dissolution was increased by one order of magnitude, indicating that passivation was almost impossible. In the uninoculated medium, however, the initial rapid hydrogen evolution was soon decelerated. The anodic dissolution was also rapidly reduced and the passive film existed in a wide range of potential. This result well demonstrated a strong interaction of Ni with the culture, in which sulfides and H_2S were able to cause severe sulfidation while metabolic products and proteins would also enhance the interaction because Ni was involved in enzymes of SRB[88].

4. 4. Characterizations of the Fe coupons exposed to SRB by DC polarization in deaerated 0.1 M HCl and XPS analysis

Finally, the resultant surface changes of pure Fe coupons due to the exposure to SRB were analyzed by the DC polarization techniques and XPS analysis. Because pure Fe is not corrosion resistant in the hydrochloric solution, the XPS analysis in this section will only introduce the surface changes of the Fe coupons immediately after the exposure.

4. 4. 1. Potentiodynamic polarization in 0.1 M HCl

The polarization diagrams did not show considerable differences between the SRB-exposed coupons and the control samples (Figure 58). The polarization diagrams were also similar to that of an "as polished" coupon after cathodic treatment[19], indicating that the surface iron oxides were not protective in 0.1 M HCl. Compared with the control samples, the SRB-exposed samples revealed a lesser surface stability by a small decrease in open circuit potential.

4. 4. 2. XPS analysis

XPS analysis was conducted immediately after the exposure, with and without the presence of the biofilm. The iron compounds were seen in the

biofilm because of its high reactivity with bacteria[89]. The Fe2p spectra from the rinsed SRB samples are shown in Figures 59a and 59b, and from the unrinsed samples in Figures 59c and 59d, at TOA's of 20° and 50°.

Without the biofilm, the outer surface region of the Fe coupons were seen to consist of a dominant proportion of ferric oxide, a large proportion of ferrous oxide and some hydroxide, in addition to a smaller amount of various types of iron sulfides including FeS, FeS_2 and $Fe_{1-x}S$. In the inner surface region, more ferric oxide could be seen, whereas the amount of ferrous iron was reduced. More iron sulfides were also detected, indicating a certain depth of sulfidation. In fact, the interaction had apparently proceeded into a deep region so that the metallic Fe was hardly visible (Figure 59b). In the presence of the biofilm, ferrous iron became dominant, while the amount of iron hydroxide was also greatly increased in the outer region. However, the amount of the iron sulfides was less, and only FeS and $Fe_{1-x}S$ were detected. More ferrous oxide was seen in the inner region, but the amount of ferric oxide and hydroxide was markedly decreased. In contrast to the outer layer, the amount of the iron sulfides was considerably increased, indicating the sulfidation of the substratum.

IV. Discussion

1. Passivity of the SRB-exposed steel samples characterized by the DC polarization tests in the deaerated 0.1 M HCl and XPS analysis

1. 1. 304 SS

In this study, it may be seen that the bacterially-induced sulfide formation can cause a marked loss of the passivity. The polarization diagrams of the SRB-exposed samples in deaerated 0.1 M HCl showed that the polarization current could increase by two orders of magnitude compared with the "as polished" coupon, in addition to a significant decrease of the open circuit potential (Figure 3). The increase of cathodic slope indicated an additional current to hydrogen evolution: the surface sulfides caused hydrogen cathodic depolarization yielding H_2S because of the low pH of the electrolyte[90]. This is consistent with the observations made with mild steels, where non-uniformly formed surface sulfide increased the corrosion rate by accelerating cathodic reaction[35]. The acceleration of anodic reaction, on the other hand, suggested that the surface sulfides were able to damage the passive films of austenitic stainless steels and increase the rate of the interaction as both unstable species in the hydrochloric solution and good electron conductors.

XPS analysis immediately after the exposure and after the potentiostatic polarization subsequent to the exposure provided an explanation about the loss of passivity. Formation of the sulfides greatly reduced the surface stability so that the passivity of a normal surface was considerably deteriorated. The sulfides appeared to be in a complex form, as indicated by the stability of some types of the sulfides under x-ray radiation which would otherwise decompose as pure compounds, such as FeS and NiS. Additionally, the deterioration of the passive film was also revealed by the formation of active components, such as Fe^{2+}, Ni^{2+} and Cr^{6+}, which were thermodynamically unfavorable[76-78]. These products indicated an additional bacterial influence other than sulfidation, which could be an intermediate stage in bacterial removal of these metal ions from the steel surface. For instance, Cr_2O_3 comprising the main kinetic barrier of the passive film would not be dissolved unless it was hydrated and further oxidized to the hexavalent state. This is different from the common knowledge about the trivalent chromium reduced by SRB[72, 73]. Biotic and abiotic simulation using anaerobic H_2S-containing solutions with and without cysteine provided further results consistent with this observation, which clearly demonstrated the cysteine-enhanced hydration of the passive film and the formation of the hexavalent chromium. Investigating the specific interactions of SRB with the alloying elements, it was also found that the anodic effect of sulfides was able

to induce dissolution of Mo via formation of molybdate, which was particularly enhanced in the presence of sulfur-containing proteins. Sulfidation of $Cr(OH)_3$ provided strong evidence of the susceptibility of the passive film to the bacterial sulfate reduction. In this study, the bacterially activated formation of the thermodynamically unfavorable products was enhanced by subsequent polarization in the hydrochloric solution at a potential where the "as polished" coupons normally became passive. The test magnified the bacterial activation because, otherwise, these products should not have been formed at the passive potential (Figure 14).

The extent of the loss of the passivity is proportional to the depth variation of the interaction, as shown in variable angle XPS analysis. During the potentiostatic polarization at -160 mV_{SCE} in the hydrochloric solution, the polarization current increased as the inner region of the surface was more sulfidized and hydrated than the outer region. Pitting was observed when undercutting took place, which thereafter further increased the extent of hydration of the inner layers of the surface film (Figures 20 and 21). Many factors may influence the degree of surface sulfidation, hydration and loss of passivity, such as, the structural consistency, sensitization, composition uniformity of the passive film, bacterial attachment to the steel substrata and

the sites of bacterial sulfate reduction and removal of metal ions. A schematic in Figure 60 qualitatively demonstrates the undercutting effect associated with the surface sulfidation and hydration. In abiotic corrosion, it is known that the passive film of a ternary austenitic stainless steel consists of an outermost $Cr(OH)_3$ layer and an intermediate Cr_2O_3 layer, covering the steel substrate with metallic Ni enriching the interface (Figure 60a)[20]. In the presence of SRB, however, the integrity of the passive film is damaged by the sulfides and bacterial uptake of the alloying elements in the order of their binding ability. Because the sulfides are better electron conductors, more readily involved in hydrogen evolution and structurally more permeable than the dense chromium (III) hydroxide and oxide, they become the sites for further interaction, causing concentration cells and assisting transport of ingressing anions, such as Cl^- and OH^-. Therefore, hydration of the passive film will result, and thereafter dissolution of the stable compounds may be induced given additional activation. In particular, the sulfides may first form in a local area where the passive Cr_2O_3 is deficient and thus develop into a certain depth rendering a greater proportion in the inner layer. Undercutting of the passive film and consequent pitting are dependent upon the extent of surface sulfidation, hydration and their variations with the depth. The plots in Figures 20 and 21 may be interpreted as follows: initiation of pitting results from undercutting of

the passive film associated with electron transferring in a highly localized volume which yields a high current density. Once the sulfides were dissolved, the substrate could be exposed, this may be one of the reasons for the appearance of the metallic Fe and Ni on the SRB-exposed coupons immediately after the exposure. In addition, the bacterial uptake may also cause migration of metallic Fe and Ni out of the interface. Thus, the conventional model of the passive film in Figure 60a is not applicable for the nonuniform bacterial interaction. This leads to the assumptions for derivation of equations (30) and (31) in describing the nonuniform sulfidation in depth, and the fractional areas of iron and nickel sulfides estimated using these formulae yielded a good consistency with the atomic percentages calculated (Table 9 and Figure 11).

1. 2. 317L SS

The formation of the sulfides on 317L SS caused a certain degree of the loss of passivity during the exposure to SRB, as shown by the decrease of OCP and the lower pitting potential in the cyclic polarization diagrams (Figure 4). Both the cathodic and anodic reactions proceeded noticeably faster than the "as polished" coupons, particularly when the samples were rinsed after the exposure. However, the degree of loss of passivity was far less compared with

the SRB-exposed 304 SS containing far less Mo. The unrinsed samples were able to maintain a low passive current close to the value of the "as polished" samples up to 0 mV_{SCE}, indicating some protection by the biofilm. Because the contents of Cr and Ni in 317L SS were comparable to those in 304 SS, the limited passivity of 317L SS was attributed to its Mo content. The results of the cyclic polarization suggested two different processes of the breakdown of passivity for the samples with and without the biofilm: crevice corrosion took place in the presence of the biofilm, whereas pitting was initiated when the biofilm was removed. Crevice corrosion associated with the biofilm was probably due to the exposure of the steel substratum in local areas resulting from dissolution of the soluble salts trapped in the biofilm and thereby generation of concentration cells.

XPS analysis provided an understanding for the limited passivity remained after the exposure. The exposure to SRB resulted in the formation of the sulfides of the constituent alloying elements mainly in the outer surface region (Figures 11, and 22 to 25). Upon anodic polarization in 0.1 M HCl, the sulfides were evenly dissolved so that the inner region was seen to contain a much smaller amount of them (Figures 26 to 29). Contrary to the bacterial activation of the hexavalent chromium observed on the surface of 304 SS, the

hexavalent chromium species formed on the surfaces of the 317L SS samples were dissolved and no further formation was induced by the subsequent polarization in the hydrochloric solution. No evidences of nonuniform islanding of the products and undercutting of the passive film were observed. The major surface species able to increase the passivity were molybdate and the SRB-induced Mo^{5+} compound only sparingly soluble in the hydrochloric solution. Therefore, the interaction of the ingressing chloride and hydroxide mainly took place in the outer layers, yielding a uniform hydration of the passive film in the outer layer. Although the passive film was very thin, its protection was clear.

It is well known that molybdate formed on the surface of Mo-bearing stainless steels increases the pitting resistance by repelling the ingressing anions[17-20]. In abiotic corrosion, molybdate was formed as the outermost layer of the passive film on the Mo-bearing stainless steels, filling the active sites and inhibiting ingressing chloride and egressing cations except proton. As a result, an intermediate chromium (III) hydroxide layer underneath the outermost molybdate may be deprotonated, and thereafter the chromium (III) oxide layer under the hydroxide is stabilized and enhanced due to the release of the protons. Figure 61a qualitatively demonstrates the bipolar effect of molybdate[14]. In this study, the unique protection effect of Mo gave rise to an interesting

issue regarding the interaction of Mo with the bacteria. Therefore, the interaction of SRB with Mo was specifically studied in order to understand its contribution to the passivity.

During the exposure of the 317L SS coupons to SRB, molybdate formation took place due to the anodic effect of the sulfides resulting from the bacterial sulfate reduction. The molybdate, on the other hand, was able to reduce the microbial activity of SRB and inhibit sulfate reduction by forming the pentavalent Mo-S complexes as described. Therefore, the interaction of SRB with the steel substratum and bacterially induced sulfidation were confined within the outer surface region. The surface depletion of Mo during the exposure provided evidence of the bacterial uptake of Mo, rendering the Mo^{5+} product insoluble in 0.1 M HCl. The stability of these Mo(V)-S complexes in the hydrochloric solution was well demonstrated by the Mo^{5+} component and the S2s of the organic sulfur peaks in the neighborhood in the Mo3d spectra from both of the rinsed and unrinsed samples after the potentiostatic polarization (Figures 31 and 33). Although the remaining biofilm was found to be so thin that the metallic elements were observed in XPS analysis after the potentiostatic polarization, its protection was obvious. Furthermore, the formation of molybdate was enhanced in the passive range in

the hydrochloric solution. Therefore, the SRB-exposed samples of 317L SS exhibited a limited passivity. Figure 61b schematically illustrates the bacterially induced change of the passivity, in contrast to the abiotic corrosion.

2. The interaction SRB with the constituent alloying elements

2. 1. The interaction of SRB with Mo

2. 1. 1. Characterization of the SRB-exposed Mo coupons

The contribution of Mo to the passivity of 317L SS was confirmed by potentiodynamic polarization of the SRB-exposed pure Mo samples in 0.1 M HCl, particularly, protective effect of the Mo-containing biofilm was clearly exhibited (Figure 37). Further XPS analysis demonstrated the surface changes at the different stages of the polarization test.

XPS analysis indicated that the formation of molybdate exclusively took place in the presence of SRB (Figure 38). This raised an interesting issue about the interaction of SRB with low concentrations of molybdate, which also arose from the results of the exposure of 317L SS to the bacteria. The sulfidation of Mo suggested that the passivity normally contributed by the stable MoO_2 would be decreased in SRB-containing environments. This explained the loss of

passivity when the biofilm was removed after the exposure (Figure 37). Because the surface molybdate had a repelling effect on the ingressing chloride, the rinsed SRB-exposed coupons retained a limited passivity. The formation of the Mo(V) complexes resulted from the interaction with the bacteria, which became more apparent when the SRB-exposed samples were subsequently polarized at -160 mV_{SCE} in deaerated 0.1 M HCl. Although immersion in the uninoculated medium also resulted in a certain amount of pentavalent Mo, it was dissolved upon the subsequent potentiostatic polarization. This difference between the biotic and abiotic Mo^{5+} species was consistent with the observations made with 317L SS (Figure 25).

The Mo^{5+} species incorporated in the biofilm became more pronounced in the XPS analysis following the potentiostatic polarization of the unrinsed SRB-exposed samples in the hydrochloric solution, which explained the limited protection of the biofilm during the polarization tests (Figure 39). The outermost layer was covered by the biospecies, including carbon, oxygen and organic sulfur. Because no sulfide was present in the biomass, the spectrum indicated that the interaction of Mo with SRB had an inhibitive effect on the bacterial sulfate reduction. In addition, this biofilm had an insulating nature, as indicated by the charge shifting of the S2s spectra (Figure 39a). Beneath the

outermost layer of the biofilm, a significant proportion of the pentavalent Mo was observed, which developed into a deeper region (Figure 39b and c). The appearance of metallic Mo from the substrate, on the other hand, suggested that the remaining biofilm was very thin after dissolution of the soluble species during the polarization tests. Namely, protection was provided by the insoluble Mo-S complexes, consistent with the protective effect of the Mo(V)-containing biofilm on 317L SS.

2. 1. 2. The interaction of SRB with Mo shown in potentiodynamic polarization in the stationary stage culture

Potentiodynamic polarization of the "as polished" Mo coupons in the 3 day old culture exhibited some unique features about the interaction of SRB with Mo, such as the increase of the open circuit potential and the slow anodic interaction. The cyclic polarization of "as polished" Mo coupons further revealed the reduction of the bacterial activity by the dissolved Mo. It was seen that the initial anodic dissolution of Mo took place at a higher rate, but was soon decelerated as more Mo was dissolved (Figure 41). The significance of this result lies in that it indicates a difference in the chemistry of the interaction of bacteria with a solid surface from the chemistry of the interaction with soluble metal ions. A careful comparison should be made by differentiating the

interactions among the bacteria themselves, the interaction between the bacteria with the dissolution products of a metal and the interaction between the bacteria and the solid metal surface.

2. 1. 3. The interaction of SRB with the dissolved Mo from the Mo thin films and Mo powders

A strong affinity of SRB for Mo was revealed by exposure of the Mo thin films. A considerable amount of Mo was dissolved, delaying the culture growth and yielding the Mo(V)-S complexes. The role of sulfur in promoting formation and stabilization of Mo(V) is well known[44, 49, 80]. In this study, the involvement of sulfur in the Mo(V) complexes was first indicated by the residual sulfate measurement 2 days after the Mo thin films were exposed to the culture, because the result was not consistent to the rate of culture growth and thereby indicated possible existence of large molecular weight sulfur compounds (Table 12). Because the dissolution of Mo was slower than the culture growth, the inhibitive effect of dissolved Mo was indicated by a significant delay in the growth of culture. However, the culture continued to grow with available nutrients so that more sulfate was reduced to sulfide as the culture was incubated for a longer period (Table 12 and Figure 47). Addition of Mo powder to the medium helped understand the result. It may be seen that

Mo dissolution did not take place until the inoculated medium grew to a certain degree. As a result, sulfate reduction was completed with Mo powders as heterogeneous sites for precipitation of sulfide. Upon addition of Mo powder to the culture previously growing for 2 days, however, dissolution of Mo took place faster so that the dissolved Mo was sufficient to interfere with the culture growth and interacted with the sulfur-containing species. The possibility of formation of the large molecular weight sulfur compounds was again indicated by the residual sulfate weight proportion (ppm) which was obviously higher than that in a normal culture without Mo. By the end of the 5 day growth period, more sulfide was formed, the ligands in the complexes were probably partially replaced by oxygen or nitrogen.

Determination of culture growth and sulfate reduction in the cultures containing different ratios of sulfate to molybdate provided further information. Because molybdate interacted with the inoculum upon inoculation, a low concentration was able to affect the culture growth drastically. As a result, the formation of the large molecular weight Mo(V)-S complexes became pronounced. In particular, the formation of the large molecular weight complex was increased with the culture growth, suggesting that the interaction took place as the culture grew and sulfate was involved in the bacterial metabolism

(Figures 43 and 44). The interaction would be most likely between molybdate and the sulfur-containing extracellular proteins, such as APS, because the sulfur reduction by SRB was a dissimilatory process in which sulfate simply participated in the electron exchange as an electron acceptor[3]. Based on this observation, it may be concluded that the dissolution of Mo during the exposure of Mo thin films and Mo powders to the culture took place via the formation of molybdate, leading to the Mo-S complexes.

A consistency with the discussion may be seen from the results of XPS analysis (Figure 46). Molybdate reduction resulted from the culture growth when the initial content of molybdate was not sufficient to completely inhibit. The Mo(V) complexes were the products. Evidence of the involvement of sulfur in the Mo(V) complexes was also shown by the decrease of the relative proportion of the organic sulfur in the S2p spectra with the decrease of molybdate. In addition, the existence of sulfite in the biomass also indicated that the interference of low concentrations of molybdate with the culture growth took place at an intermediate stage so that a certain intermediate products, such as sulfite, were able to remain in the biomass. It became evident that the low concentrations of molybdate were able to inhibit the growth of SRB by forming the Mo(V)-S complexes with the intermediate sulfur

containing species.

The sulfur containing intermediate extracellular proteins were most likely the reducing agents in reduction of molybdate. In dissimilatory sulfate reduction by SRB, sulfate entering the bacterial cells would be activated into APS by extracellular ATP at the first stage of sulfate reduction, subsequently formed sulfite and/or thiosulfate and finally reduced to sulfide through a series of enzymatic catalysis. The sulfide would be released to the external environment. Although residual cysteine may be found in cytochrome c and enzyme systems, almost all of the sulfur in the intermediate sulfur-containing proteins should eventually be released as sulfide[3, 84, 91]. Without protein catalysts, the formation of the Mo(V)-S complexes with inorganic sulfur would be thermodynamically difficult. By the UV spectroscopic analysis, it was shown that the organic salts were unable to induce the Mo(V)-S complexes. However, a synthetic solution of 10 mM Na_2S, 1 g/l Mo powder and 1 g/l NH_4Cl was able to induce the Mo(V)-S products to a limited degree, whereas the presence of biocells greatly enhanced the interaction (Figures 47 and 48). Additionally, the enhanced interaction of the 3 day old culture with Mo powder may also be contributed by the increased dissolution of Mo due to the bacterial affinity. Furthermore, the formation of the Mo(V)-S complexes was not simply dependent on the amount of sulfide resulting from the sulfate reduction. Upon

adding Mo powders to the supernatants of the cultures growing for different periods, the maxima of absorption were observed in the supernatant of the 2 day old culture in which the sulfate reduction was not yet complete, whereas the supernatant of the 3 day old culture showed the minima of absorption after Mo was added. We have previously determined that the culture reached the stationary stage after incubation for 3 days[52]. The result indicated that the interaction took place to a greater degree before sulfate was totally reduced to sulfide, when involved in the extracellular proteins. As a ligand promoting the formation of the Mo(V) and stabilizing it, sulfur showed a variable degree of influence dependent on its form. The sulfur bonds in proteins showed a particularly strong effect, as demonstrated by the Mo(V)-cysteine complex.

2. 2. The interaction of SRB with Cr

2. 2. 1. DC polarization tests and XPS analysis

The exposure of the pure Cr coupons to SRB did not result in obvious changes of the passivity (Figure 49). For both of the rinsed and unrinsed samples, the decrease of the open circuit potential in 0.1 M HCl was an indication of the surface hydration. Whereas, the open circuit potential of the "as polished" coupons was the steady state of Cr_2O_3 in 0.1 M HCl. The biofilm

exhibited certain protection, and in particular, it markedly reduced the rate of the anodic dissolution, indicating a certain insulation.

XPS analysis provided further information about the surface changes (Figure 50). The hydration of the surface was found to have taken place during the exposure, consistent with the drop of open circuit potential observed in the polarization tests in 0.1 M HCl. The appearance of the hexavalent chromium indicated the bacterial influence on the surface. However, no sulfidation was observed if the samples were rinsed. Once polarized in 0.1 M HCl, the hydrated surface was susceptible to dissolution due to the low pH of the hydrochloric solution. Therefore, the relative proportions of the Cr_2O_3 and metallic Cr were increased. The appearance of a noticeable amount of metallic Cr indicated that the hydrated layer was rather thin, because the underlayer of Cr_2O_3 was stable in the hydrochloric solution. Furthermore, the relative proportion of the hexavalent Cr was increased, suggesting a pathway of dissolution of $Cr(OH)_3$, consistent with the observations made with 304 SS. With the biofilm, the SRB-exposed Cr coupons confirmed the hydration and formation of the hexavalent chromium arising from the exposure, because their relative proportions were significantly increased. In particular, the small amount of Cr_2S_3 on the surface suggested that the bacterial sulfidation took place with

the soluble chromium species[92]. This result was a further evidence of the formation of the hexavalent chromium, because, otherwise, $Cr(OH)_3$ should not have been sulfidized as an insoluble compound in a neutral solution.

2. 2. 2. The potentiodynamic polarization of "as polished" Cr coupons in the stationary stage culture and the influence of $Cr(OH)_3$ on the culture growth

The decrease of the surface stability of Cr in SRB was exhibited by the decrease in open circuit potential and accelerated cathodic and anodic interactions compared with the control test (Figure 53). But the corrosion resistance was not considerably reduced. This was because chromium was far less vulnerable to sulfidation than the other metal elements in this study. In particular, the surface compounds of the Cr coupons were comprised of stable Cr_2O_3 and $Cr(OH)_3$, protecting the metallic substrate. Therefore, the decrease of the open circuit potential in the culture was, in a sense, a reflection of a change of the interfacial energy due to the presence of the sulfides.

The formation of the hexavalent chromium species during the exposure of the steel and Cr coupons to SRB was verified by addition of a low concentration of $Cr(OH)_3$ to the growth medium. As demonstrated by the obvious interference with the culture growth and sulfate reduction, formation of

the hexavalent chromium was deduced, because, otherwise, the trivalent chromium would remain stable in the culture[87]. Because chromate has a very strong inhibitive effect on sulfate reduction which was a fast process in the culture growth, this result may be considered as a pathway of dissolution of $Cr(OH)_3$ after the culture have reached a certain activity. Because $Cr(OH)_3$ is highly stable in neutral pH, the limited inhibition indicated that the amount of the hexavalent chromium formed during the culture growth was very low, and could have been subsequently sulfidized.

In XPS analysis, it was noted that Cr_2S_3 resulted from the culture growth since more Cr_2S_3 was formed as the culture grew (Figure 54). This indicated that the passive film on the steel surfaces comprised of Cr_2O_3 could be sulfidized once hydrated. This explained the severe loss of the passivity of 304 SS. The formation of Cr_2S_3 with the culture growth indicates that the stability of $Cr(OH)_3$ may be deteriorated in the presence of SRB, and the hexavalent chromium was the intermediate products of dissolution because their amount appeared to be independent of the growth period. Furthermore, the incomplete sulfate reduction was also shown in the S2p spectra, where the organic sulfur species were dominant. It is known that a low concentration of chromate may form complexes with the extracellular proteins[87].

2. 3. The interaction of SRB with Ni

The decrease of the surface stability of Ni coupons due to the exposure was shown by the subsequent potentiodynamic polarization in 0.1 M HCl (Figure 55). Because NiS in the outer region had been decomposed before the polarization tests, the hydrogen cathodic depolarization was not exhibited. In this test, the anodic rate was very fast, because pure Ni was not passive in the hydrochloric solution.

XPS analysis of the SRB-exposed Ni coupons explained the surface changes shown in the polarization diagrams. The Ni coupons were found to have been covered by the hydroxide resulting from decomposition of NiS. Therefore, the polarization diagrams in 0.1 M HCl did not reveal a significant cathodic hydrogen depolarization. Once anodically polarized at -210 mV_{SCE} in the hydrochloric solution, the outer layer of $Ni(OH)_2$ was dissolved and NiS in the inner region was revealed. Because of the rapid anodic dissolution at this potential, the existence of NiS independent of the sampling depth indicated that the sulfidation of Ni had developed into a certain depth. Furthermore, the metallic Ni was also detected, independent of the take-off angles used in the analysis, suggesting a nonuniform interaction of SRB with Ni. The metal substratum would be exposed in certain areas once the sulfides were dissolved,

which confirmed the assumptions made for evaluation of the depth-dependent interactions [eqns (30) and (31)].

Finally, the interaction of SRB with Ni was studied by potentiodynamic polarization in the stationary stage culture. The marked decrease of the open circuit potential, compared with the control test, exhibited the susceptibility of Ni to the bacterial interactions[88].

2. 4. The interaction of SRB with Fe

The DC polarization tests in 0.1 M HCl following the exposure to SRB were unable to effectively analyze the surface changes of Fe because it was not corrosion resistant in the hydrochloric solution.

XPS analysis after the exposure provided the information about the interaction. A strong bacterial uptake of Fe was shown in this study, indicating the bacterial affinity[89]. As a result, the surface was more oxidized, and more sulfides were formed in the biofilm. Furthermore, the interaction was not uniform so that undercutting took place. The absence of metallic Fe indicated a considerable depth of the interaction into the substratum (Figure 59).

V. Conclusion

1. 304 SS

SRB influenced the passivity of 304 SS in two ways, direct sulfide formation and additional activation. The sulfides appeared to be in a complex form, including FeS, FeS_2, $Fe_{1-x}S$, Cr_2S_3 and NiS, nonuniformly formed at the sites where the passive film was activated and developed into the sublayer, rendering islanding and undercutting. The degree of the loss of passivity was proportional to the vertical variation of the interaction in the surface film. The additional bacterial activation was featured with initiation of hexavalent chromium that was subsequently enhanced by polarization in 0.1 M HCl.

2. 317L SS

The sulfides were also formed on the surface of 317L SS. However, the interaction took placed more evenly in the outer surface layers. The bacterial activation was not observed by polarization in 0.1 M HCl, although the formation of the hexavalent chromium also took place during the exposure. The surface passivity was retained by hydrated chromium (III). Mo played the major role in enhancing the passivity. A certain amount of molybdate was

formed on the surface of 317L SS and reduced the bacterial activity by involving in the enzymatic reactions with the sulfur-containing extracellular proteins. The biofilm containing the interaction product, Mo^{5+}, provided a protection for the SRB-exposed 317L SS in 0.1 M HCl due to its insolubility and insulating nature. On the other hand, the involvement of Mo in the biofilm provided some information about the bonding mechanism of biofilm to Mo-bearing steels.

FUTURE WORK

1. Expanding the investigation to high Mo content stainless steels, such as AL6X and AL6XN;

2. Investigation of the role of nitrogen in the passivity behavior of nitrogen bearing steels;

3. Investigation of MIC resistance of martensitic stainless steels and duplex steels, weldment structures;

4. Investigation of the interactions of SRB with other alloys, such as Cu, Cu-Ni alloys and Ti.

5. Investigation of the modification of sulfur-containing proteins on the surfaces of the alloys and its influence on the electrochemical process of corrosion in the presence of oxygen, chloride and various types of sulfides including H_2S.

REFERENCES

1. M. G. Fontana, in "Corrosion Engineering" McGraw-Hill Book Company, New York, USA, 392 (3rd edn., 1987).

2. B. J. Little, P. A. Wagner and W. G. Characklis et al, in "Biofilms", W. G. Characklis and K. G. Marshall (eds), Wiley Interscience, John Wiley and Sons, Inc., New York, USA, 635 (1990).

3. J. R. Postgate, in "Sulphate-Reducing Bacteria", Cambridge University Press, Cambridge, UK, 82 (2nd edn., 1984).

4. H. L. Drake and J. M. Akagi, J. Bact., **132**, 139 (1977).

5. H. D. Peck, Jr, in "The Sulfate-Reducing Bacteria: Contemporary Perspectives", Brock/Springer Series in Contemporary Bioscience, Springer-Verlag, New York, USA, 60 (1993).

6. B. F. Taylor, and R. S. Oremland, Current Microbiology, 3, 101 (1979).

7. J. R. Postgate, Nature, **164**, 670 (1949).

8. I. M. Banat and D. B. Nedwell, Estuarine, Coastal and Shelf Science, **18**, 361 (1984).

9. J. S. Lou, X. Campaignolle, J. Bullen, M. W. Mittelman, D. C. White and J. F. Zibrida, Corrosion/92, Paper No. 186, NACE, Houston, USA (1992).

10. H. D. Peck, Proceedings of National Academic Science USA, **45**, 701 (1959).

11. J. M. Akagi and L. L Campbell, J. Bacteriology, **84**, 1194 (1962).

12. A. B. Ray and P. A. Trudinger, in "The Biochemistry of Inorganic Compound of Sulfur", Cambridge, Cambridge University Press, UK (1970).

13. J. R. Pilbrow, in "Transition Ion Electron Paramagnetic Resonance", Oxford

Science Publications, Clarendon Press, Oxford, 521 (1990).

14. G. N George, J. Magnetic Resonance, **64**, 384 (1985).

15. D. R. Lovley and E. J. P Phillips, J. Appl. and Environ. Microbiol., **2**, 726 (1994).

16. P-C Wang, T. Mori, K. Toda and H. Ohtake, J. Bacteriology, **3**, 1670 (1990).

17. M. G. Fontana, in "Corrosion Engineering", McGraw-Hill Book Company, New York, USA, 282 (3rd edn., 1987).

18. H. H. Uhlig, in "Corrosion and Corrosion Control", John Wiley and Sons Inc., New York, USA, 257 (2nd edn., 1971).

19. C. R. Clayton, Y. C. Lu, Corrosion Science, **29**, 7, 881 (1989).

20. C. R. Clayton and I. Olefjord, in Corrosion Mechanisms in Theory and Practice, by P. Marcus and J. Oudar (eds), Marcel Dekker, Inc., New York, 184 (1st edn., 1995).

21. C. A. H. von Wolzogen and L. S. van de Vlught, Water, **18**, 16, 147 (1934).

22. R. C. Newman, B. J. Webster and R. G. Kelly, Iron and Steel Inst. of Japan, **31**, 2, 201 (1991).

23. P Marcus and H. Talah, Corrosion Science, **29**, 4, 455 (1989).

24. J. S. Smith and J. D. A. Miller, Br. Corrosion J., **10**, 3, 136 (1975).

25. G. Schmidt, Corrosion, **47**, 4, 285 (1991).

26. B. Little, P. Wagner and F. Mansfeld, *Electrochemica Acta*, **37**, 12, 2185 (1992).

27. P. F Sanders and W. A. Hamilton, Corrosion/86, Paper No. 47, NACE, Houston, Texas, USA (1986).

28. G. H. Booth, J. A. Robb and D. S. Wakerley, Proc. 3rd Int. Congr. Metall. Corros., **2**, 542 (1966).

29. G. H. Booth, L. Elford and D. S. Wakerley, *ibid.*, **3**, 242 (1968).

30. J. D. A. Miller and D. S. Wakerley, J. Gen Microbiol., **43**, 101 (1966).

31. R. A. King and D. S. Wakerley, Br. Corros. J., **8**, 41 (1973).

32. R. A. King, J. D. A. Miller and D. S. Wakerley, *ibid.*, **8**, 89 (1973).

33. G. H. Booth, P. M. Cooper and D. S. Wakerley, Br. Corros. J., **1**, 345 (1975).

34. W. Lee and W. G. Characklis, Corrosion, **49**, 3, 186 (1993).

35. R. C. Newman, K. Rumash and B. J. Webster, Corrosion Science, **33**, 12, 1877 (1992).

36. T. Hemmingsen, H. Vangdal and T. Våland, Corrosion, **48**, 6, 475 (1992).

37. J. W. Costerton, G. G. Geesey and P. A. Jones, Materials Performance, NACE, Houston, TX, USA, 3, 49 (1988).

38. A. Mohagheni, D. M. Updegraff and M. B. Oldhaber, Geomicrobiology, **5**, 4, 153 (1984).

39. W. G. Characklis, G. A. McFeters and K. C. Marshall, in "Biofilms", W. G. Characklis and K. G. Marshall (eds), Wiley Interscience, John Wiley and Sons, Inc., New York, USA, 341 (1990).

40. Z. Lewandowski, P. Stoodley and F. Roe, "Corrosion/95", Paper No. 222, NACE, Orlando, Florida, USA, March, 1995

41. Wayne Dickinson and Z. Lewandowski, "Corrosion/95", Paper No. 223, NACE, Orlando, Florida, USA, March, 1995.

42. G. Chen, C. R. Clayton, A. J. Francis, to be published.

43. G. Chen, C. R. Clayton, R. A. Sadowski, J. R. Kearns and A. J. Francis, Corrosion/95, Paper No. 217, NACE, Orlando, Florida, USA, March, 1995.

44. L. P. Wackett, W. H. Orme-Johnson and C. T. Walsh, in "Metal Ions and Bacteria", T. J. Beveridge and R. J. Doyle (eds), John Wiley and Sons, New York, USA, 165 (1989).

45. J. R. Postgate, in "The Sulphate-Reducing Bacteria", Cambridge University Press, Cambridge, UK, 96 (2nd edn., 1984).

46. S. C. Dexter, D. J. Duquette, O. W. Siebert and H. A. Videla, Corrosion, **47**, 4, 308 (1991).

47. J. R. Postgate, in "The Sulfate-Reducing Bacteria", second edition, Cambridge University Press, Cambridge, UK, 32 (2nd edn., 1984).

48. J. R. Postgate, in "The Sulfate-Reducing Bacteria", Cambridge University Press, Cambridge, UK, 9 (2nd edn., 1984).

49. P. Kroneck and J. T. Spence, J. Inorg. Chem., **35**, 3391 (1973).

50. A. L. Page et al (eds), in "Methods of Soils Analysis, Part II- Chemical and Microbiological Characteristics", American Society of Agronomy, Inc. Madison, Wisconsin, USA, 175 (1982).

51. A. J. Francis, C. J. Dodge, J. B. Gillow and J. E. Cline, *Radiochimica Acta,* **52- 53**, 311 (1991).

52. R. A. Sadowski, G. Chen, C. R. Clayton, J. R. Kearns, J. B. Gillow and A. J. Francis, Corrosion/95, Paper No. 218, NACE, Orlando, Florida, USA, March, 1995.

53. S. W. Dean, Jr., W. D. France, Jr., and S. J. Ketcham, in "Handbook on Corrosion Testing and Evaluation", by W. H. Ailor (ed), John Wiley & Sons, New York, USA, 174 (1971).

54. S. W. Dean, Jr., W. D. France, Jr., and S. J. Ketcham, in "Handbook on Corrosion Testing and Evaluation", by W. H. Ailor (ed), John Wiley & Sons, New York, USA, 182 (1974).

55. M. Stern and A. L. Geary, J. electrochem. Soc., **104**, 56 (1957).

56. C. D. Wagner, W. M. Riggs, L. E. Davis, J. F. Moulder and G. E. Muilenberg (eds), in "Handbook of X-ray Photoelectron Spectroscopy", Perkin-Elmer corporation, Eden Prairie, Minnesota, USA, 12 (1979).

57. K. Siegbahn *et al*, "ECSA Applied to Free Molecules", North Holland, Amsterdam (1969).

58. U Gelius, *Physica Scripta*, **9**, 133 (1974).

59. D. A. Shirley, in "Advances in Chemical Physics", **XXIII** by I. Prigogine and S. A. Rice (eds), John Wiley & Sons, New York, USA, 85 (1973).

60. M. E. Schwartz, Chem. Phys. Lett., **5**, 50 (1970).

61. C. R. Brundle, M. B. Robin, H. Basch, J. Chem. Phys., **53**, 2196 (1971).

62. W. E. Spicer, Phys. Rev., Lett., **11**, 243 (1963).

63. C. D. Wagner, L. E. Davis, M. V. Zeller, J. A. Taylor, R. H. Raymond and L. H. Gale, Surf. and Interf. Anal., **3**, 5, 211 (1981).

64. D. Briggs and J. C. Rivière, in "Practical Surface Analysis by Auger and X-ray Photoelectron Spectroscopy", by D. Briggs and M. P. Seah (eds), John Wiley & Sons, New York, USA, 133 (1st edn., 1983).

65. M. P. Seah, in "Practical Surface Analysis by Auger and X-ray Photoelectron Spectroscopy", D. Briggs and M. P. Seah (eds), John Wiley & Sons Inc., New York, 211 (1st edn., 1983).

66. M. P. Seah and W. A. Dench, surf. and Interf. Anal., **1**, 2 (1979).

67. D. A. Shirley, Physics. Review. **B5**, 4709 (1972).

68. P. M. A. Sherwood, in "Practical Surface Analysis by Auger and X-ray Photoelectron Spectroscopy", by D. Briggs and M. P. Seah (eds), John Wiley & Sons, New York, USA, 445 (1st edn., 1983).

69. A. Savitsky and M. J. E. Golay, Anal. Chem., **36**, 1627 (1964).

70. A. Proctor and P. M. A. Sherwood, Anal. Chem., **54**, 13 (1982).

71. H. P. Yule, Anal. Chem., **38**, 103 (1966).

72. R. H. Smillie, K. Hunter and M. Loutit, Water Research, **5**, 1351 (1981).

73. F. Li, B. Harris, M. M. Urrutia and T. J. Beveridge, Appl. & Environ. Microbiol., 5, 1525 (1994).

74. G. P. Halada and C. R. Clayton, J. Electrochemical Society, **138**, 10, 2921 (1991).

75. T. Dickinson, A. F. Povey and P. M. A. Sherwood, J. Chem. Soc., Faraday Transaction I, 1, 327 (1977).

76. M. Pourbaix and N. De Zoubov, in "Atlas of Electrochemical Equilibria", M. Pourbaix (ed), Pergamon Press, Long Island City, New York, USA, 307 (1st edn., 1966).

77. E. Deltombe, N. De Zoubov and M. Pourbaix, in "Atlas of Electrochemical Equilibria", M. Pourbaix (ed), Pergamon Press, Long Island City, New York, USA, 256 (1st edn., 1966).

78. E. Deltombe, N. De Zoubov and M. Pourbaix, in "Atlas of Electrochemical Equilibria", M. Pourbaix (ed), Pergamon Press, Long Island City, New York, USA, 330 (1st edn., 1966).

79. F. C. Richard and A. C. M. Bourg, Water Research, **25**, 7, 807 (1991).

80. J. T. Spence, Model Reactions of Molybdenum Complxes, in "Molybdenum and Molybdenum Containing Enzymes", by M. Coughlan (ed), Pergamon Press, New York, 101 (1st edn., 1980).

81. S. O. Grim and L. J. Matienzo, Inorganic Chemistry, **14**, 5, 1014 (1975).

82. B. J. Brisdon, W. S. Mialki and R. A. Walton, J. Organometallic Chemistry, **187**, 341 (1980).

83. N. W. Ashcroft and N. D. Mermin, in "Solid State Physics", Saunders College, USA, 396 (1976).

84. J. R. Postgate, in "The Sulfate-Reducing Bacteria", Cambridge University Press, Cambridge, UK, 86 (2nd edn., 1984)

85. J. Johnson, The Molybdenum Cofactor Common to Nitrate Reductase, Xanthine Dehydrogenase and Sulfide Oxidase, in "Molybdenum and Molybdenum Containing Enzymes", by M. Coughlan (ed), Pergamon Press, New York, 365 (1st edn., 1980).

86. E. B. Sandell, in "Colorimetric Determination of Traces of Metals", Interscience, New York, USA, 388 (3rd edn, 1959).

87. J. P. M. Drummond and J. R. Postgate, J. Appl. Bact., **18**, 307 (1955).

88. J. R. Pilbrow, in "Transition Ion Electron Paramagnetic Resonance", Oxford Science Publications, Clarendon Press, Oxford, UK, 529 (1990).

89. J. D. A. Miller, in "Microbial Aspects of Metallurgy", by J. D. A. Miller (ed), American Elsevier Publishing Co., Inc., New York, USA, 22 (1970).

90. G. Valensi, J. van Muylder and M. Pourbaix, in "Atlas of Electrochemical Equilibria", M. Pourbaix (ed), Pergamon Press, Long Island City, New York, USA, 545 (1st edn., 1966).

91. G. Voordouw, in "The Sulfate-Reducing Bacteria: Contemporary Perspectives", by J. M. Odom and R. Singleton, Jr. (eds), Spring-Verlag, New York, USA, 88 (1st edn., 1993).

92. C. R. Clayton, G. P. Halada, J. R. Kearns, J. B. Gillow and A. J. Francis, in "Microbiologically Influenced Corrosion Testing", ASTM STP 1232, by J. R. Kearns and B. J. Little (eds), ASTM, Philadelphia, USA, 141 (1994).

Appendix 1

METAL ION AND EXOPOLYMER INTERACTION: A SURFACE ANALYTICAL STUDY

G. Chen, S. V. Kagwade, G. E. French, C. R. Clayton
Department of Materials Science & Engineering
State University of New York at Stony Brook
Stony Brook, NY 11974

T. E. Ford and R. Mitchell
Division of Applied Sciences
Harvard University
Cambridge, MA 02138

ABSTRACT

Various concentrations of molybdate were added to the protein-containing and deproteinated exopolymers of a marine bacterium, *Deleya marina*. The interaction was investigated by X-ray photoelectron spectroscopy (XPS) and electron spin resonance (ESR). Molybdate reduction was observed exclusively in the deaerated protein-containing exopolymer, resulting in the formation of a Mo^{5+} species. This species appeared to be susceptible to reoxidation in the presence of soluble oxygen. Thus, only hexavalent molybdenum was seen in the aerated suspension. The "reducing agents" could be the residual proteins which remained in the exopolymer without subsequent deproteination. The influence of this reduction on the corrosion resistance of Mo-bearing stainless steels was simulated with an austenitic stainless steel, 304 SS, whose surface was treated with molybdate prior to exposure to the exopolymer. In addition to the formation of the Mo^{5+} species, a small amount of MoO_2 was detected, and hydration of the passive film of the steel was increased. No evidence was found to indicate that the exopolymer attachment compromised the corrosion resistance of the steel in deaerated 0.1 M HCl.

Keywords: Exopolymer, X-ray photoelectron spectroscopy (XPS), electron spin resonance (ESR), reduction of molybdate, potentiodynamic polarization.

INTRODUCTION

As the importance of biofilms in microbiologically influenced corrosion (MIC) is increasingly understood, the interactions between bacterial exopolymers and metal substrata have received considerable interest from both microbiologists and material scientists[1,2]. The exopolymers comprise the outermost extracellular polymeric envelope of many types of bacteria. They contribute a structural component to the biofilm, providing the basis for bacterial attachment to a substratum[3, 4]. The exopolymers provide protection for the bacteria and may influence uptake of ions and molecules into the microorganisms[5, 6]. The binding ability of an exopolymer to a metal ion may be an important factor in the adhesion of the biofilm to a metal substratum and may determine its ability to attract and assimilate metal ions from the substratum and media[7, 8]. In the present work, the interaction of the exopolymer of a marine bacterium, *Deleya marina*, with a group VI oxyanion, molybdate, was studied.

The assimilation of trace metal ions by the bacterium, *Deleya marina*, is of the order: Fe > Cd > Cu > Zn > Pb = Ni = Mn[2, 7]. Whereas, the interaction of the metal ions with the crude exopolymer of this bacterium, measured by their maximum binding abilities, varies in a different order: Mn > Cu > Ni > Fe. This interaction does not take place once the exopolymer is purified by deproteination. Therefore, the interaction is attributed to species that may be removed during deproteination, including functional amino groups and residual proteins[2]. In the present work, X-ray photoelectron spectroscopy (XPS), electron spin resonance (ESR) and electrochemical methods were used to study the interaction of the exopolymer with molybdate. XPS provides information about the electron transfer process of the interaction through valence state analysis. The unique feature of ESR lies in its ability to identify unpaired electrons. It was utilized to characterize the products and confirm XPS observations of odd valence states. Various concentrations of molybdate, ranging from 0.01 to 0.05 M, were added to both the protein-containing and deproteinated exopolymers in order to determine if any reduction would take place. Subsequently, an austenitic stainless steel, type 304, was surface-treated with molybdate, exposed to the exopolymer, and then characterized with XPS. The surface changes induced by the exopolymer were also characterized by potentiodynamic polarization in deaerated 0.1 M HCl. The importance of this work lies in the knowledge that molybdate species are present in the outer region of the passive film formed on Mo-bearing stainless steels, where it is

believed that molybdate is most effectively able to repel ingressing chloride ions which are powerful producers of pitting corrosion[9, 10, 11].

EXPERIMENTAL PROCEDURE

1. Preparation of the exopolymer

The bacterium *Deleya* (*Pseudomonas*) *marina* (ATCC 25374) was obtained from the American Type Culture Collection (Rockville, MD). The culture was maintained on slants of Marine Agar 2216 (Difco, Detroit, MI) and stored at -20 °C in glycerol. For exopolymer extraction, bacteria in batch cultures were grown to stationary phase (A_{660} = 2.7) in a defined minimal medium with glucose as carbon source.

Once the batch cultures reached stationary stage, they were centrifuged at 20,000 rpm for 20 minutes to separate cells from extracellular material. The supernatant was filtered through sterilized 0.2 μm filters (Millipore) and then concentrated in a stirred ultrafiltration cell (Amicon, Danvers, MA) with a nominal molecular weight (MW) cut-off of 5,000. The concentrated supernatant was precipitated with 3 volumes of 95% (v/v) ethanol and stored at 4 °C for 24 hours. The precipitate was collected through centrifugation, dissolved in deionized water (18.2 MΩ) and dialyzed extensively with deionized water prior to lyophilization. The solution was finally lyophilized. This lyophilized product was considered crude exopolymer (protein-containing).

For subsequent deproteination, samples of the crude exopolymer was treated as follows: ether extraction was used to remove lipids followed by extensive dialysis with deionized water. Deproteination was then conducted several times with chloroform/ isopentanol followed by extensive dialysis. The deproteinated exopolymer was then lyophilized. Both crude and deproteinated exopolymers were stored in a desiccator prior to experimentation. Chemical analysis of the exopolymer has been reported elsewhere[2, 12].

2. Addition of molybdate to the exopolymer

Rehydration and sample preparation were performed in a nitrogen purged glove bag. Deionized water was deaerated by boiling and purging with ultra high purity nitrogen for at least 20 minutes, cooled on ice and then placed in the glove bag. 1 mg exopolymer was dissolved in 0.1 ml deaerated deionized

water. Sodium molybdate solution was deaerated, transported into the glove bag and then pipetted into 3 aliquots of the exopolymer, to give final concentrations of molybdate of 0.01 M, 0.02 M and 0.05 M. Aerated suspension was prepared without deaerating deionized water and the molybdate solution. Both types of the suspensions were allowed to equilibrate for 4 hours, and then dropped onto a 1 cm^2 piece of silicon wafer which had been previously rinsed in 5% HF solution to remove the surface oxide and followed by thoroughly rinsing in deionized water. As soon as a droplet started to dry, it was gently rinsed by deaerated deionized water to obtain a relatively thin exopolymeric film. The film was dried overnight in nitrogen before XPS analysis. Titanium (99.99%) coupons, polished to 6 μm diamond finish, ultrasonically degreased in acetone and rinsed in deionized water, were used in place of Si wafer to investigate the influence, if any, of the substrata.

3. Processing of 304 SS samples

The composition of 304 SS used for the study was (%wt): Fe: 69.62, Cr: 19.27; Ni: 8.49; Mo: 0.35; Mn: 1.77; Si: 0.41; P: 0.031; S: 0.008; and C: 0.053. 1 mm thick foils were cut into 1 cm^2 coupons, annealed at 1080 °C for 1 hour in an evacuated quartz tube and then quenched in water. The quenching-stabilized coupons were polished to a 6 μm diamond finish and ultrasonically degreased in acetone. Subsequently, two categories of samples were prepared: (1) For XPS analysis, the coupons were molybdate surface-treated and exposed to the exopolymer directly and, (2) For electrochemical characterization, the coupons were mounted on 2 x 1.5 x 0.5 cm^3 plexiglass sample holders by epoxy resin before the molybdate treatment and exposure. Connection from the electrode to the potentiostat was completed by a copper wire which was previously placed between the sample and the plexiglass block passing through an 8 mm outer diameter glass tube mounted on the plexiglass block. Both types of the samples were then placed in a nitrogen filled glove box. They were thoroughly rinsed in deaerated deionized water and then immersed in deaerated 0.1 M molybdate solution for 2 hours. After the surface molybdate treatment, they were rinsed with deaerated deionized water and dried by blowing nitrogen over the surface. A droplet of the exopolymer suspension was subsequently placed on each sample and left in a sealed glass flask for 12 hours. The samples were finally processed for XPS and electrochemical characterization under two surface conditions, one thoroughly rinsed with deaerated deionized water and the other unrinsed.

In addition to the samples processed above, another type of samples were prepared by direct exposure to the protein-containing exopolymer for 5 minutes, in order to study the effect of the adsorbed exopolymer on the electrochemical behavior. The quenching-stabilized coupons were polished, rinsed and then mounted on the plexiglass sample holders. They were placed in the glove box, rinsed with deaerated deionized water and then immersed in the deaerated exopolymer suspension for 5 minutes, under two conditions: one without disturbance and the other was mechanically stirred to aid in adsorption.

4. X-ray photoelectron spectroscopy

A VG Scientific ESCA 3 Mark II XPS spectrometer was used for the analysis. It was controlled by a VGX900 interface and data acquisition software. The samples were transported into the XPS chamber in an argon purged glove bag. The vacuum was maintained below 4×10^{-9} torr. To prevent outgassing, liquid nitrogen cooling was provided. An Al K_α (1486.6 eV, 400 watts) X-ray source was used, providing a full width at half maximum (FWHM) of 1.35 eV for $Au4f_{7/2}$. The entrance and exit slit widths were set at 4 mm during the analysis. Analyzer energies were set at 100 eV for wide survey scans and 20 eV for region scans. Charge shifting was corrected with the adventitious carbon 1s line at 284.6 eV. Spectra were obtained at several photoelectron take-off angles, ranging from 20° to 50°, with respect to the sample surface. Nonlinear least square curve fitting was performed. The parameters included the Gaussian/Lorentzian ratio, constant tail ratio, exponential tail slope and constant/exponential tail mixing ratio. Background subtraction was performed with the Shirley method[13]. Peak subtraction and secondary differentiation were carried out to aid in peak identification[14-16]. The peak parameters used as standards were obtained with the pure elements and compounds using the same spectrometer settings (Table 1).

5. Electron spin resonance

An X-band Varian E-12 ESR spectrometer was used in the present work. The microwave frequency was set at 9.51 GHz and the magnetic field was scanned to find the resonant condition for the given species. The suspension containing 0.02 M molybdate was cooled with liquid nitrogen to a temperature of 77 °K during the analysis. Suitable standards for Mo^{5+} were analyzed, yielding characteristic **g** values under the same conditions[17, 18].

6. Electrochemical characterization

A Gamry CMS 100 potentiostat was employed. The experiment was conducted in the glove box at room temperature, using a 1 liter Greene cell and a saturated calomel reference electrode. Counter electrodes were made of 1 mm diameter Pt wires. The electrolyte, 0.1 M HCl solution, was deaerated in the Greene cell for at least two hours before the working electrode was inserted. Potentiodynamic polarization was started at a sweep rate of 1 mV/sec from the open circuit potential. No cathodic surface conditioning was applied to avoid the influence of cathodic reactions on the surface. This test simulated typical pitting conditions in a local area which was associated with a low pH and high chloride content.

RESULTS AND DISCUSSION

1. XPS analysis of the molybdate doped exopolymers

The wide scan qualitatively revealed that the exopolymer primarily consisted of C, O, N, Ca, Si, and S, of which Ca, Si and S signals were detectable only in the protein-containing exopolymer (Figure 1). The S signal indicated a possible disulfide bond which is often seen in extracellular proteins[19], whereas Si could be a contaminant. The spectra showed a certain amount of charge shifting, compared with the results of previous work where the surface charge was neutralized with an electron flood gun[7]. The binding energy difference between the C1s in the present work and that with the electron flood gun was about 2.3 eV, equal to the binding energy difference of the other component peaks in these two investigations[7].

Figure 2a and b are the Mo3d photoelectron spectra obtained from the respective deaerated and aerated protein-containing exopolymers doped with 0.02 M molybdate. By comparison, it was seen that reduction of molybdate to Mo^{5+} took place only in the deaerated protein-containing exopolymer. The residual hexavalent molybdenum might have existed as sodium molybdate and molybdenum trioxide and/or molybdic acid[20]. The molybdenum trioxide and molybdic acid are fitted into one peak because their binding energy values are very close (Table 1). The absence of Mo^{5+} in the Mo3d spectra of the aerated sample indicated its susceptibility to oxidation when soluble oxygen was present. In addition, it was interesting to note that the addition of molybdate substantially decreased the sulfur signal, while the molybdenum signal also

became reduced. This indicated an interaction between the molybdate and sulfur species in the exopolymer. The fact that the molybdenum and sulfur signals became reduced suggested the formation of two possible products, a high vapor pressure product that evaporated in the spectrometer chamber, or a cluster of Mo and S compounds attenuating the emission of the photoelectrons. On the other hand, the deaerated deproteinated exopolymer did not reveal this reduction effect when molybdate was provided. The spectroscopic features of the other major component peaks, such as C1s, O1s and N1s, did not show obvious differences from those of the protein-containing exopolymer. Therefore, the major functional groups of the exopolymer are most likely not the "reducing agents". It was postulated in the previous study that the binding moieties to the metal ions probably were the functional amino groups and residual proteins from the biomass which remained in the crude exopolymer prior to subsequent deproteination processing[2]. The results of the present work indicate that this reduction is more likely caused by the residual proteins, and specifically, the sulfide groups. The enzymatic interactions of sulfur-containing proteins with Mo and their influence on microbial metabolism have been well recognized[21].

The reduction of molybdate resulted in a decrease in charging by 1.1 eV (Figure 2a and b). By the charge shifting only, it was difficult to derive any information regarding the molecular changes in the exopolymer induced by the reduction since no characteristic changes were seen in the spectra of C1s, O1s and N1s. The decreased charge shifting could be due to the decrease of the relative proportion of MoO_4^{2-}, because a pure sodium molybdate standard usually showed 4 eV charge shifting toward the high binding energy side, due to its insulating nature.

The influence of molybdate concentration on the interaction was studied with the deaerated suspensions containing 0.01 M, 0.02 M and 0.05 M molybdate respectively. It was observed that the most remarkable reduction was seen when the molybdate content was 0.02 M, in terms of the relative proportions of peak areas. An increase of molybdate concentration did not increase the degree of reduction, indicating that the amount of the "reducing agents" was limited. The reduction process ended once the "reducing agents" were consumed.

In order to distinguish the role of the substratum in the reduction, similar studies were performed with the titanium coupons. Reduction of

molybdate was also seen to occur. There was no evidence to suggest that the selected substrata played a role in the reduction process.

2. ESR analysis of the molybdate doped exopolymer

The reduction of molybdate in the deaerated protein-containing exopolymer was confirmed by ESR analysis, as shown in Figure 3. The corresponding **g**-factor was 1.969, close to the **g** values of Mo^{5+} found in Mo containing enzymes[22, 23]. By contrast, no molybdate reduction was found in the deproteinated exopolymer, consistent with the XPS results.

3. The reduction of molybdate on the surface of 304 SS

The reduction effect of the exopolymer gives rise to the question as to whether the corrosion resistance of Mo-bearing stainless steels is compromised by the attachment of the exopolymer, since externally bound molybdate salts are effective pitting inhibitors in chloride containing media. The interaction was therefore investigated with the molybdate treated 304 SS, in order to simulate the surface condition of Mo-bearing stainless steels, such as SS 316, but without the interference of a constant source of molybdenum from the alloy. The samples were immersed in 0.1 M Na_2MoO_4 for 2 hours, rinsed and then analyzed by XPS before and after exposure to the exopolymer.

Molybdate surface treatment of 304 SS resulted in formation of $FeMoO_4$. The spectra of Mo3d showed the existence of molybdate on the steel surface (Figure 4a). In contrast to the remarkable charge shifting in the Mo3d spectra of Na_2MoO_4 standard, the spectra revealed little charging, indicating a close contact of the molybdate to the steel substratum. No sodium signal was detectable. $Fe2p_{3/2}$ spectra correspondingly revealed the formation of $FeMoO_4$, associated with a significant decrease of the relative proportions of ferrous iron and oxyhydroxide usually existing on the surface of a freshly polished coupon (Figure 5a)[24]. On the other hand, the Cr2p spectra essentially remained unchanged (Figure 6a), and Ni remained in its metallic form[24]. The relative proportions of the metal element on the surface are given in Table 2. It was seen that there was a certain degree of depletion of iron and enrichment of chromium, particularly in the outer region of the surface.

After the molybdate treated surface was exposed to the deaerated protein-containing exopolymer, XPS analysis was performed, and the relative

proportions of the surface metal elements calculated (Table 2). It was seen that the surface molybdate was reduced by 50%, associated with a greater degree of surface depletion of iron and enrichment of chromium. The nickel signal was then no longer visible. The changes in the valence states of Mo3d, $Fe2p_{3/2}$ and Cr2p spectra are shown in Figure 4b, 5b, and 6b respectively. The reduction of molybdate to Mo^{5+} took place to a greater extent in a few top monolayers of the steel surface (Figure 4b). Comparing Figure 2 and 4b, it is noted that these Mo3d spectra differ from those obtained from the suspension droplets by formation of MoO_2 on the surface. The formation of MoO_2 could be due to the inter-influence of the alloying elements, since the conversion of molybdate to MoO_2 usually takes place under aerobic conditions[9]. Consistency of the results may be seen from the $Fe2p_{3/2}$ spectra (Figure 5). The amount of ferrous molybdate was greatly reduced, showing a little depth dependence. A dominant amount of Fe^{3+} existed in the outer layer, with a certain amount of ferrous oxide and oxyhydroxide. The $Fe2p_{3/2}$ spectra from the sublayer consisted of a considerable amount of metallic Fe, Fe^{3+} and oxyhydroxide, as well as a small quantity of Fe^{2+}. Finally, an increased proportion of $Cr(OH)_3$ appeared in Cr2p spectra, particularly in the outer layer, indicating an increase of surface hydration (Figure 6).

4. The electrochemical aspects

Potentiodynamic polarization was conducted in deaerated 0.1 M HCl to study the influence of molybdate treatment and subsequent exposure to the exopolymer on the passivation performance of 304 SS. The evidence of surface modification by molybdate was revealed by a greater degree of anodic dissolution and a stable passivity at a higher overpotential (Figure 7). The influence of exopolymer was not considerable: the potentiodynamic polarization result was almost identical in the exopolymer-exposed and the non-exposed steels. However, this does not mean that the surface will remain intact once a thick biofilm has developed. The interaction of the exopolymer with molybdate indicated a potential mechanism for the bacterial attachment to the Mo-bearing steel substrata. In an environment where the bacteria exist, depletion of surface molybdenum will reduce the corrosion resistance of Mo-bearing steels.

The influence of the adsorbed exopolymer on the potentiodynamic behavior of 304 SS in deaerated 0.1 M HCl is illustrated in Figure 8. The anodic dissolution was reduced, despite the lack of uniformity of the adsorbed layer of the exopolymer. However, a uniformly adsorbed layer, resulting from

mechanical stirring, led to a better surface stability, as indicated by the lower current density in the passive region.

CONCLUSIONS

The protein-containing exopolymer of the bacterium *D. marina* has a reducing effect on molybdate, yielding products of Mo^{5+} under anaerobic conditions. The reduction could be induced by the sulfur-containing residual proteins. This reduction was also seen on the surface of the molybdate treated austenitic stainless steel, 304 SS, associated with the formation of molybdenum dioxide. The exposure to the exopolymer resulted in the surface depletion of iron and enrichment of chromium, rendering an increased hydration of chromium. However, no evidence indicated that the corrosion resistance of the steel was compromised by the exopolymer attachment.

ACKNOWLEDGEMENT

The program was supported in part by a grant from the Office of Naval Research to the State University of New York at Stony Brook under the contract number N0001485K0437(Dr. A. J. Sedriks, Contract Officer).

REFERENCE

1. W. G. Characklis and K. C. Marshall, (Editors), in Biofilms, John Wiley & Sons, Inc., New York, USA, 635, 1990.

2. T. E. Ford et al, Corrosion/87, paper No. 380, Moscone Center, San Francisco, USA, 1987.

3. B. J. Little et al, Corrosion, NACE, **42**, 9, September, 533 (1986).

4. G. G. Geesey, and M. W. Mittelman, Corrosion/85, Paper No. 297, NACE, Houston, Texas, 1985.

5. W. G. Characklis and K. C. Marshall, (Editors), in Biofilms, John Wiley & Sons, Inc., New York, USA, 341, 1990.

6. J. S. Nickels et al, Appl. and Environ. Microbiol., **41**, 1442 (1981).

7. T. E. Ford et al, American Society for Microbiology Annual Meeting, Paper Abstract, No. I-77, Miami, Florida, USA, 1988.

8. G. G. Geesey et al, Materials Performance, **25**, 2, 37 (1986).

9. H. H. Uhlig and R. W. Revie, in Corrosion and Corrosion Control, John Wiley & Sons, New York, USA, Third Edition, 263 (1985).

10. Y. C. Lu, C. R. Clayton,and A. B. Brooks, Corrosion Sc., **29**, 863 (1989).

11. Y. C. Lu, C. R. Clayton and A. B. Brooks, Corrosion Sc., **29**, 881 (1989).

12. T. Ford, E. Sacco, J. Black, T. Kelly, R. Goodacre, R. C. W. Berkeley and R. Mitchell, Applied and Environ. Microbiol., **57**, No. 6 1595 (1991).

13. D. A. Shirley, Physics Review B, **55**, 4709 (1972).

14. A. Savitsky and M. J. E. Golay, Anal. Chem., **36**, 1627 (1964).

15. A. Proctor and P. M. A. Sherwood, Anal. Chem., **54**, 13 (1982).

16. H. P. Yule, Anal. Chem., **38**, 103 (1966).

17. J. E. Wertz and J. R. Bolton, in Electron Spin resonance - Elementary Theory and Practical Applications, Chapman and Hall, New York, USA, 17, 1986.

18. R. Aasa et al, in Single Crystal EDTA" *Arkiv FörKemi*, Band **25**, 29, 309 (1966).

19. L. Stryer, in Biochemistry, W. H. Freeman and Company, 3rd edn, 23, 1988.

20. C. R. Clayton and Y. C. Lu, Surface and Interface Analysis, **14**, 66 (1989).

21. P. Kroneck and J. T. Spence, J. Inorg. Nucl. Chem., **35**, 3391 (1973).

22. B. Ghani, M. Takai, and N. Z. Hisham et al, Appl. and Environ. Microbiol., **59**, 4, 1176 (1993).

23. J. R. Pilbrow, in Transition Ion Electron Paramagnetic Resonance, Oxford Science Publication, Clarendon Press, Oxford, UK, 521, 1990.

24. G. Chen, C. R. Clayton, R. A Sadowski et al Corrosion/95, paper number 95217, Orlando, Florida, USA, 1995.

TABLE 1
RELATIVE PROPORTIONS OF ALLOY ELEMENTS ON THE SURFACE OF 304 SS AFTER MOLYBDATE SURFACE TREATMENT AND THE SUBSEQUENT EXPOSURE TO THE EXOPOLYMER OF *D. MARINA*

Treatment	Atomic percentages of metal elements				TOA
	Fe	Cr	Ni	Mo	
Polished to 6 μm	70	28	2	--	20°
	72	25	3	--	50°
MoO_4^{2-} treated	50	35	3	12	20°
	60	27	2	11	50°
MoO_4^{2-} treated and exposed to *D. Marina*	46	49	--	5	20°
	45	50	--	5	50°

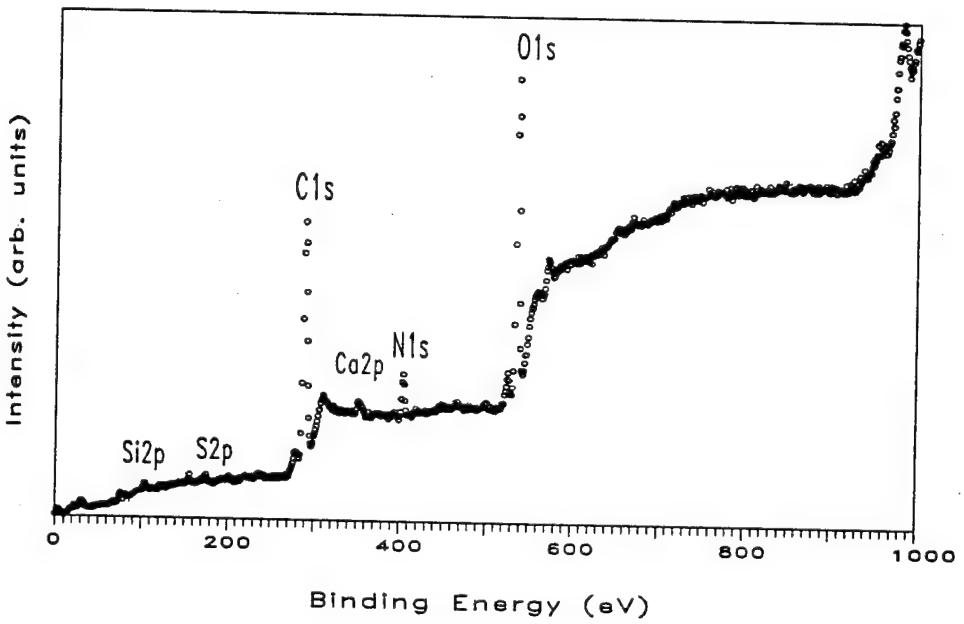

Figure 1 Composition of the protein containing exopolymer of bacterium *D. marina* shown in XPS wide scan

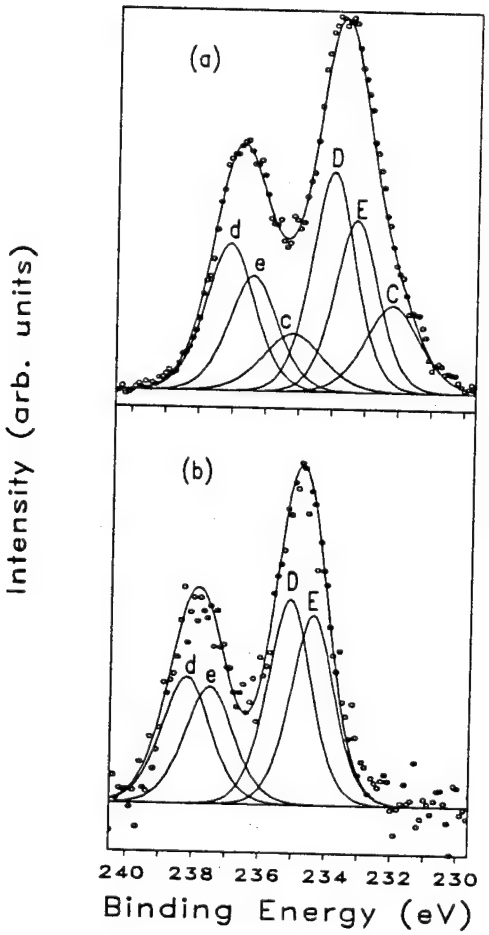

Figure 2 Molybdate reduction induced by the deaerated protein containing exopolymer of *D. marina*, take-off angle 25°.
(a) deaerated suspension with 0.02 M molybdate;
(b) aerated suspension with 0.02 M molybdate.
C, c: Mo^{5+}, D, d: MoO_3/H_2MoO_4; E, e: MoO_4^{2-}.

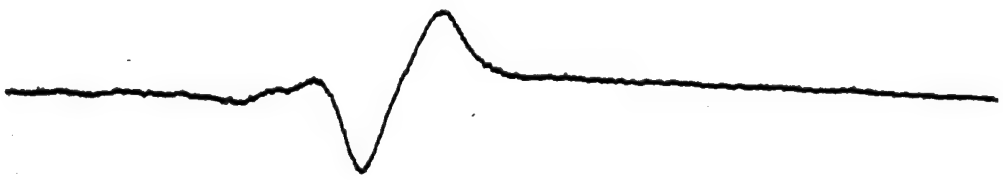

Figure 3 Mo^{5+} shown in an ESR spectrum of the deaerated protein-containing exopolymer of *D. marina* with 0.02 M molybdate. Field Center: 3450.0 G, Scan width: 1000 G, T = 77°K, g=1.969

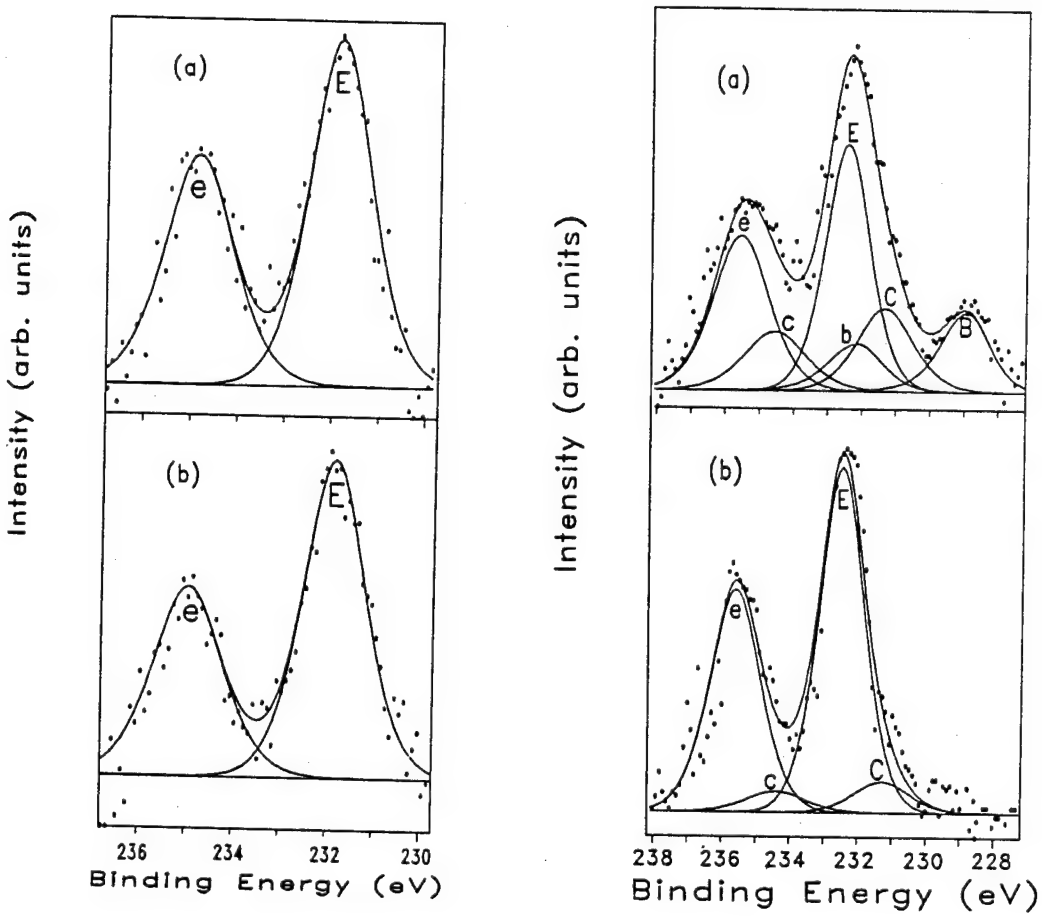

4a Before exposure to the exopolymer

4b After exposure to the exopolymer

Figure 4 The influence of the deaerated protein-containing exopolymer of *D. marina* on Mo3d on the surface of 304 SS following molybdate treatment.
(a) take-off angle 20°; (b) take-off angle 50°.
B, b: MoO_2; C, c: Mo^{5+}; E, e: MoO_4^{2-}.

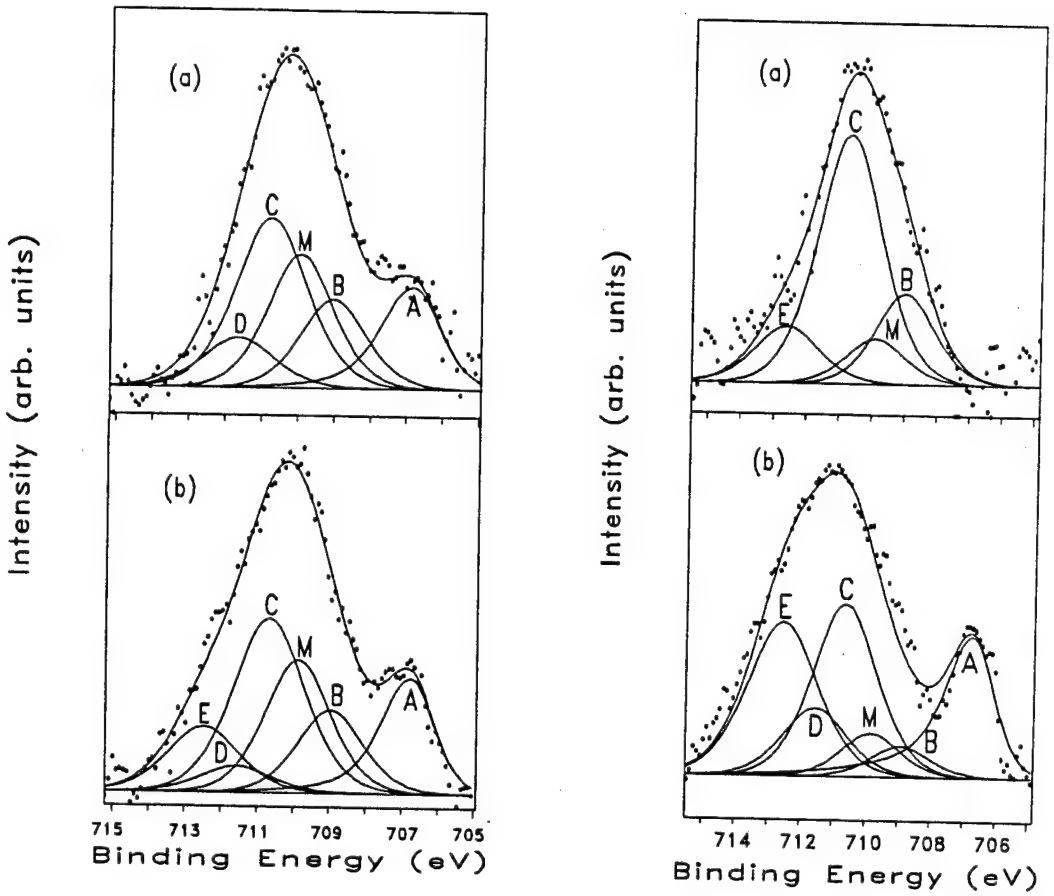

5a Before exposure to the exopolymer 5b After exposure to the exopolymer

Figure 5 The influence of the deaerated protein containing exopolymer of *D. marina* on Fe2p on the surface of 304 SS following molybdate treatment.
(a) take-off angle 20°; (b) take-off angle 50°.
A: Fe; B: FeO, C: Fe_2O_3; D: $Fe(OOH)_\gamma$; E: $Fe(OOH)_\alpha$; M: $FeMoO_4$.

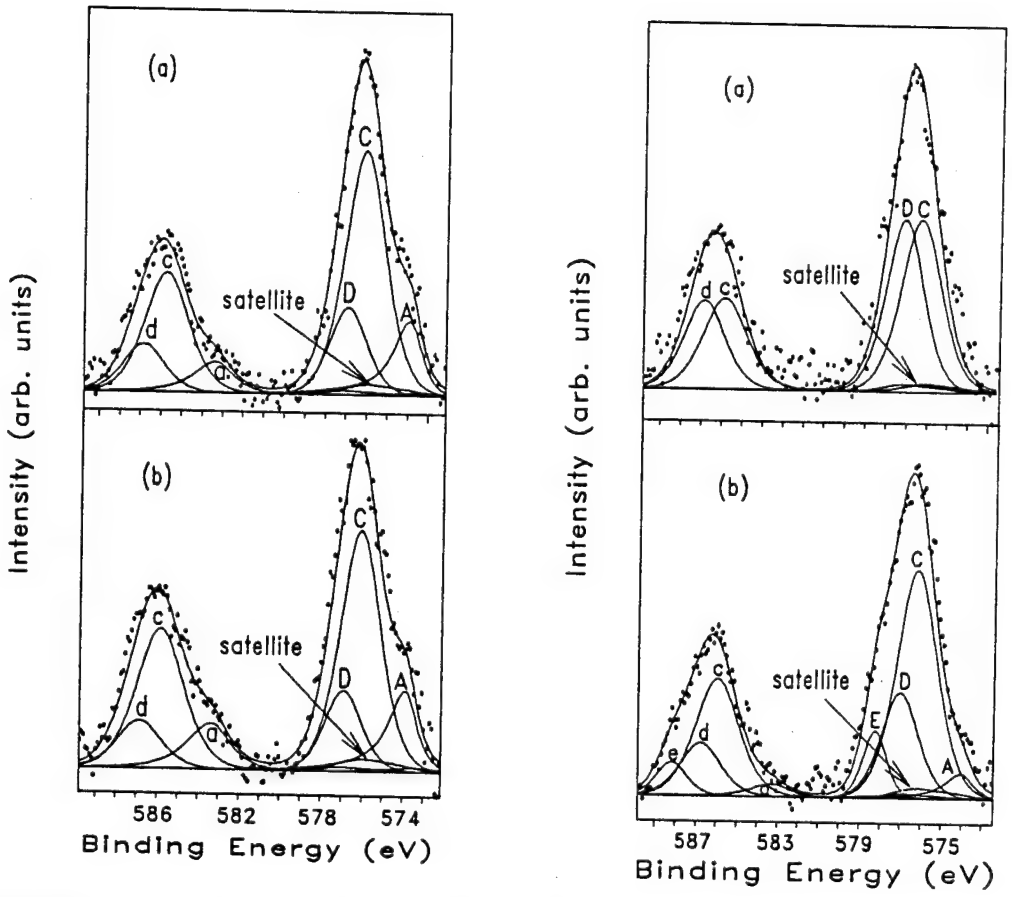

6a Before exposure to the exopolymer 6b After exposure to the exopolymer

Figure 6 The influence of the deaerated protein containing exopolymer of *D. marina* on Cr2p on the surface of 304 SS following molybdate treatment.
(a) take-off angle 20°; (b) take-off angle 50°.
A, a: Cr; C, c: Cr_2O_3; D, d: $Cr(OH)_3$; E, e: CrO_3.

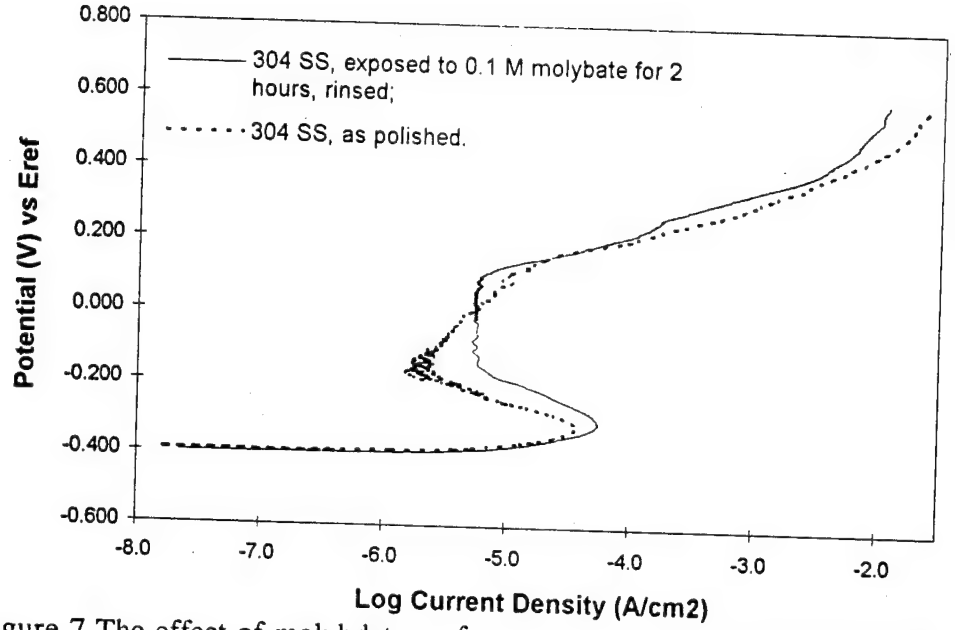

Figure 7 The effect of molybdate surface treatment on the potentiodynamic polarization of 304 SS in deaerated 0.1 M HCl.

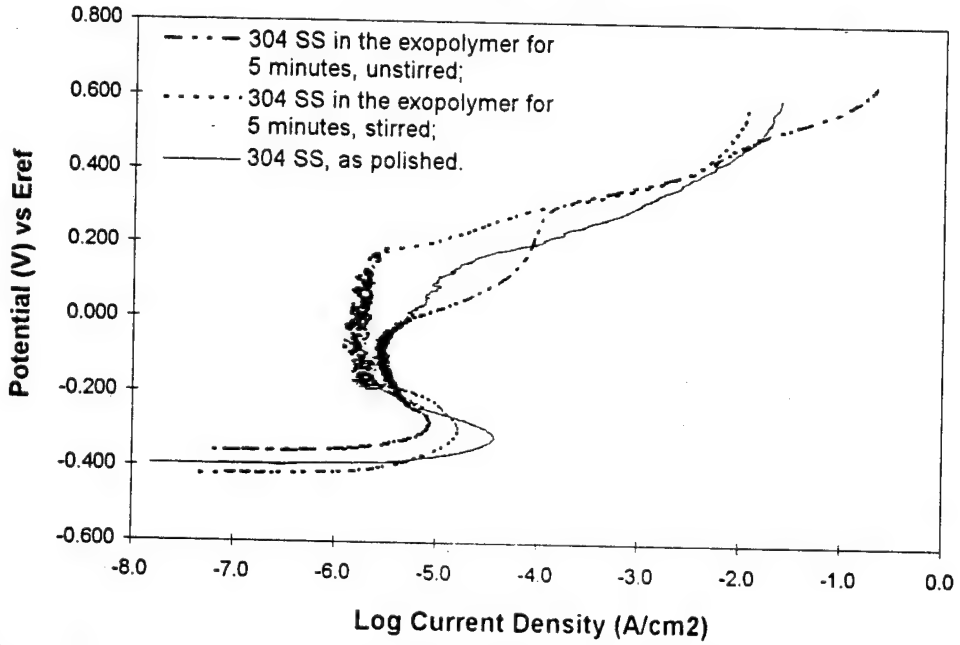

Figure 8 Potentiodynamic polarization diagrams of 304 SS in deaerated 0.1 M HCl after the exposure to the deaerated protein-containing exopolymer of *D. marina* for 5 minutes.

Table 1
Different ratios of sulfate to molybdate added to the modified Postgate medium C (SO_4^{2-} + MoO_4^{2-} = 20 mM)

SO_4^{2-} (mM)	0	0	5	10	15	18	19	19.5	19.9	20
MoO_4^{2-} (mM)	0	20	15	10	5	2	1	0.5	0.1	0

Table 2
Content of the organic salt mixtures simulating the organic salts in the stationary stage culture (mM)

Solutions	Lactate	Acetate	Propionate	Sulfite
Solution 1a	10	--	--	--
Solution 1b	10	--	--	2
Solution 2a	--	10	--	--
Solution 2b	--	10	--	2
Solution 3a	--	--	10	--
Solution 3b	--	--	10	2
Solution 4a	2	10	--	--
Solution 4b	2	10	--	2
Solution 5a	2	--	10	--
Solution 5b	2	--	10	2
Solution 6a	--	10	10	--
Solution 6b	--	10	10	2
Solution 7a	2	10	10	--
Solution 7b	2	10	10	2

Table 3
Contents of the constituent alloying elements of 304 and 317L SS used for this study

Type of steels	Alloy elements		
	Mo	Cr	Ni
304 SS	0.34	19.27	8.49
317L SS	3.34	18.43	13.13

Table 4
The empirical sensitivity factors of the main elements used in this study (F1s=1.00)

Metal element	Area		Height ($2p_{3/2}/3d_{5/2}$)
	$2p_{3/2}/3d_{5/2}$	2p/3d	
Fe	2.0	3.0	2.0
Ni	3.0	4.5	3.0
Mo	1.66	2.75	1.740
Cr	1.5	2.3	1.5

Table 5

The inelastic mean free paths of the photoelectrons and the maximum sampling depth into the surfaces of 304 and 317L SS

($\lambda_{elem}= 538/E^2 + 0.41\ (aE)^{0.5}$; $\lambda_{comp}= 2170/E^2 + 0.72\ (aE)^{0.5}$; $a^3= (A \times 10^{24})/\rho nN$)

Compounds		Molecular weight	Density (g/cm^3)	a (nm)	λ (nm)	d=3λsinα, nm (α=TOA)	
Mo	Mo	95.94	10.2	0.25	1.8	1.8	20°
						4.1	50°
	MoO_2	127.94	6.47	0.22	2.6	2.7	20°
						6.0	50°
	MoS_2	160.07	4.80	0.26	3.4	3.5	20°
						7.8	50°
	Mo_2O_5	271.88	3.60	0.26	3.4	3.5	20°
						7.8	50°
	MoO_3	143.94	4.69	0.23	2.8	2.9	20°
						6.4	50°
	H_2MoO_4	161.95	3.11	0.23	2.8	2.9	20°
						6.4	50°
Cr	Cr	51.996	7.20	0.22	1.3	1.3	20°
						3.0	50°
	Cr_2O_3	151.99	5.21	0.21	2.1	2.2	20°
						4.8	50°
	CrO_3	99.99	2.70	0.25	2.7	2.8	20°
						6.2	50°
	Na_2CrO_4	161.97	2.71	0.24	2.6	2.7	20°
						6.0	50°
	Cr_2S_3	200.18	3.77	0.26	2.9	3.0	20°
						6.7	50°

Table 5 (continued)
The inelastic mean free paths of the photoelectrons and the maximum sampling depth into the surfaces of 304 and 317L SS

Compounds		Molecular weight	Density (g/cm^3)	a (nm)	λ (nm)	d=3λsinα, nm (α=TOA)	
Ni	Ni	58.71	8.90	0.22	1.1	1.1	20°
						2.5	50°
	NiO	74.71	6.67	0.21	1.7	1.7	20°
						3.9	50°
	$NiCl_2$	129.62	3.55	0.27	2.5	2.6	20°
						5.7	50°
	NiS	90.77	5.45	0.24	2.1	2.2	20°
						4.8	50°
Fe	Fe	55.847	7.86	0.23	1.3	1.3	20°
						2.9	50°
	$FeCl_2$	126.75	3.16	0.28	3.0	3.1	20°
						6.9	50°
	FeO	71.85	5.7	0.22	2.1	2.2	20°
						4.8	50°
	$Fe(OH)_2$	89.86	3.4	0.24	2.4	2.5	20°
						5.5	50°
	Fe_2O_3	159.69	5.24	0.22	2.1	2.2	20°
						4.8	50°
	FeS	87.91	4.74	0.25	2.5	2.6	20°
						5.7	50°
	FeS_2	119.98	4.87	0.24	2.4	2.5	20°
						5.5	50°

Table 6
Standard parameters used for XPS spectrum deconvolution

Valence state		compound	B. E. (eV)	FWHM (eV)	G/L	Tail height	Expontl Slope	Tail Mix ratio
Fe	$Fe2p_{3/2}$	Fe	706.8	0.900	0.500	0.001	0.075	0.500
		FeS_2	707.2	0.700	0.650	0.001	0.200	0.500
		$Fe_{1-x}S$	708.0	1.200	0.500	0.001	20.0	0.500
		FeO	709.0	1.100	0.500	0.001	20.0	0.500
		$FeMoO_4$	710.1	1.200	0.500	0.001	20.0	0.500
		$FeCl_2$	710.3	1.200	0.500	0.001	20.0	0.500
		Fe_2O_3	710.7	1.200	0.500	0.001	20.0	0.500
		$Fe(OOH)_\gamma$	711.6	1.200	0.500	0.001	20.0	0.500
		FeS	711.8	1.200	0.500	0.001	20.0	0.500
		$Fe(OOH)_\alpha$	712.6	1.200	0.500	0.001	20.0	0.500
Ni	$Ni2p_{3/2}$	Ni	852.3	0.800	0.600	0.001	0.070	0.500
		NiS	853.1	0.900	0.500	0.001	20.0	0.500
		NiO	854.5	0.900	0.500	0.001	20.0	0.500
		$Ni(OH)_2$	856.6	1.300	0.500	0.001	20.0	0.500
Cr	$Cr2p_{3/2}$	Cr	574.1	0.700	0.650	0.001	0.050	0.500
		Cr_2S_3	575.0	0.900	0.650	0.001	0.045	0.500
		Cr_2O_3	576.3	1.200	0.500	0.001	20.0	0.500
		$Cr(OH)_3$	577.1	1.100	0.500	0.001	20.0	0.500
		CrO_3	578.3	0.700	0.500	0.001	20.0	0.500
		CrO_4^{2-}	579.3	0.700	0.500	0.001	20.0	0.500
	$Cr2p_{1/2}$	Cr	583.3	1.000	0.650	0.001	0.060	0.500
		Cr_2S_3	584.5	1.000	0.750	0.001	0.050	0.500
		Cr_2O_3	586.0	1.300	0.500	0.001	20.0	0.500
		$Cr(OH)_3$	586.8	1.200	0.500	0.001	20.0	0.500
		CrO_3	587.5	0.900	0.500	0.001	20.0	0.500
		CrO_4^{2-}	588.5	0.900	0.500	0.001	20.0	0.500

Table 6 (continued)
Standard parameters used for XPS spectrum deconvolution

Valence States			Compound	B. E. (eV)	FWHM (eV)	G/L	Tail Hight	Expnt Slope	Tail Mix
Mo	$Mo3d_{5/2}$	Mo	metal	227.7	0.600	0.75	0.001	0.150	0.500
		Mo^{4+}	MoO_2	229.0	0.800	0.50	0.001	0.110	0.500
			MoS_2	228.9	0.800	0.50	0.001	0.110	0.500
		Mo^{5+}	--	230.8	1.000	0.50	0.001	20.0	0.500
		Mo^{6+}	MoO_3	232.5	0.800	0.50	0.001	20.0	0.500
			MoO_4^{2-}	231.9	1.000	0.50	0.001	20.0	0.500
	$Mo3d_{3/2}$	Mo	metal	230.8	0.700	0.75	0.001	0.110	0.500
		Mo^{4+}	MoO_2	232.2	0.900	0.70	0.001	0.110	0.500
			MoS_2	232.0	0.900	0.70	0.001	0.110	0.500
		Mo^{5+}	--	233.9	1.100	0.50	0.001	20.0	0.500
		Mo^{6+}	MoO_3	235.8	0.900	0.50	0.001	20.0	0.500
			MoO_4^{2-}	235.1	1.100	0.50	0.001	20.0	0.500
S	S2p	S^{2-}	MoS_2	161.9	0.600	0.65	0.001	0.250	0.500
		SO_3^{2-}	Na_2SO_3	166.4	0.900	0.50	0.001	20.0	0.500
		$S_2O_3^{2-}$	$Na_2S_2O_3$	162.4	0.900	0.50	0.001	20.0	0.500
				168.5	0.900	0.50	0.001	20.0	0.500
		SO_4^{2-}	Na_2SO_4	169.6	0.900	0.50	0.001	20.0	0.500
		S2p, organic S in inoculated media		165.0	0.800	0.50	0.001	20.0	0.500
	S2s	S^{2-}	MoS_2	225.9	0.900	0.50	0.001	20.0	0.500
		SO_3^{2-}	Na_2SO_3	231.3	1.100	0.50	0.001	20.0	0.500
		$S_2O_3^{2-}$	$Na_2S_2O_3$	227.1	1.100	0.50	0.001	20.0	0.500
				232.2	1.100	0.50	0.001	20.0	0.500
		SO_4^{2-}	Na_2SO_4	233.0	1.100	0.50	0.001	20.0	0.500

Table 7

The cathodic slopes and open circuit potentials (OCP) of the SRB-exposed 304 and 317L SS coupons shown in potentiodynamic polarization in deaerated 0.1 M HCl

Cathodic slope		The sample conditions prior to the polarization test	
		In SRB for 5 days, rinsed/unrinsed	Control, rinsed/unrinsed
$-\beta_c$	304SS	-100 ± 45 mV/decade	-150 ± 28 mV/decade
	317LSS	-65 ± 20 mV/decade	-50 ± 18 mV/decade
OCP	304 SS	-510 ± 75 mV_{SCE}	-350 ± 20 mV_{SCE}
	317LSS	-470 ± 45 mV_{SCE}	-335 ± 20 mV_{SCE}

Table 8
Atomic percentages of the constituent alloying elements on the surfaces of the same batch of SRB-exposed 304 SS samples at different stages of the investigation

Surface conditions	Atomic percentage of alloy elements (%at)			TOA
	Fe	Cr	Ni	
as polished (6 μm diamond finish).	70	28	2	20°
	72	25	3	50°
Control, rinsed	35	56	9	20°
	36	56	8	50°
exposed to SRB for 5 days, rinsed	32	57	11	20°
	39	54	7	50°
Control, unrinsed	--	--	--	20°
	--	--	--	50°
exposed to SRB for 5 days, unrinsed	--	--	--	20°
	--	--	--	50°
control, rinsed, and then polarized at -160 mV_{SCE} in 0.1 M HCl.	21	78	1	20°
	22	76	2	50°
exposed to SRB, rinsed and then polarized at -160 mV_{SCE} in 0.1 M HCl.	43	41	16	20°
	33	46	21	50°
control, unrinsed, and then polarized at -160 mV_{SCE} in 0.1 M HCl (Ar^+ etched 5 seconds).	24	72	4	20°
	21	76	3	50°
exposed to SRB, unrinsed and then polarized at -160 mV_{SCE} in 0.1 M HCl (Ar^+ etched 5 seconds).	63	28	10	20°
	66	19	15	50°

Table 9

Fractional areas of iron sulfides and nickel sulfides remaining in the outer (TOA=20°) and inner (TOA=50°) surface regions of the same batch of the SRB exposed-samples after the potentiostatic polarization in deaerated 0.1 M HCl

Sample		TOA	FeS (%)	NiS (%)
304SS	Immediately after the exposure to SRB	20°	6.9 ~ 7.3	5.3 ~ 5.5
		50°	~ 11.2	~ 5.6
	Exposed to SRB, rinsed and then polarized at -160 mV_{SCE} in 0.1 M HCl	20°	--	--
		50°	~ 7.6	~ 9.2
317LSS	Immediately after the exposure to SRB	20°	~ 7.0	~ 6.4
		50°	~ 5.9	~ 1.9
	Exposed to SRB, rinsed and then polarized at -160 mV_{SCE} in 0.1 M HCl	20°	~ 5.0	--
		50°	~ 1.5	--

Table 10
Atomic percentages of the constituent alloying elements on the surfaces of the same batch of SRB-exposed 317L SS samples at different stages of the investigation

Surface conditions	Atomic percentage of alloy elements (5%at)				TOA
	Fe	Cr	Mo	Ni	
as polished, (6 μm diamond finish)	73.5	18.5	4	4	20°
	71.5	20.5	3	5	50°
control, rinsed	33	54	5	8	20°
	36	48	9	7	50°
exposed to SRB for 5 days, rinsed	37.5	50	2.5	10	20°
	44	46	2	8	50°
Control, unrinsed	--	--	--	--	20°
	--	--	--	--	50°
exposed to SRB for 5 days, unrinsed.	--	--	--	--	20°
	--	--	--	--	50°
Control, rinsed and then polarized at -160 mV_{SCE} in 0.1 M HCl.	14	75	7	4	20°
	22	64	7	7	50°
exposed to SRB, rinsed and then polarized at -160 mV_{SCE} in 0.1 M HCl.	34	51	9	6	20°
	26	59	6	9	50°
Control, unrinsed and then polarized at -160 mV_{SCE} in 0.1 M HCl.	35	57	6.5	1.5	20°
	33	55	5	7	50°
exposed to SRB, unrinsed and then polarized at -160 mV_{SCE} in 0.1 M HCl.	49	47	3	1	20°
	43	45	6	6	50°

Table 11
The atomic percentage of Mo compounds on the surfaces of the pure Mo coupons at different stages of the investigation

Table 11a. From the rinsed surfaces of Mo coupons

Samples	Type of Mo compounds (%at)						
	Mo	MoO_2	MoS_2	Mo^{5+}	MoO_4^{2-}	MoO_3	TOA
SRB-exposed, rinsed	36	6	15	27	16	--	10°
	42	9	16	23	10	--	20°
	55	9	15	15	6	--	50°
Control, rinsed	48	26	--	26	--	--	10°
	59	25	--	16	--	--	20°
	72	17	--	11	--	--	50°
SRB-exposed, rinsed and then polarized at -160 mV_{SCE} in 0.1 M HCl	43	19	14	18	6	--	10°
	47	16	14	15	8	--	20°
	60	17	10	13	--	--	50°
Control, rinsed and then polarized at -160 mV_{SCE} in 0.1 M HCl	52	31	--	17	--	--	10°
	64	28	--	8	--	--	20°
	76	19	--	5	--	--	50°

Table 11 (continued)
The atomic percentage of Mo compounds on the surfaces of the pure Mo coupons at different stages of the investigation

Table 11b. From the unrinsed surfaces of Mo coupons*

Samples	Type of Mo compounds (%at)						
	Mo	MoO_2	MoS_2	Mo^{5+}	MoO_4^{2-}	MoO_3	TOA
SRB-exposed, unrinsed and then polarized at -160 mV_{SCE} in 0.1 M HCl	--	--	--	--	--	--	10°
	36	12	19	33	--	--	20°
	39	13	17	31	--	--	50°
Control, unrinsed and then polarized at -160 mV_{SCE} in 0.1 M HCl	42	26	--	22	10	--	10°
	47	26	--	18	9	--	20°
	56	25	--	19	--	--	50°

* Note: The data from the unrinsed Mo coupons were not obtained immediately after the exposure because the surfaces were covered by the excess biomass.

Table 12
The culture growth and sulfate reduction during the exposure of the Mo thin films and Mo powders

Sample	Turbidity (600nm)	pH	Residual sulfate (ppm)
2 day growth			
culture without Mo	0.62	7.36	167
culture w/ Mo thin film	0.41	7.39	1120
culture w/ 1 g/l Mo	0.74	7.36	100
culture w/ 1.44 g/l MoO_3*	0.06	6.69	1320
culture previously grew for 2 days, then 1 g/l Mo added and incubated for 2 days	0.50	7.70	400
uninoculated medium	0.02	7.34	1410
5 day growth			
culture without Mo	0.19	7.18	111
culture w/ Mo thin film	0.32	7.20	447
culture w/ 1 g/l Mo	0.26	7.37	50
culture w/ 1.44 g/l MoO_3	0.06	6.72	1280
culture previously grew for 2 days, then 1 g/l Mo added and incubated for 5 days	0.20	7.45	130
uninoculated medium	0.03	7.40	1380

* Solubility of MoO_3 in cold water: 7.41 mM.

Table 13
The culture growth and sulfate reduction
in the medium containing 0.21 g/l $Cr(OH)_3$

Sample	Turbidity (600nm)	pH	Residual sulfate (ppm)
2 day growth			
culture without $Cr(OH)_3$	0.62	7.36	167
culture w/ 0.21 g/l $Cr(OH)_3$	0.56	7.30	310
	0.57	7.25	315
culture w/ 2 mM $Cr_2(SO_4)_3$	0.61	7.28	350
	0.60	7.25	330
uninoculated medium	0.02	7.34.	1410
5 day growth			
culture without Mo	0.19	7.18	111
culture w/ 0.21 g/l $Cr(OH)_3$	0.21	7.21	100
	0.22	7.10	130
culture w/ 2 mM $Cr_2(SO_4)_3$	0.18	7.17	140
	0.19	7.15	135
uninoculated medium	0.03	7.40	1380

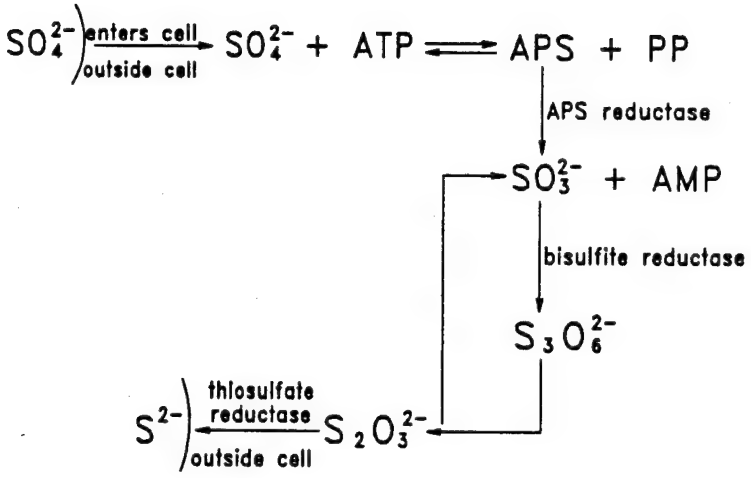

Figure 1. A possible metabolic pathway of sulfate reduction by SRB

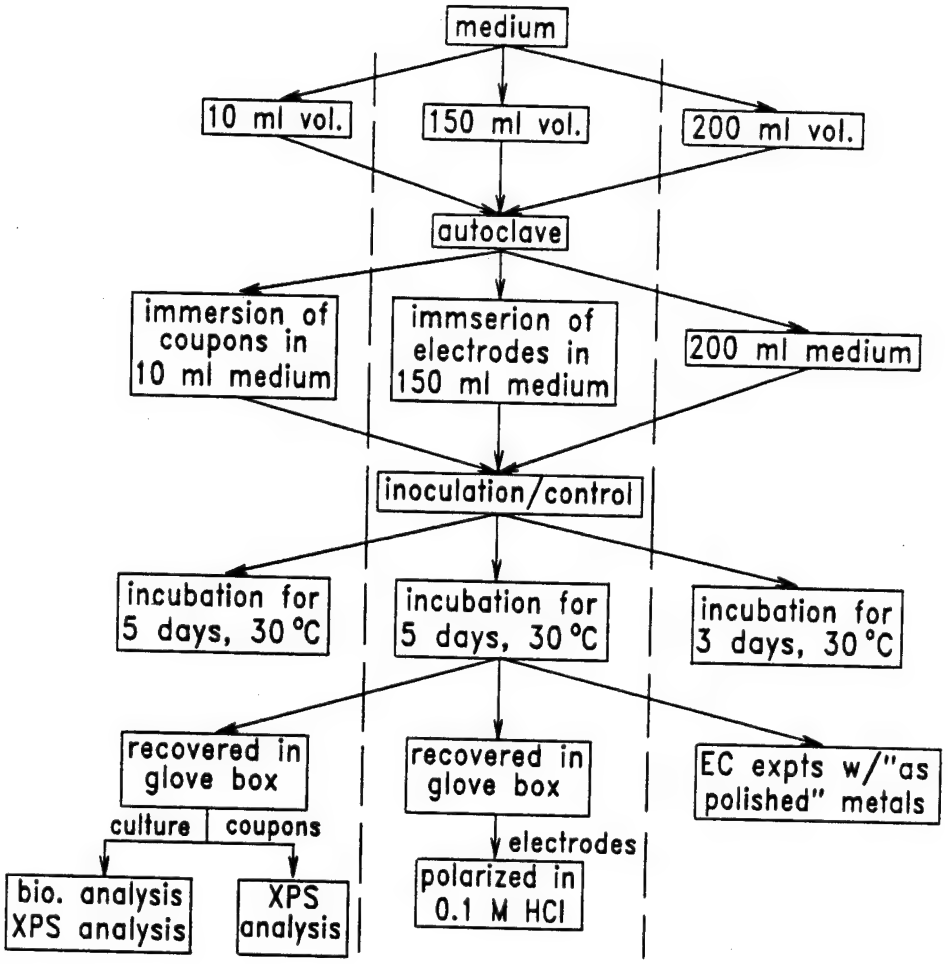

Figure 2a. Flow diagram of the experimental procedures for exposure of metal samples to SRB and subsequent analyses by XPS and DC polarization in deaerated 0.1 M HCl, and for potentiodynamic polarization of the "as polished" metal coupons in stationary stage culture

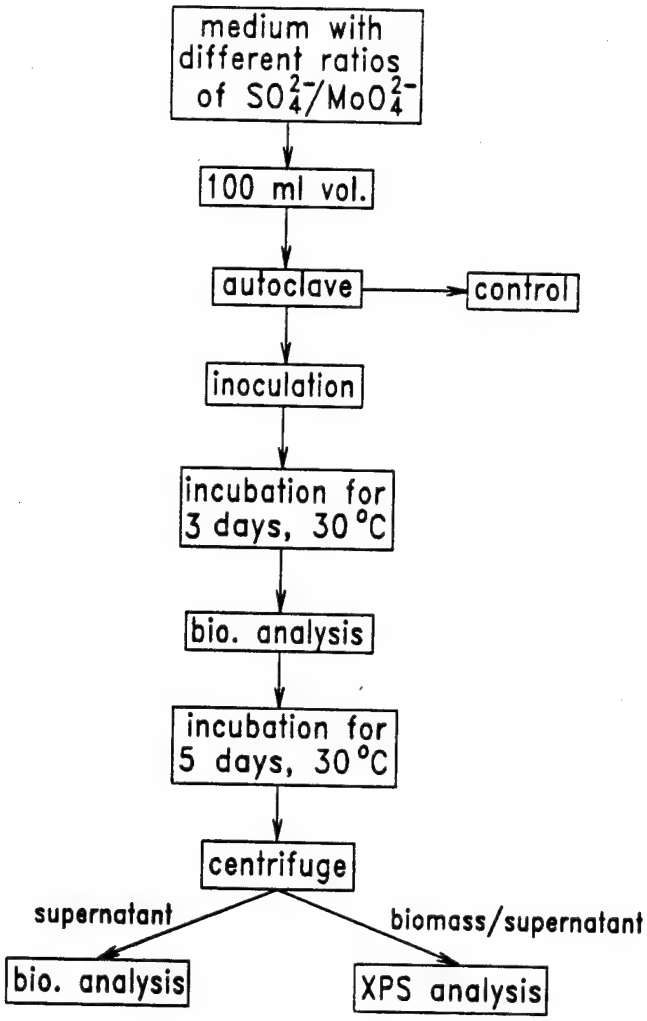

Figure 2b. Flow diagram for study of interaction of SRB with low concentrations of molybdate

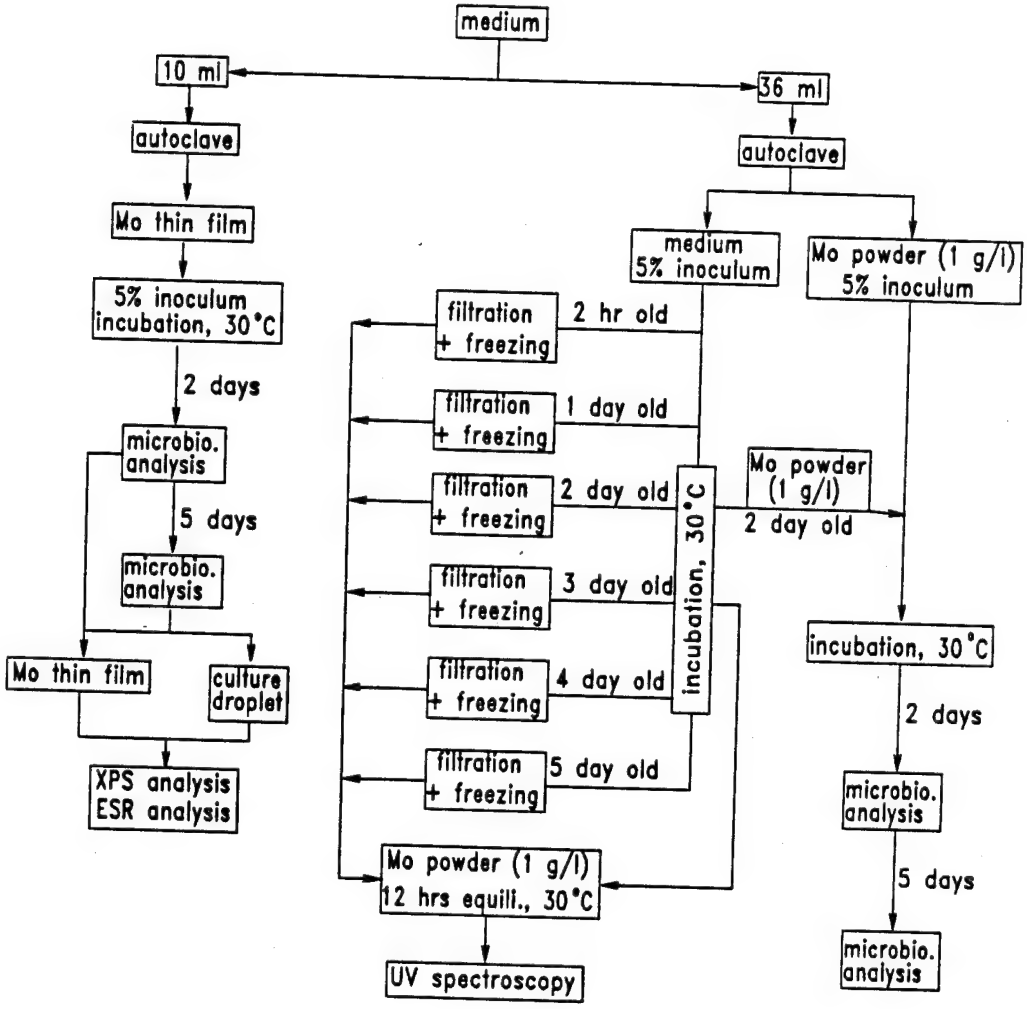

Figure 2c. Flow diagram for XPS and UV analyses of the interaction of SRB with Mo thin films and Mo powders

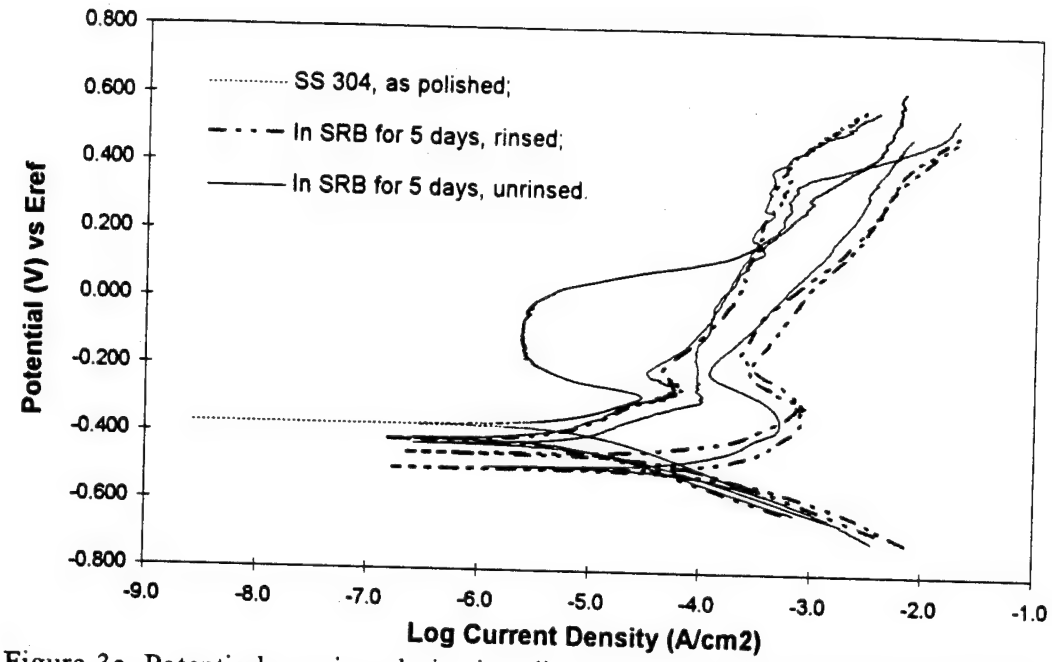

Figure 3a. Potentiodynamic polarization diagrams of 304 SS in deaerated 0.1 M HCl following exposure to SRB for 5 days

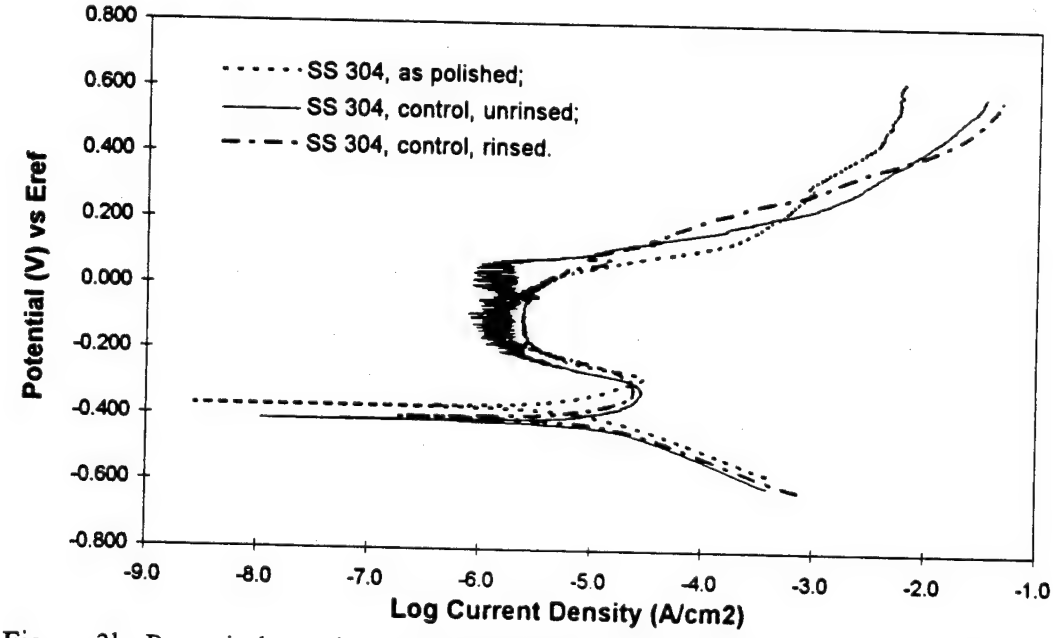

Figure 3b. Potentiodynamic polarization diagrams of the control samples of 304 SS in deaerated 0.1 M HCl

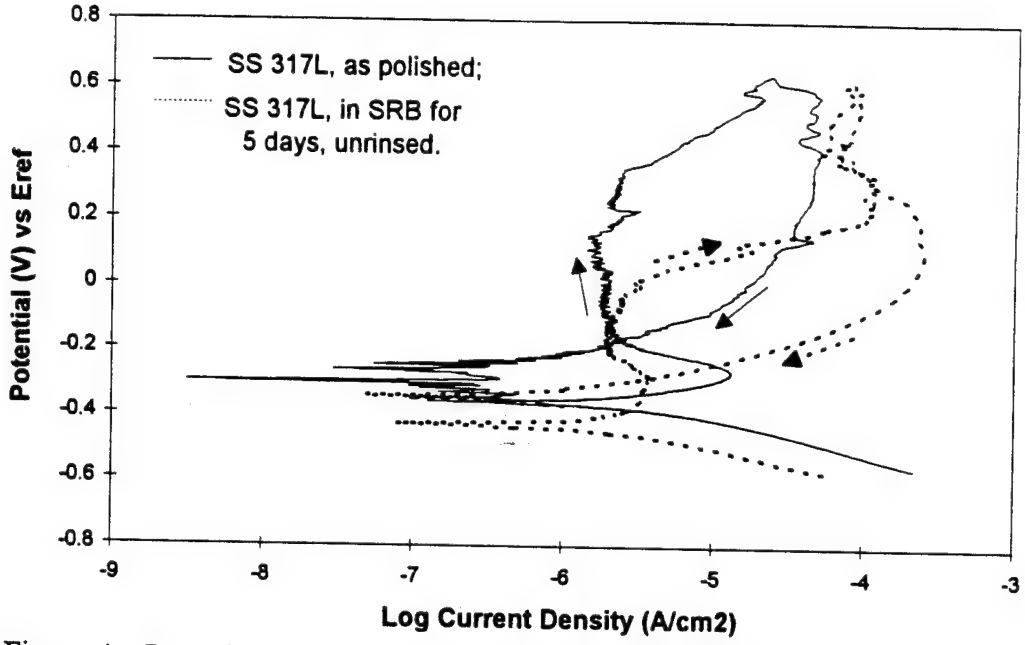

Figure 4a. Potentiodynamic polarization diagrams of 317L SS in deaerated 0.1 M HCl following exposure to SRB for 5 days, unrinsed prior to the test

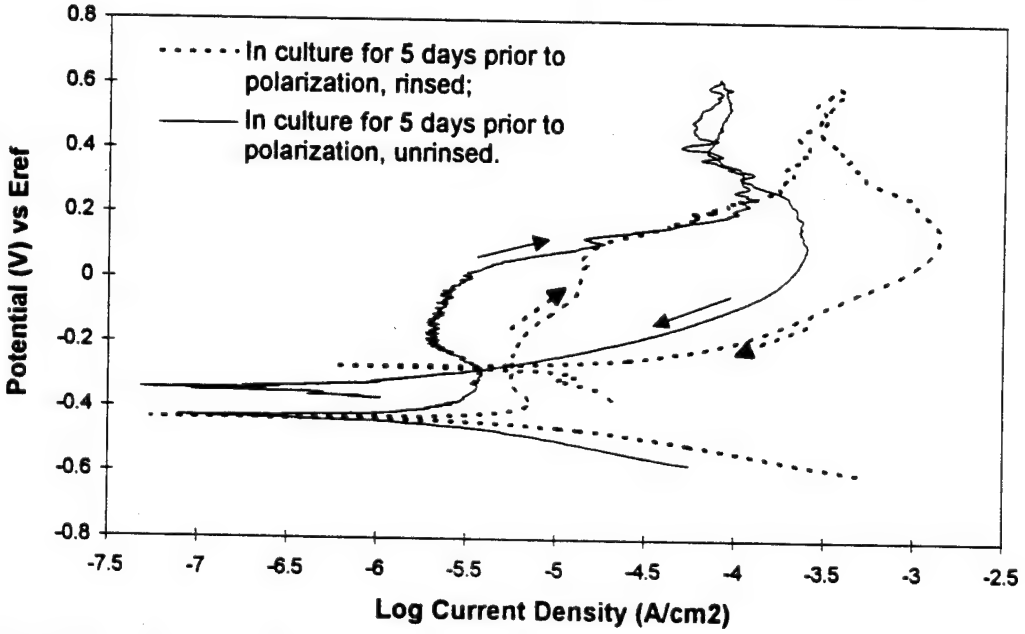

Figure 4b. The role of biofilm in the passivation performance of the SRB exposed 317L SS shown in the polarization diagrams in 0.1 M HCl.

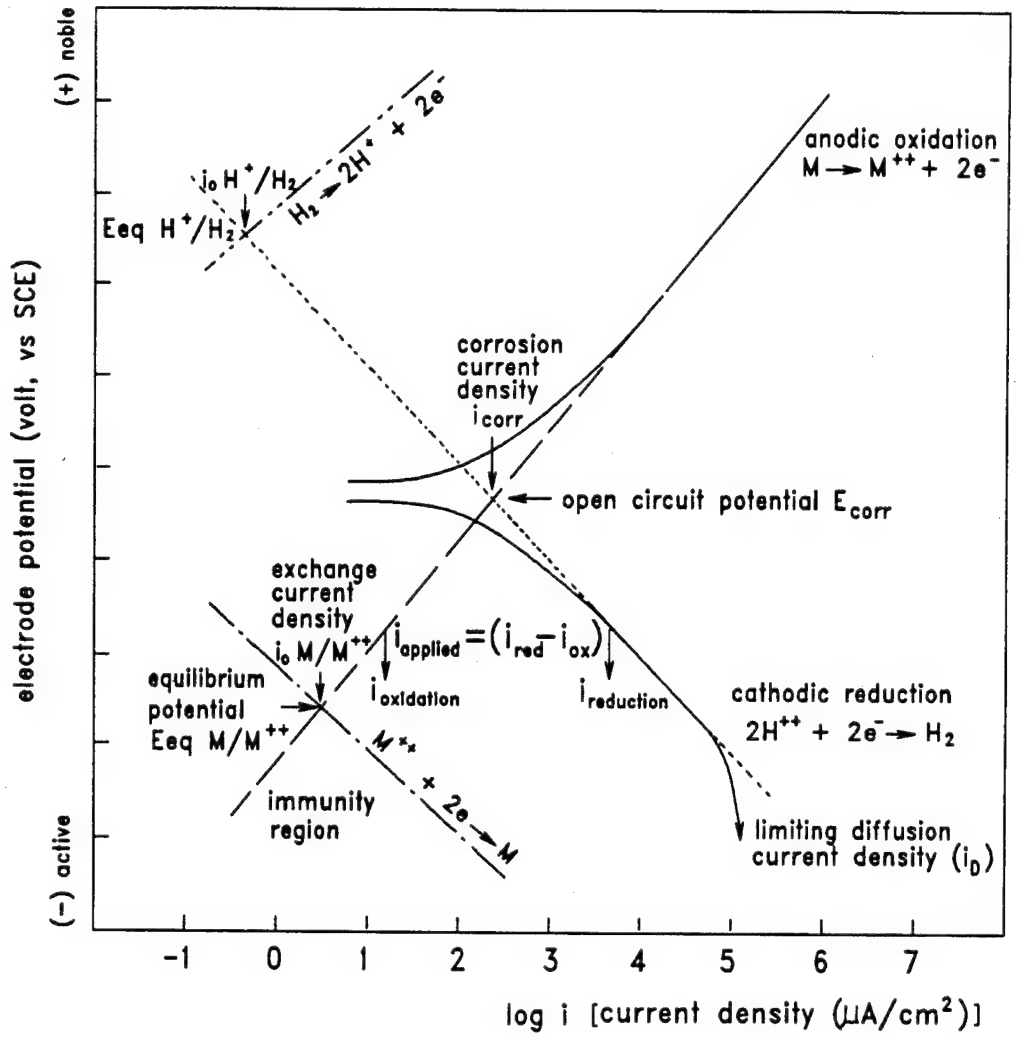

Figure 5. An illustration of the electrochemical significance of the Stern-Geary equation.

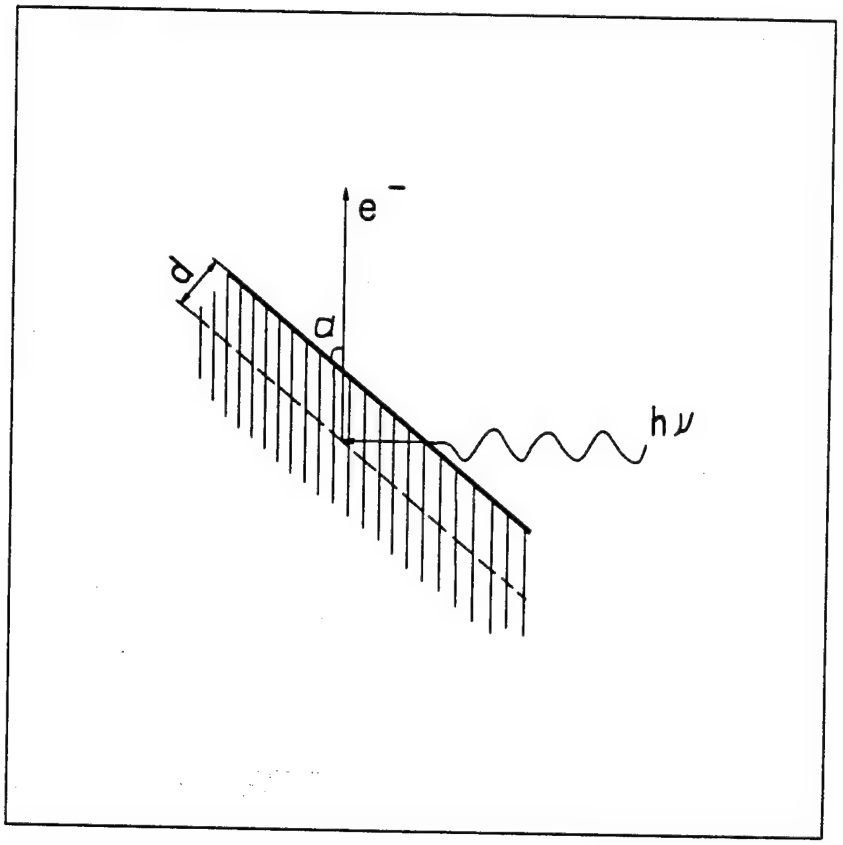

Figure 6. A schematic of sampling depth vs. take-off angles of photoelectrons in XPS analysis

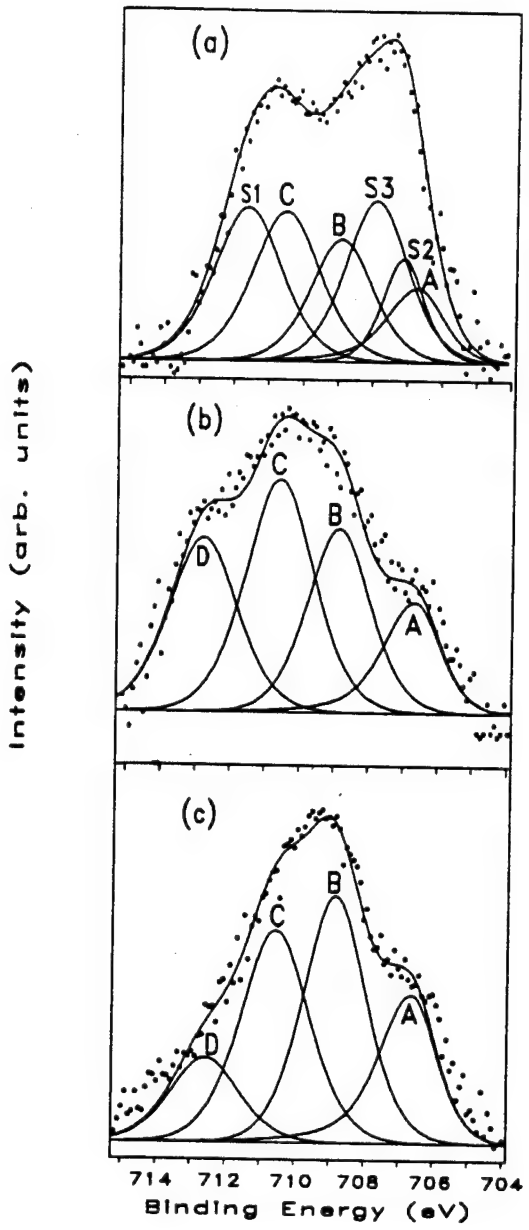

A: Fe; B: Fe^{2+}; C: Fe^{3+}; D: $Fe(OOH)_{\alpha}$; S1: FeS; S2: FeS_2; S3: $Fe_{1-x}S$.

Figure 7. Fe2p spectra from the surfaces of 304 SS, TOA: 20°. (a) In SRB for 5 days, rinsed; (b) A control sample; (c) "As polished".

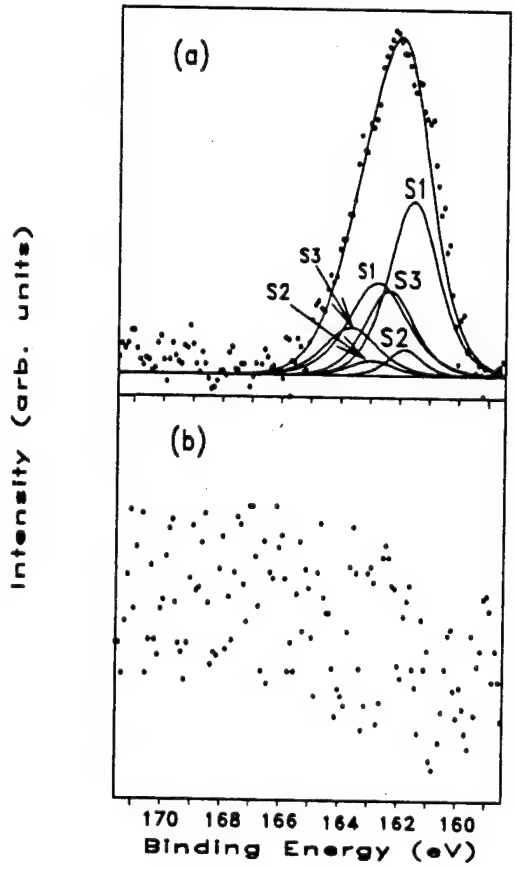

S1: FeS, NiS, Cr_2S_3; S2: FeS_2; S3: $Fe_{1-x}S$.

Figure 8. S2p spectra from the surfaces of 304 SS after the exposure, TOA: 20°. (a) In SRB for 5 days, rinsed; (b) A control sample

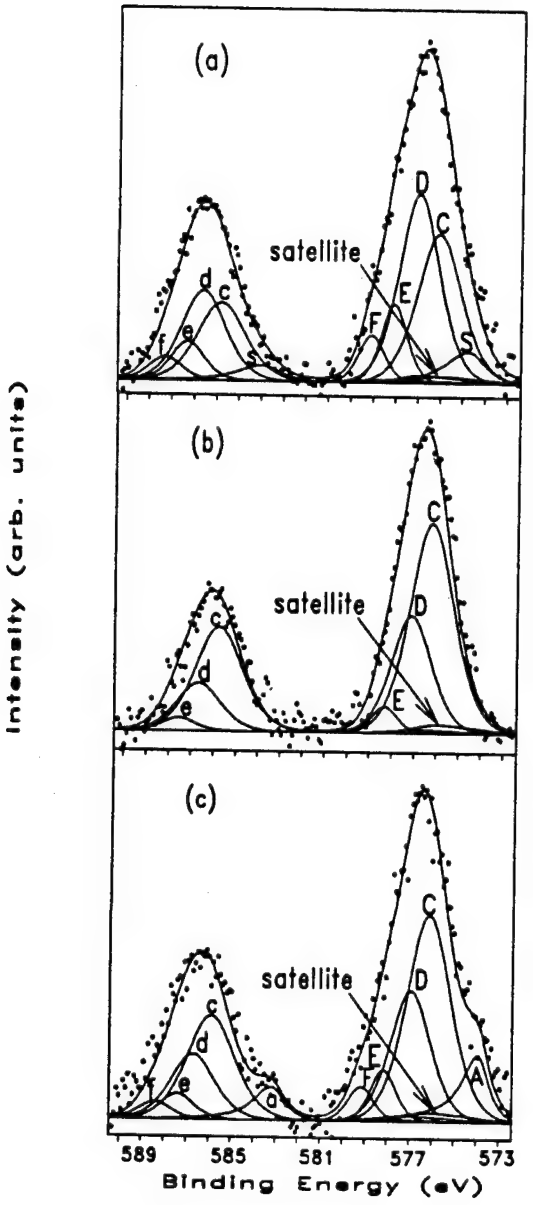

A, a: Cr; C, c: Cr_2O_3; D, d: $Cr(OH)_3$; E, e: CrO_3; F, f: CrO_4^{2-}; S, s: Cr_2S_3.

Figure 9. Cr2p spectra from the surfaces of 304 SS, TOA: 20°. (a) In SRB for 5 days, rinsed; (b) A control sample; (c) "As polished".

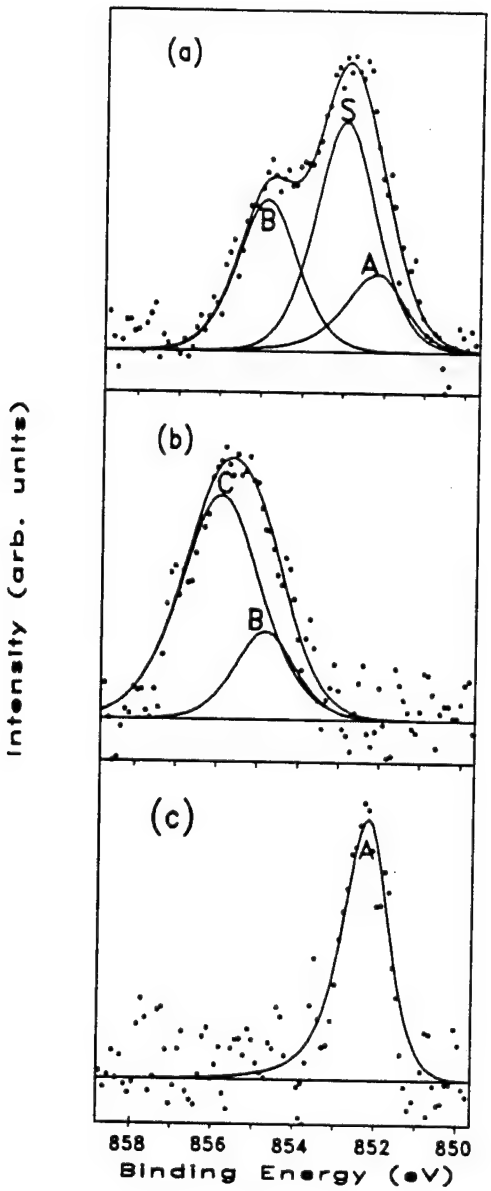

A: Ni; B: Ni^{2+}; C: $Ni(OH)_2$; S: NiS.

Figure 10. Ni2p spectra from the surfaces of 304 SS, TOA: 20°. (a) In SRB for 5 days, rinsed; (b) A control sample; (c) "As polished"

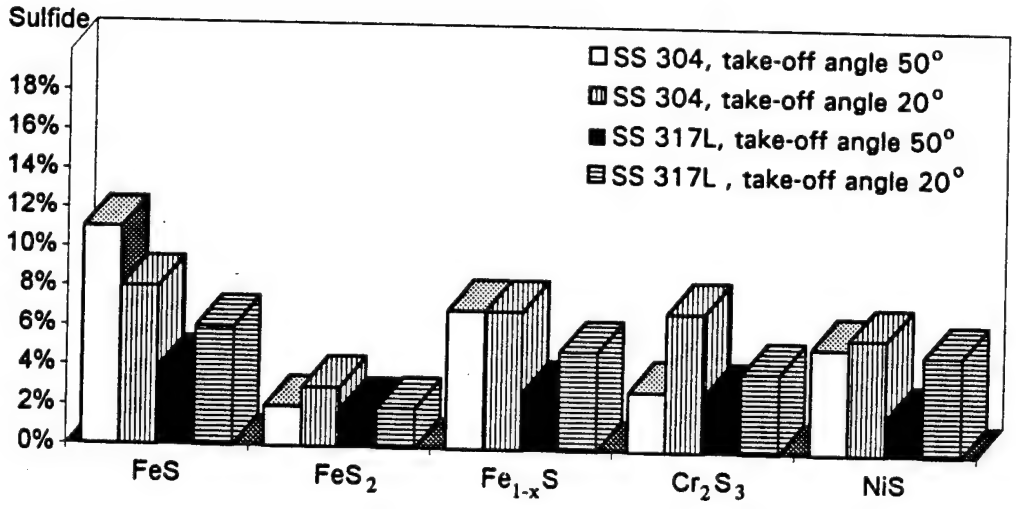

Figure 11. Relative proportions of sulfides in the percentage of total metal content, formed on the surfaces of 304 and 317L SS coupons during the exposure to SRB

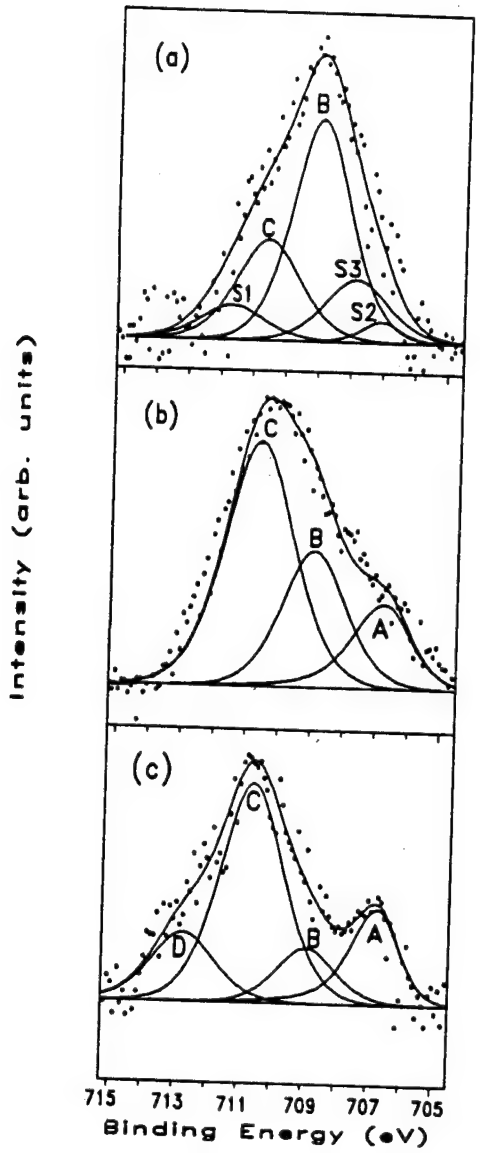

A: Fe; B: Fe^{2+}; C: Fe^{3+}; D: $Fe(OOH)_{\alpha}$; S1: FeS; S2: FeS_2; S3: $Fe_{1-x}S$.

Figure 12. Fe2p spectra on the surfaces of 304 SS after the potentiostatic polarization at -160 mV_{SCE} for 5 minutes in deaerated 0.1 M HCl, TOA: 20°. (a) Previously in SRB for 5 days, rinsed; (b) A control sample; (c) "As polished".

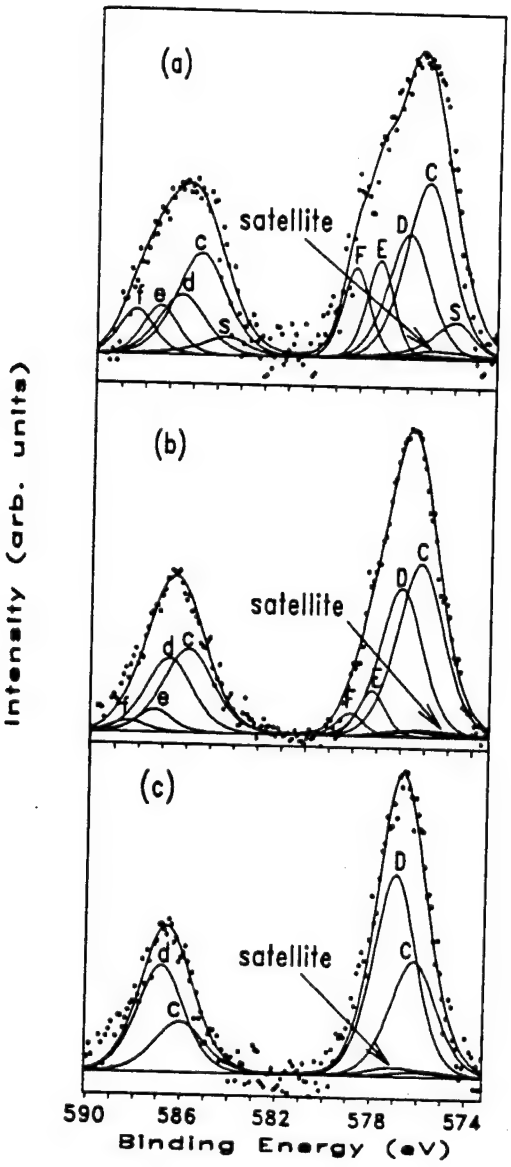

C, c: Cr_2O_3; D, d: $Cr(OH)_3$; E, e: CrO_3; F, f: CrO_4^{2-}; S, s: Cr_2S_3.

Figure 13. Cr2p spectra on the surfaces of 304 SS after the potentiostatic polarization at -160 mV_{SCE} for 5 minutes in deaerated 0.1 M HCl, TOA: 20°. (a) Previously in SRB for 5 days, rinsed; (b) A control sample; (c) "As polished".

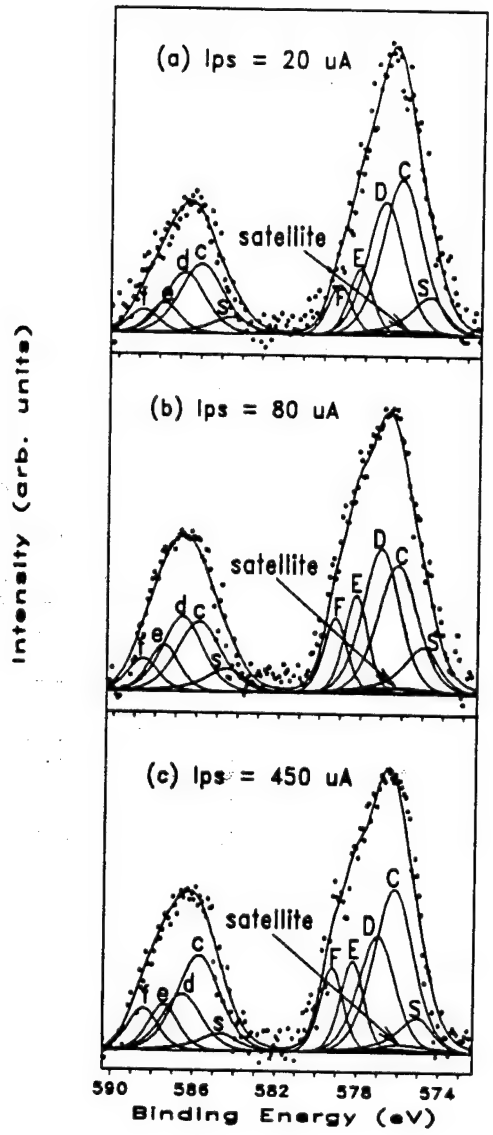

C, c: Cr_2O_3; D, d: $Cr(OH)_3$; E, e: CrO_3; F, f: CrO_4^{2-}; S, s: Cr_2S_3.

Figure 14. Polarization current vs the resultant hexavalent chromium on the surfaces of 304 SS formed during the potentiostatic polarization at -160 mV_{SCE} in deaerated 0.1 M HCl for 5 minutes after the exposure to SRB, TOA: 20°. (a) I_{ps} = 20 μA; (b) I_{ps} = 80 μA; (c) I_{ps} = 450 μA.

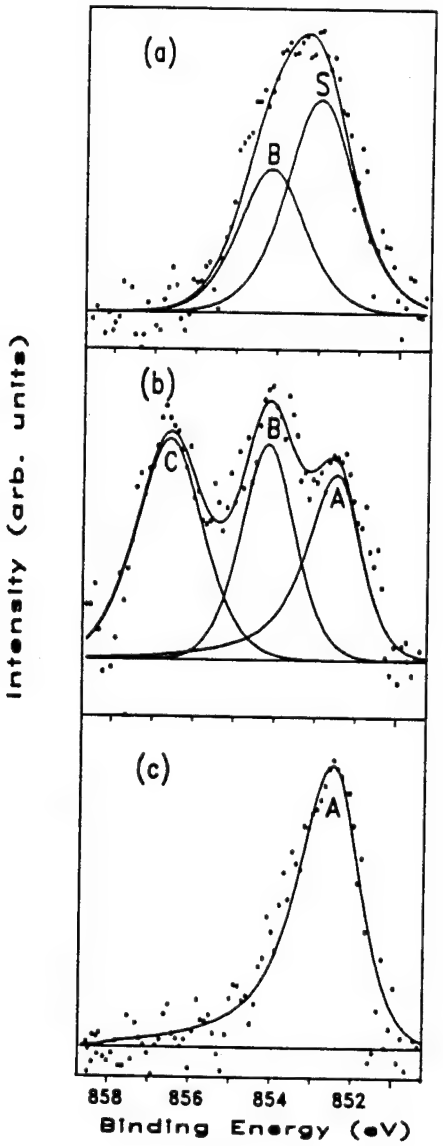

A: Ni; B: Ni^{2+}; C: $Ni(OH)_2$; S: NiS.

Figure 15. Ni2p spectra on the surfaces of 304 SS after the potentiostatic polarization at -160 mV_{SCE} for 5 minutes in deaerated 0.1 M HCl, TOA: 20°. (a) Previously in SRB for 5 days, rinsed; (b) A control sample; (c) "As polished".

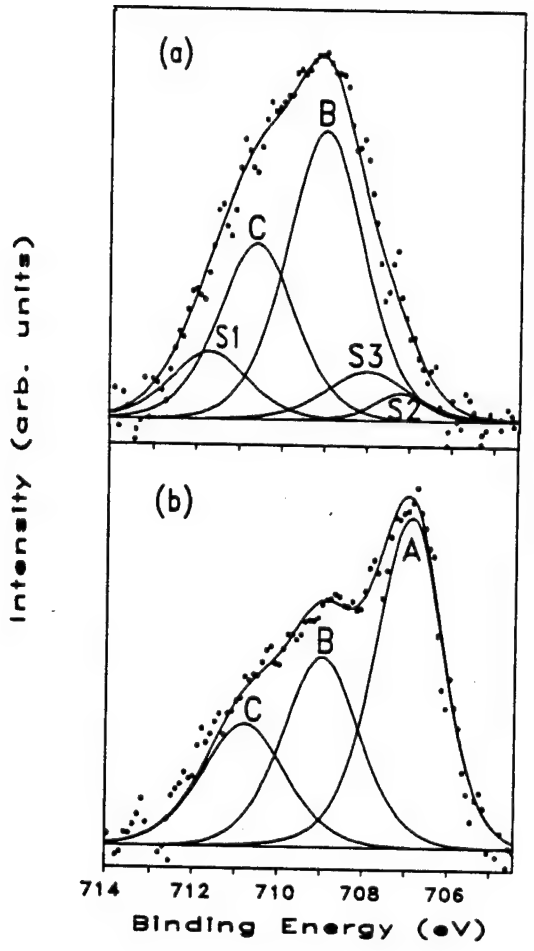

A: Fe; B: Fe^{2+}; C: Fe^{3+}; S1: FeS; S2: FeS_2; S3: $Fe_{1-x}S$.

Figure 16. Fe2p spectra from the surfaces of 304 SS after the potentiostatic polarization at -160 mV_{SCE} for 5 minutes in deaerated 0.1 M HCl, TOA: 50°, Ar^+ etched for 5 seconds. (a) Previously in SRB for 5 days, unrinsed; (b) A control sample.

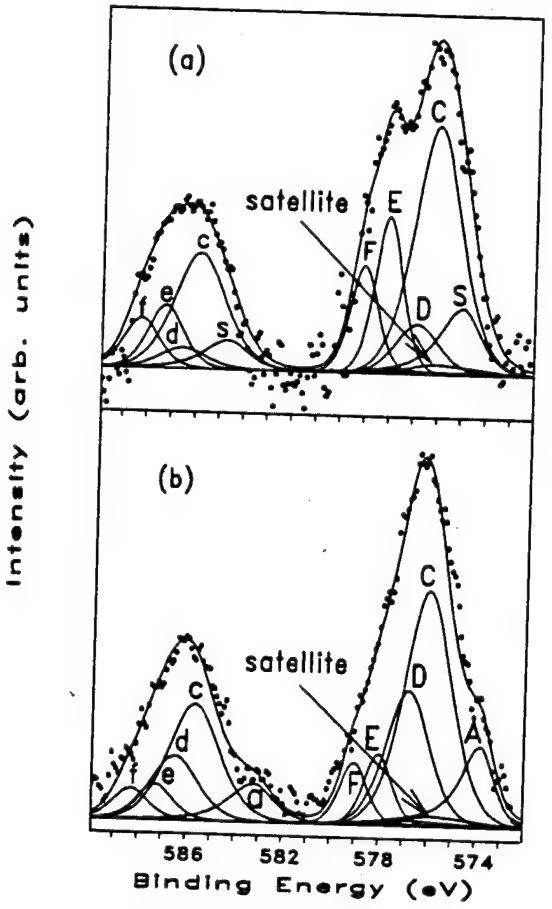

A, a: Cr; C, c: Cr_2O_3; D, d: $Cr(OH)_3$; E, e: CrO_3; F, f: CrO_4^{2-}; S, s: Cr_2S_3.

Figure 17. Cr2p spectra from the surfaces of 304 SS after the potentiostatic polarization at -160 mV_{SCE} for 5 minutes in deaerated 0.1 M HCl, TOA: 50°, Ar^+ etched for 5 seconds. (a) Previously in SRB for 5 days, unrinsed; (b) A control sample.

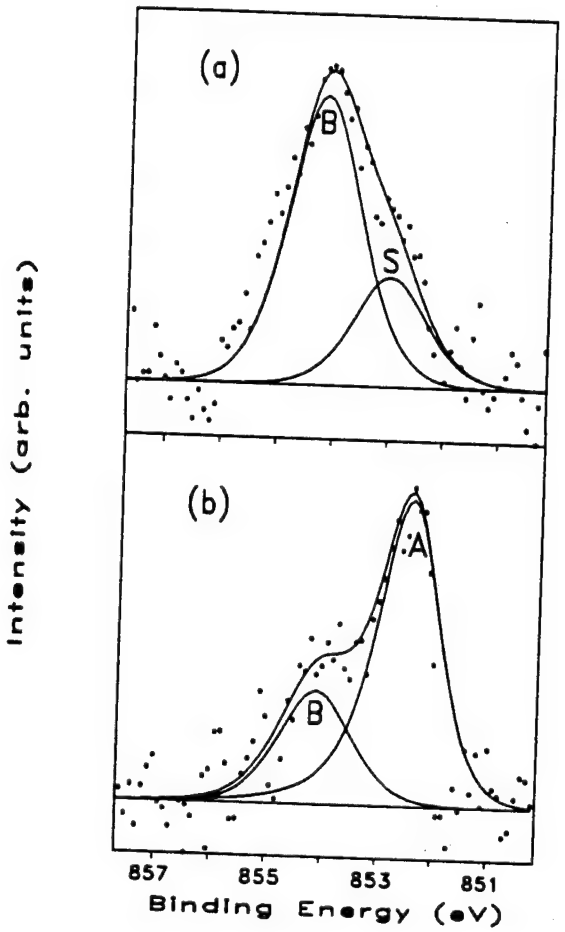

A: Ni; B: Ni^{2+}; S: NiS.

Figure 18. Ni2p spectra from the surfaces of 304 SS after the potentiostatic polarization at -160 mV_{SCE} for 5 minutes in deaerated 0.1 M HCl, TOA: 50°, Ar^+ etched for 5 seconds. (a) Previously in SRB for 5 days, unrinsed; (b) A control sample.

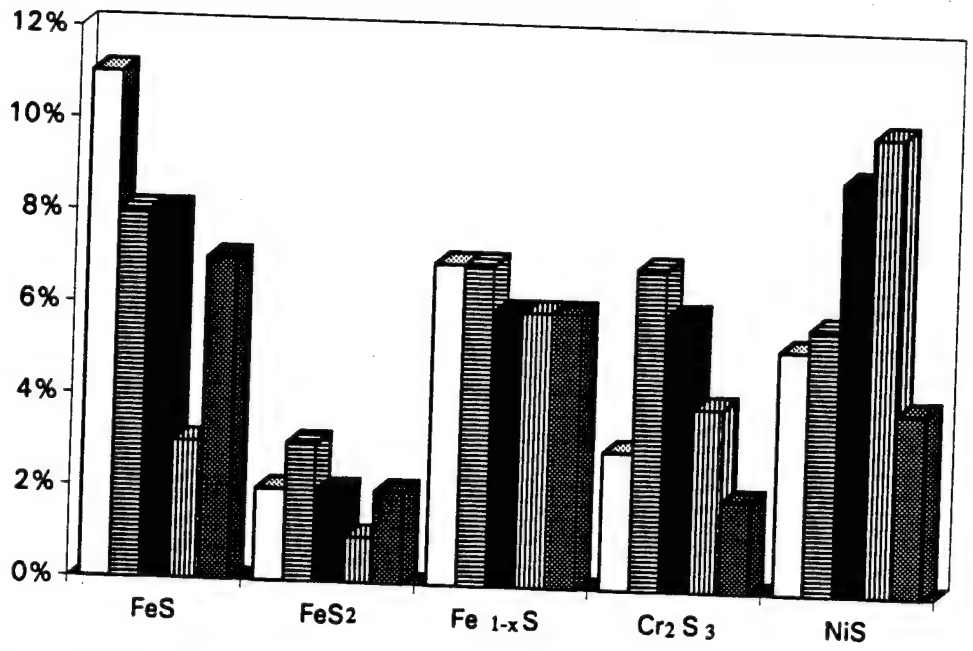

Figure 19. Relative proportions of sulfides on the surfaces of 304 SS in the percentage of total contents of the alloying elements.

- Immediately after the 5 day exposure to SRB, rinsed, toa: 50°;
- Immediately after the 5 day exposure to SRB, rinsed, toa: 20°;
- After polarization at -160 mV_{SCE} for 5 minutes in 0.1 M HCl following the 5 day exposure to SRB, rinsed, toa: 50°;
- After polarization at -160 mV_{SCE} for 5 minutes in 0.1 M HCl following the 5 day exposure to SRB, rinsed, toa: 20°;
- After polarization at -160 mV_{SCE} for 5 minutes in 0.1 M HCl following the 5 day exposure to SRB, unrinsed, toa: 50°.

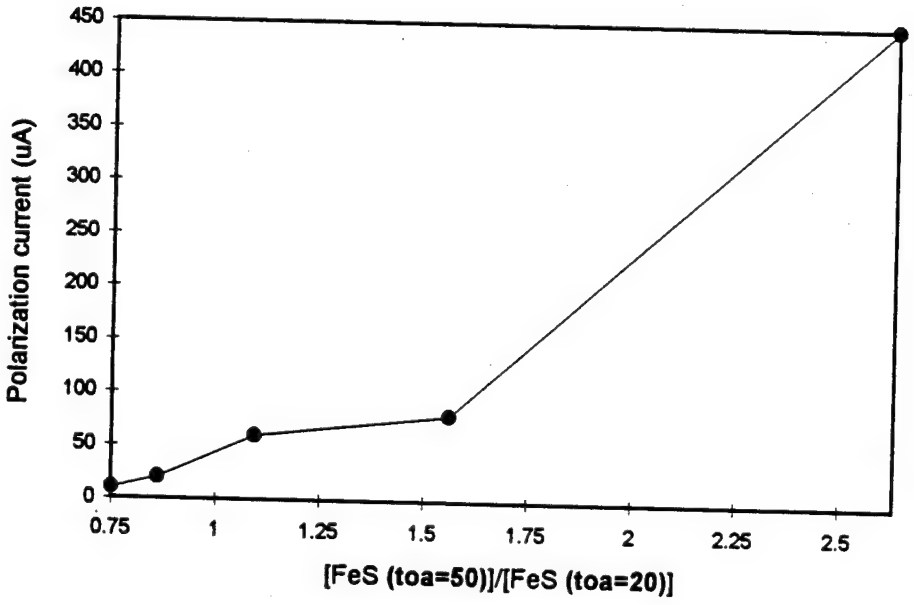

Figure 20. The polarization current vs the ratios of the residual FeS in the inner region (TOA = 50°) to the one in the outer region (TOA = 20°) of the SRB-exposed 304 SS coupons determined by variable angle XPS analysis after the potentiostatic polarization in the hydrochloric solution.

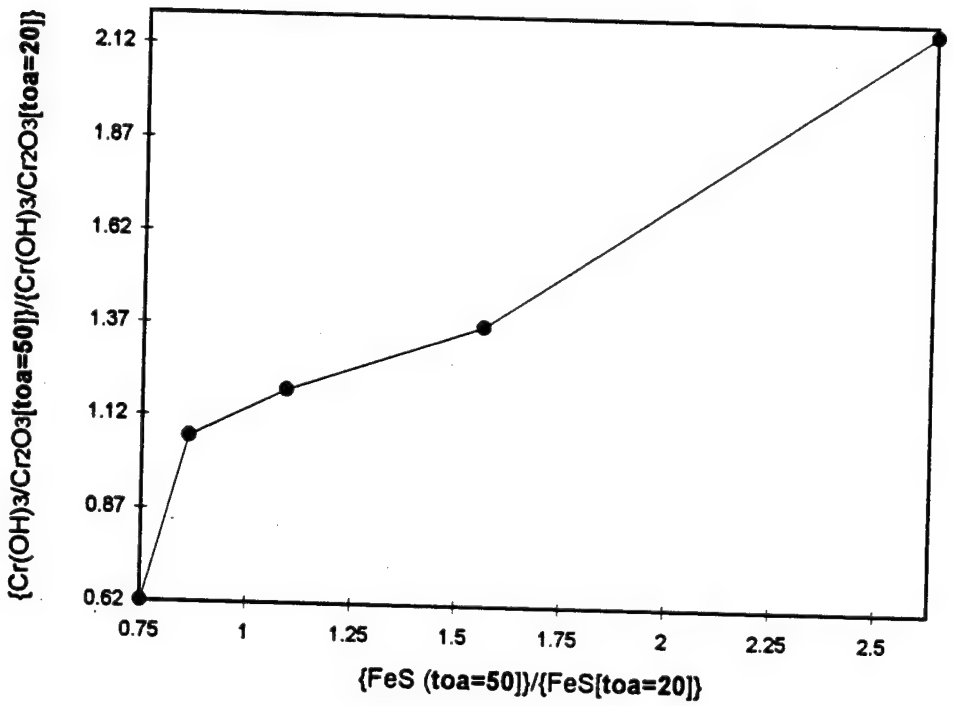

Figure 21. The ratios of the relative proportion of $Cr(OH)_3$ to Cr_2O_3 in the inner region to the one in the outer region vs the variable sulfidation with the depth of the surface films of SRB-exposed 304 SS coupons determined by variable angle XPS after the potentiostatic polarization in the hydrochloric solution.

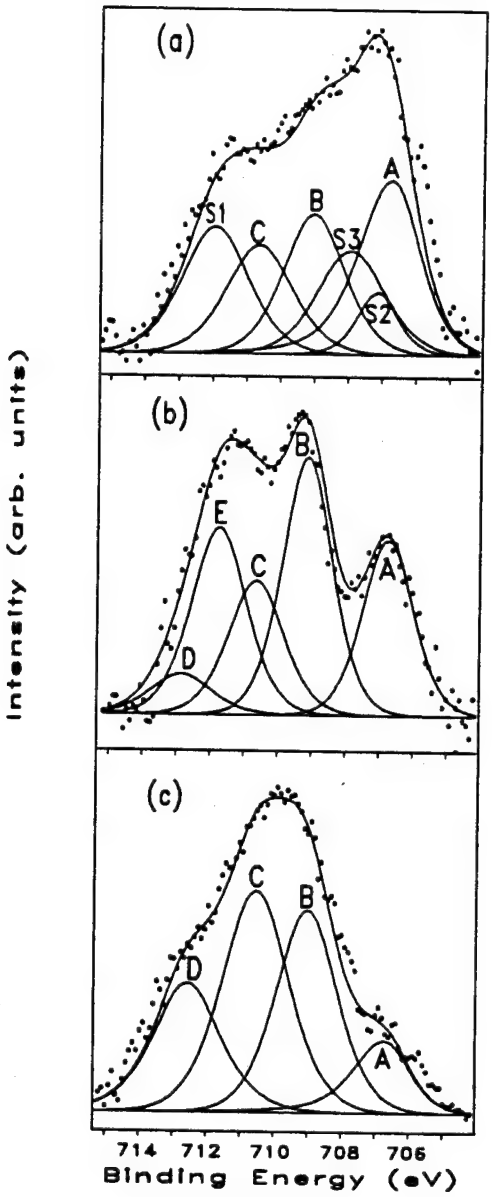

A: Fe; B: Fe^{2+}; C: Fe^{3+}; D: $Fe(OOH)_{\alpha}$; E: $Fe(OOH)_{\gamma}$;
S1: FeS; S2: FeS_2; S3: $Fe_{1-x}S$.

Figure 22. Fe2p spectra from the surfaces of 317L SS, TOA: 20°. (a) In SRB for 5 days, rinsed; (b) A control sample; (c) "As polished".

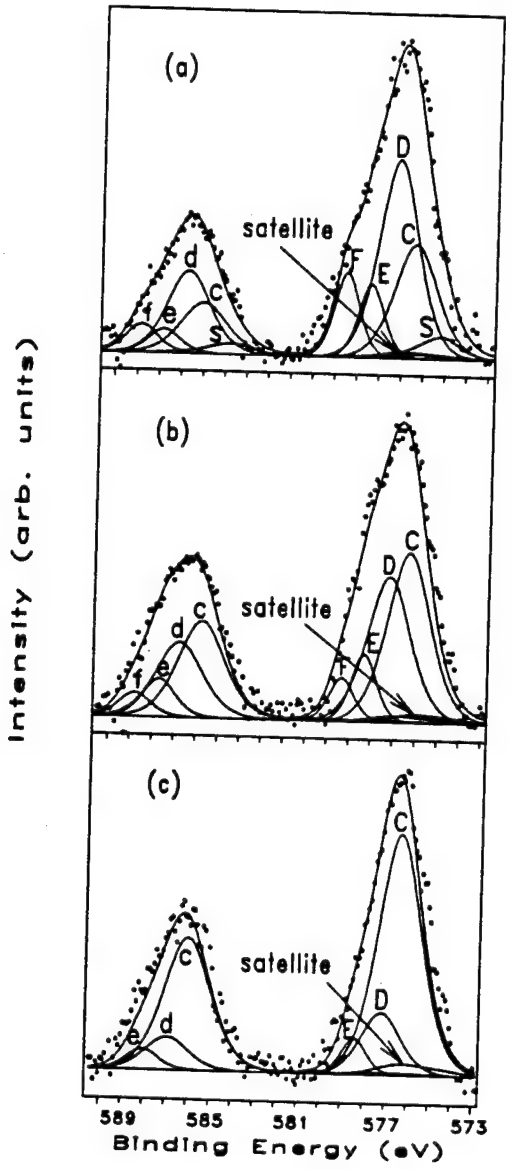

C, c: Cr_2O_3; D, d: $Cr(OH)_3$; E, e: CrO_3; F, f: CrO_4^{2-}; S, s: Cr_2S_3.

Figure 23. Cr2p spectra from the surfaces of 317L SS, TOA: 20°. (a) In SRB for 5 days, rinsed; (b) A control sample; (c) "As polished".

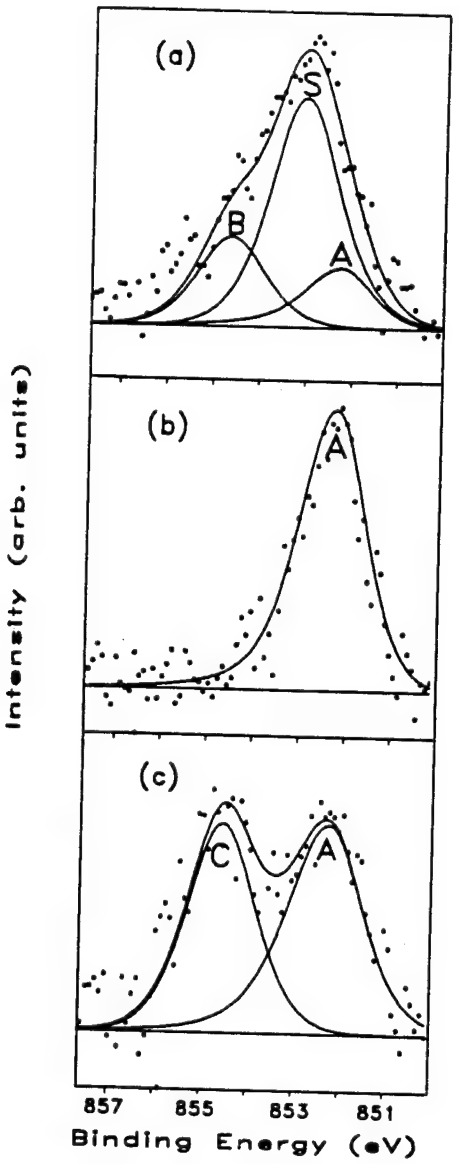

A: Ni; B: Ni^{2+}; C: $Ni(OH)_2$; S: NiS.

Figure 24. Ni2p spectra from the surfaces of 317L SS, TOA: 20°. (a) In SRB for 5 days, rinsed; (b) A control sample; (c) "As polished".

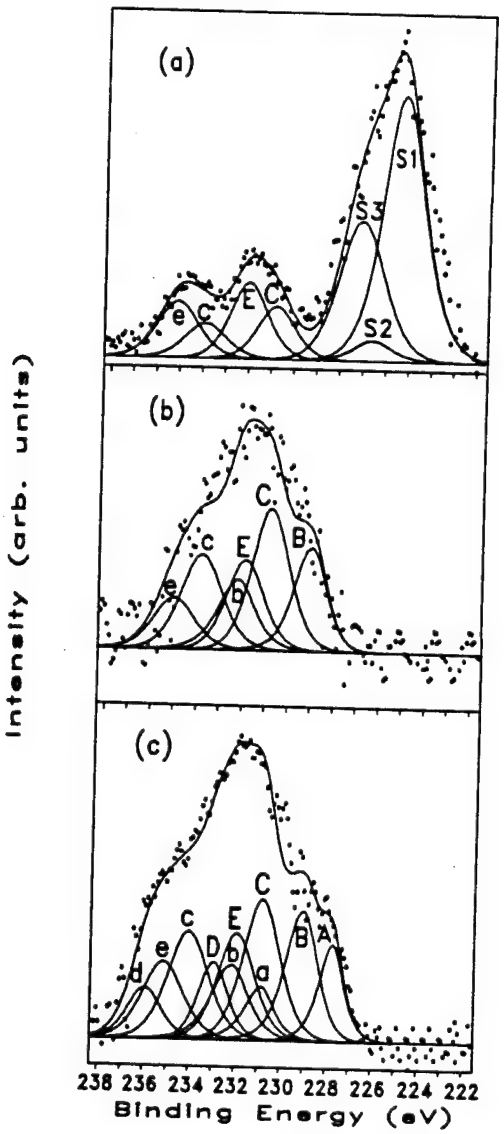

A, a: Mo; B, b: Mo^{4+}; C, c: Mo^{5+}; D, d: MoO_3; E, e: MoO_4^{2-}; S1: S2s of FeS, NiS, Cr_2S_3 and MoS_2; S2: S2s of FeS_2; S3: S2s of $Fe_{1-x}S$.

Figure 25. Mo3d spectra from the surfaces of 317L SS, TOA: 20°. (a) In SRB for 5 days, rinsed; (b) A control sample; (c) "As polished".

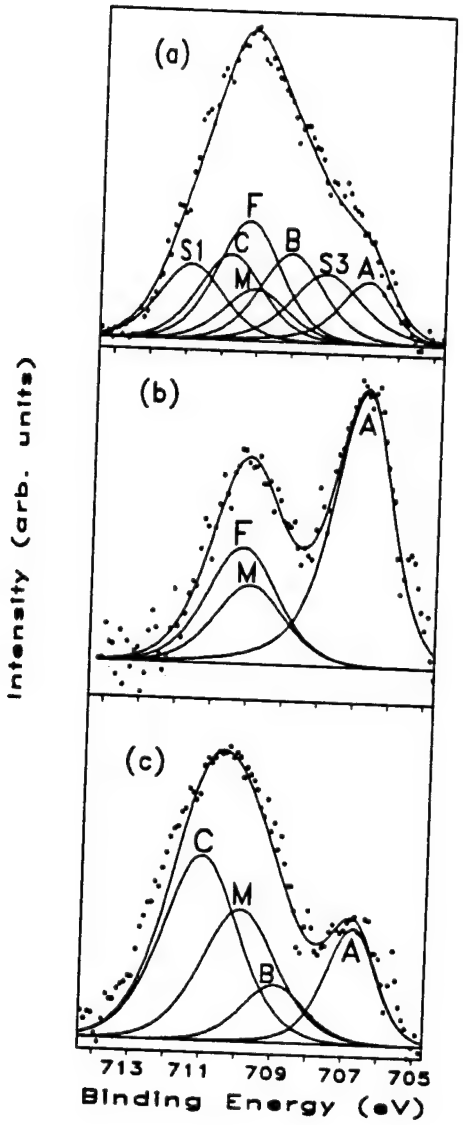

A: Fe; B: Fe^{2+}; C: Fe^{3+}; F: $FeCl_2$; M: $FeMoO_4$; S1: FeS; S3: $Fe_{1-x}S$.

Figure 26. Fe2p spectra on the surfaces of 317L SS after the potentiostatic polarization at -160 mV_{SCE} for 5 minutes in deaerated 0.1 M HCl, TOA: 20°. (a) Previously in SRB for 5 days, rinsed, (b) A control sample; (c) "As polished".

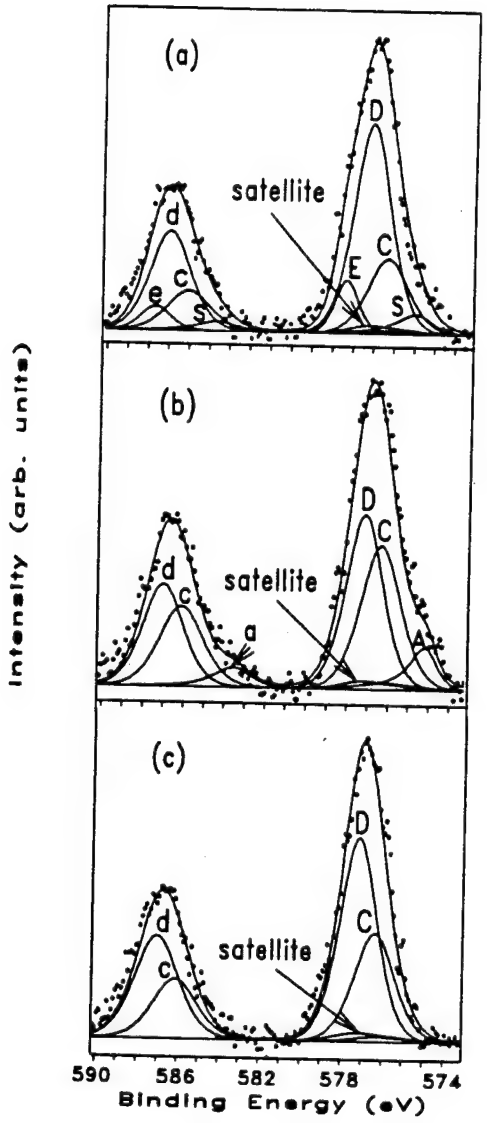

A, a: Cr; C, c: Cr_2O_3; D, d: $Cr(OH)_3$; E, e: CrO_3; S, s: Cr_2S_3.

Figure 27. Cr2p spectra on the surfaces of 317L SS after the potentiostatic polarization at -160 mV_{SCE} for 5 minutes in deaerated 0.1 M HCl, TOA: 20°. (a) Previously in SRB for 5 days, rinsed; (b) A control sample; (c) "As polished".

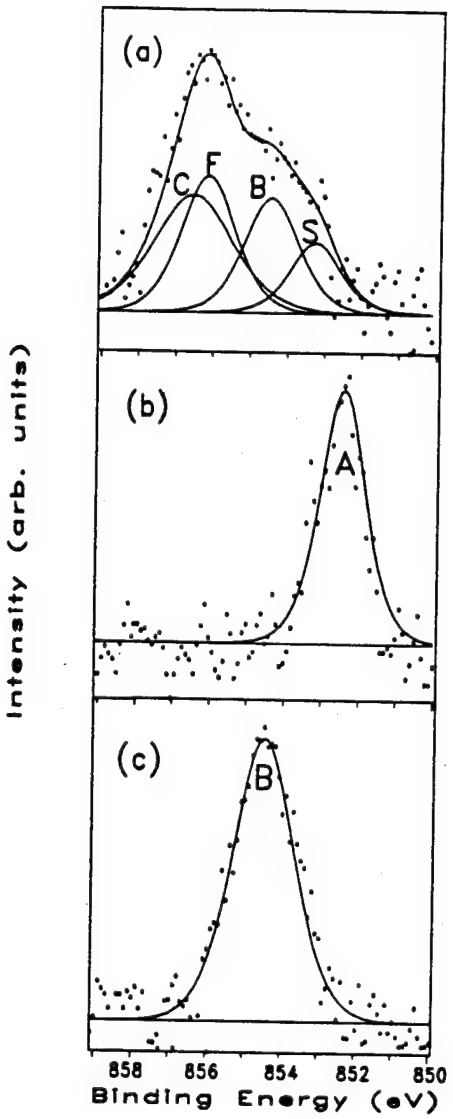

A: Ni; B: Ni^{2+}; C: $Ni(OH)_2$; F: $NiCl_2$; S: NiS.

Figure 28. Ni2p spectra on the surfaces of 317L SS after the potentiostatic polarization at -160 mV_{SCE} for 5 minutes in deaerated 0.1 M HCl, TOA: 20°. (a) Previously in SRB for 5 days, rinsed; (b) A control sample; (c) "As polished".

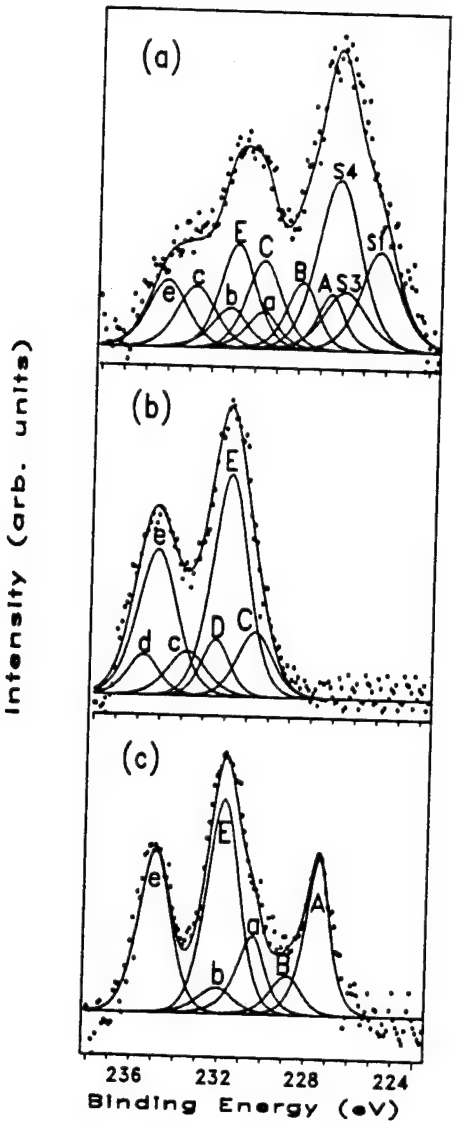

A, a: Mo; B, b: Mo^{4+}; C, c: Mo^{5+}; D, d: MoO_3; E, e: MoO_4^{2-}; S1: S2s of FeS, NiS, Cr_2S_3 and MoS_2; S3: S2s of $Fe_{1-x}S$, S4: S2s of organic sulfur.

Figure 29. Mo3d spectra on the surfaces of 317L SS after the potentiostatic polarization at -160 mV_{SCE} for 5 minutes in deaerated 0.1 M HCl, TOA: 20°. (a) Previously in SRB for 5 days, rinsed; (b) A control sample; (c) "As polished".

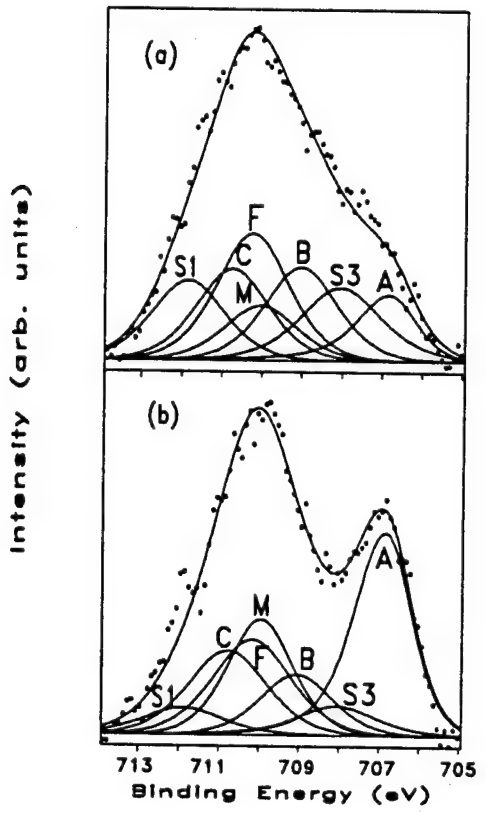

A: Fe; B: Fe^{2+}; C: Fe^{3+}; F: $FeCl_2$; M: $FeMoO_4$; S1: FeS; S3: $Fe_{1-x}S$.

Figure 30. Variable angle Fe2p spectra on the surface of 317L SS after the potentiostatic polarization at -160 mV_{SCE} for 5 minutes in deaerated 0.1 M HCl following the 5 day exposure to SRB, rinsed prior to the polarization.
(a) TOA: 20°; (b) TOA: 50°.

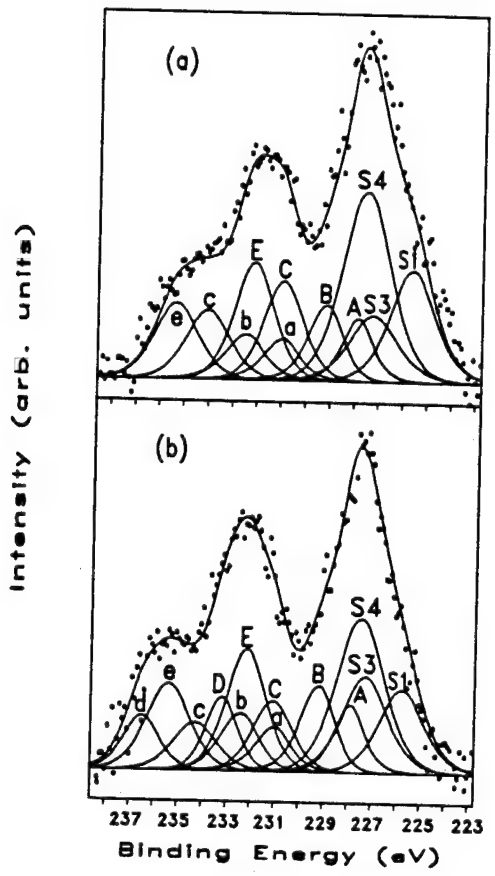

A, a: Mo; B, b: Mo^{4+}; C, c: Mo^{5+}; D, d: MoO_3; E, e: MoO_4^{2-}; S1: S2s of FeS, NiS, Cr_2S_3 and MoS_2; S3: S2s of $Fe_{1-x}S$; S4: S2s of organic sulfur.

Figure 31. Variable angle Mo3d spectra on the surface of 317L SS after the potentiostatic polarization at -160 mV_{SCE} for 5 minutes in deaerated 0.1 M HCl following the 5 day exposure to SRB, rinsed prior to the polarization.
(a) TOA: 20°; (b) TOA: 50°.

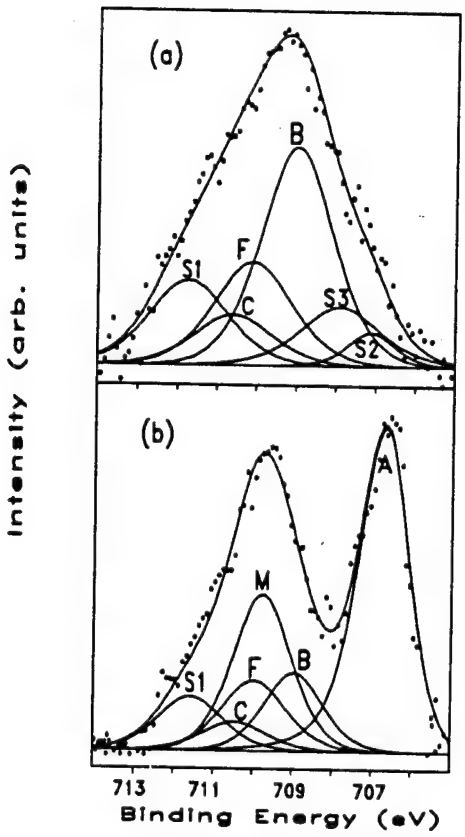

A: Fe; B: Fe^{2+}; C: Fe^{3+}; F: $FeCl_2$; M: $FeMoO_4$; S1: FeS; S2: FeS_2; S3: $Fe_{1-x}S$.

Figure 32. Variable angle Fe2p spectra on the surface of 317L SS after the potentiostatic polarization at -160 mV_{SCE} for 5 minutes in deaerated 0.1 M HCl following the 5 day exposure to SRB, unrinsed prior to the polarization. (a) TOA: 20°; (b) TOA: 50°.

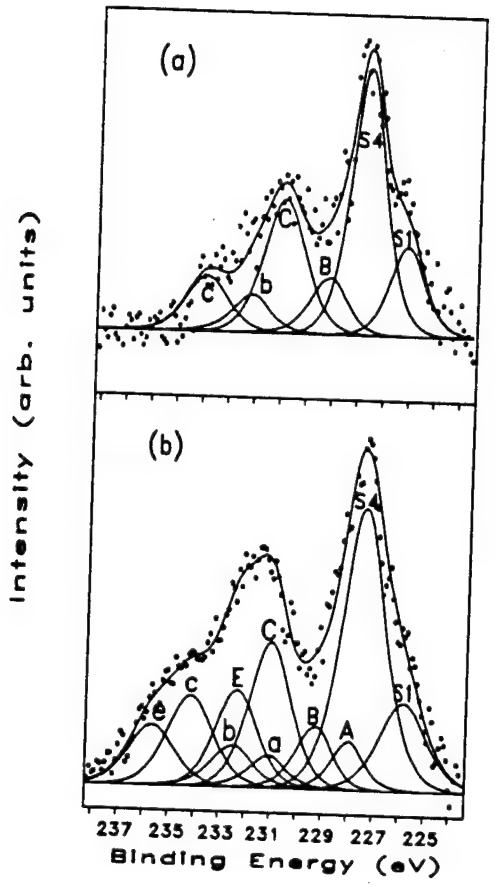

A, a: Mo; B, b: Mo^{4+}; C, c: Mo^{5+}; E, e: MoO_4^{2-}; S1: S2s of FeS, NiS, Cr_2S_3 and MoS_2; S4: S2s of organic sulfur.

Figure 33. Variable angle Mo3d spectra on the surface of 317L SS after the potentiostatic polarization at -160 mV_{SCE} for 5 minutes in deaerated 0.1 M HCl following the 5 day exposure to SRB, unrinsed prior to the polarization. (a) TOA: 20°; (b) TOA: 50°.

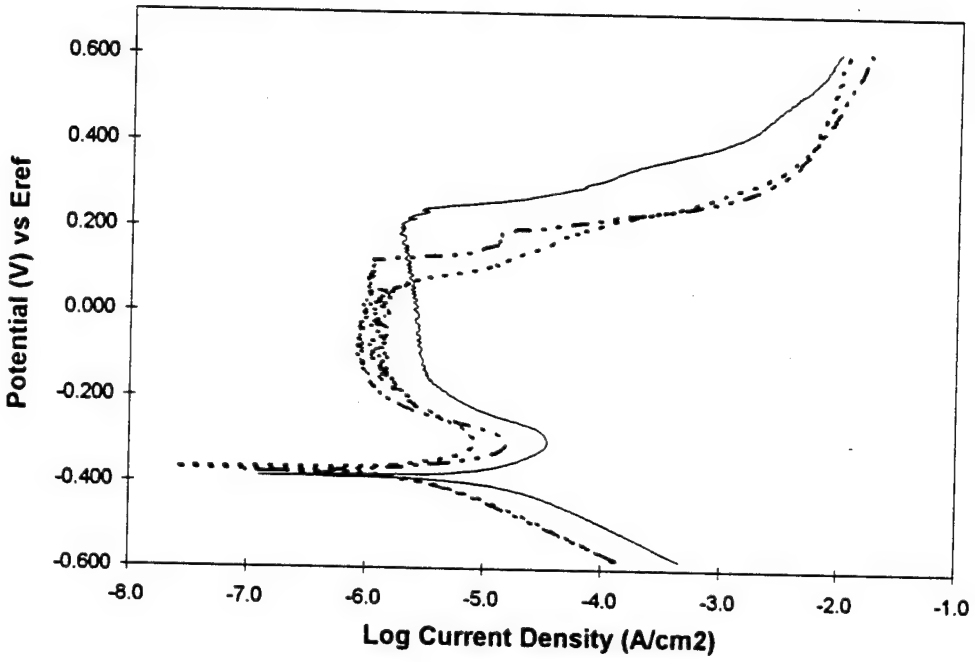

Figure 34a Polarization diagrams of 304 SS in 0.1 M HCl following the exposure to anaerobic 10 mM cysteine.

Figure 34. Comparison of potentiodynamic polarization diagrams of 304 SS in 0.1 M HCl following exposure to the H_2S-containing synthetic solutions with those previously exposed to SRB.

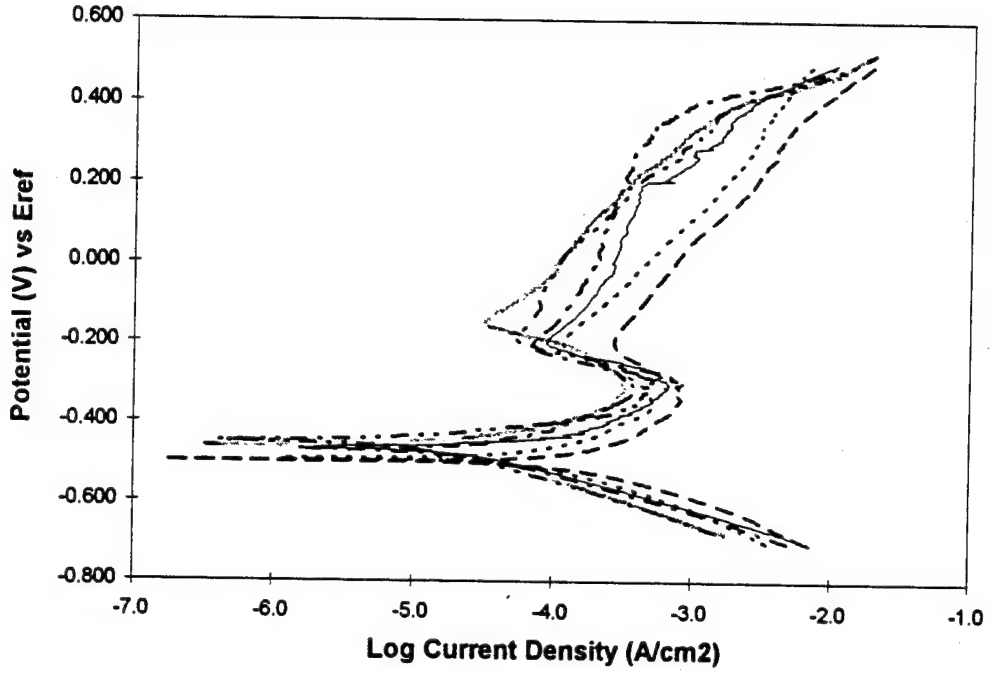

Figure 34b Potentiodynamic polarization diagrams of 304 SS in 0.1 M HCl following the exposure to anaerobic H_2S-containing solutions for 5 days

Figure 34. Comparison of potentiodynamic polarization diagrams of 304 SS in 0.1 M HCl following exposure to the H_2S-containing synthetic solutions with those previously exposed to SRB.

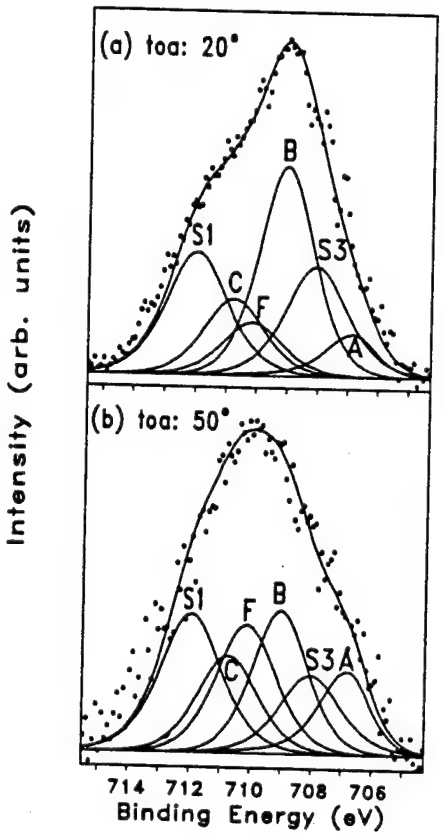

Figure 35a

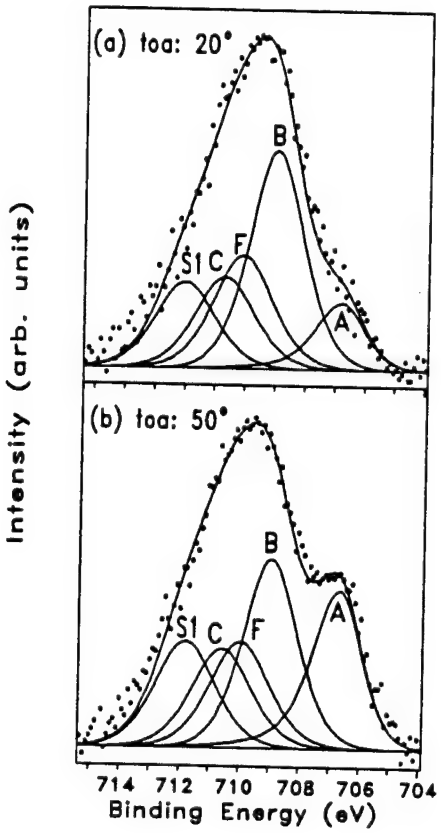

Figure 35b

A: Fe; B: Fe^{2+}; C: Fe^{3+}; F: $FeCl_2$; S1: FeS; S3: $Fe_{1-x}S$.

Figure 35. Fe2p spectra of 304 SS samples subsjected to the exposure to the anaerobic H_2S-containing solutions and subsequent anodic polarization at -160 mV_{SCE} in 0.1 M HCl for 5 minutes. (a) previously exposed to deaerated 10 mM Na_2S + 1 g/l NH_4Cl for 5 days, not rinsed; (b) previously exposed to deaerated 10 mM Na_2S + 1 g/l NH_4Cl + 10 mM cysteine for 5 days, not rinsed.

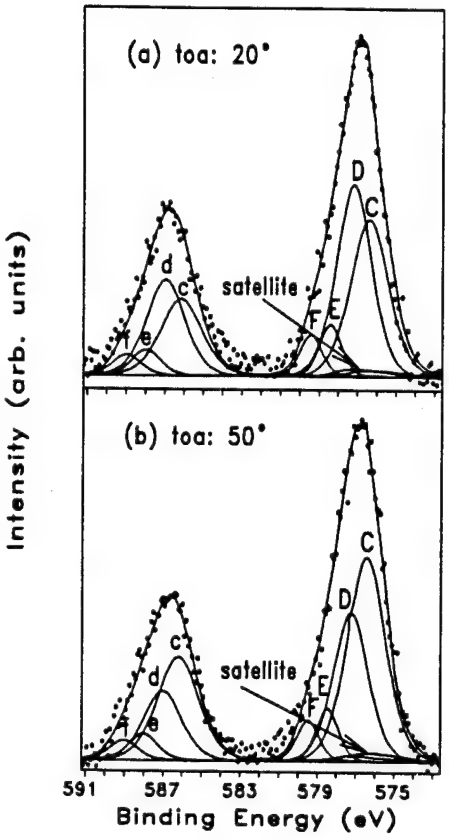

Figure 36a

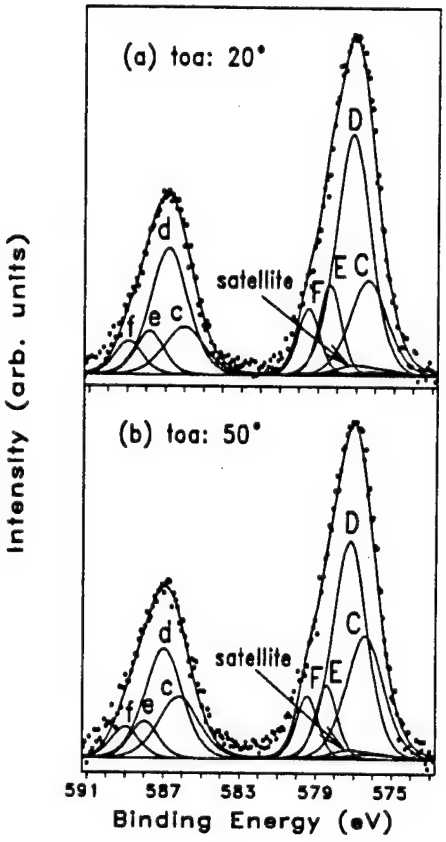

Figure 36b

C, c: Cr_2O_3; D, d: $Cr(OH)_3$; E, e: CrO_3; F, f: CrO_4^{2-}.

Figure 36. Cr2p spectra of 304 SS samples subsjected to the exposure to the anaerobic H_2S-containing solutions and subsequent anodic polarization at -160 mV_{SCE} in 0.1 M HCl for 5 minutes. (a) previously exposed to deaerated 10 mM Na_2S + 1 g/l NH_4Cl for 5 days, not rinsed; (b) previously exposed to deaerated 10 mM Na_2S + 1 g/l NH_4Cl + 10 mM cysteine for 5 days, not rinsed.

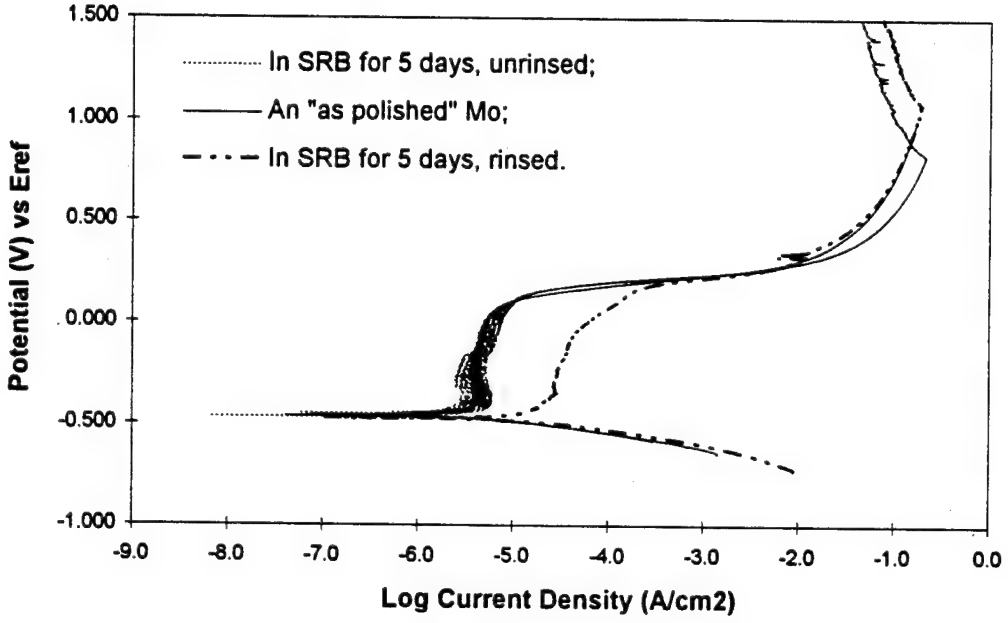

Figure 37. Potentiodynamic polarization diagrams of the SRB-exposed pure Mo coupons in deaerated 0.1 M HCl.

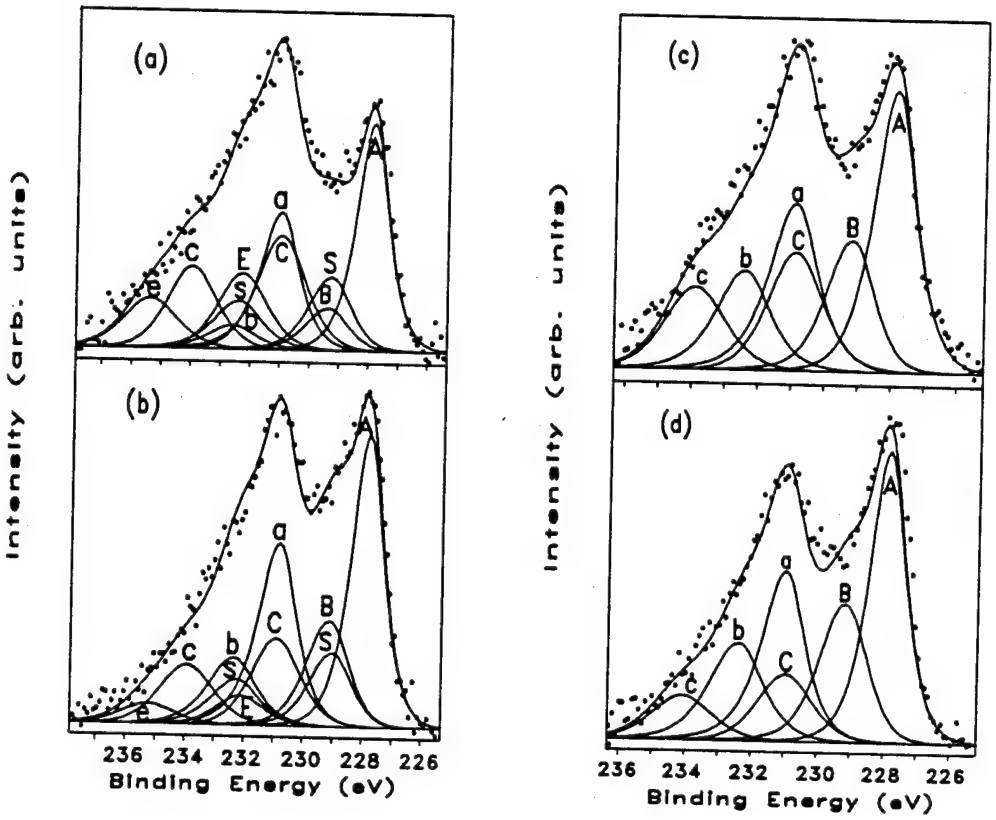

A, a: Mo; B, b: Mo^{4+}; C, c: Mo^{5+}; E, e: MoO_4^{2-}; S, s: MoS_2.

Figure 38. Mo3d spectra from the surfaces of Mo coupons, TOA: 10°. (a) In SRB for 5 days, rinsed; (b) In SRB for 5 days, rinsed and then polarized at -160 mV_{SCE} for 5 minutes in deaerated 0.1 M HCl; (c) A control sample corresponding to (a); (d) A control sample corresponding to (b).

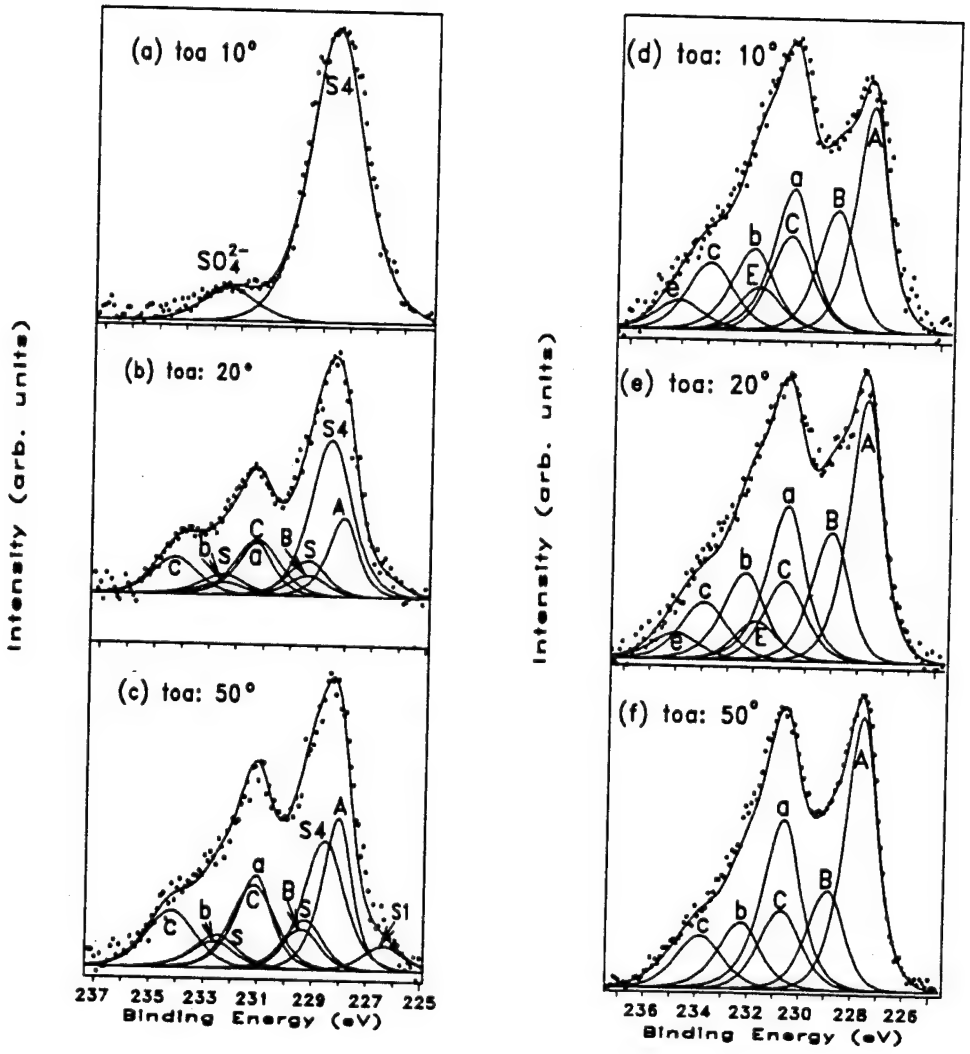

A, a: Mo; B, b: Mo^{4+}; C, c: Mo^{5+}; E, e: MoO_4^{2-}; S, s: MoS_2; S1: S2s of MoS_2; S4: S2s of the organic sulfur.

Figure 39. Variable angle Mo3d spectra from the surfaces of Mo coupons. (a), (b) and (c) In SRB for 5 days, unrinsed and then polarized at -160 mV_{SCE} for 5 minutes in deaerated 0.1 M HCl; (d), (e) and (f) A control sample.

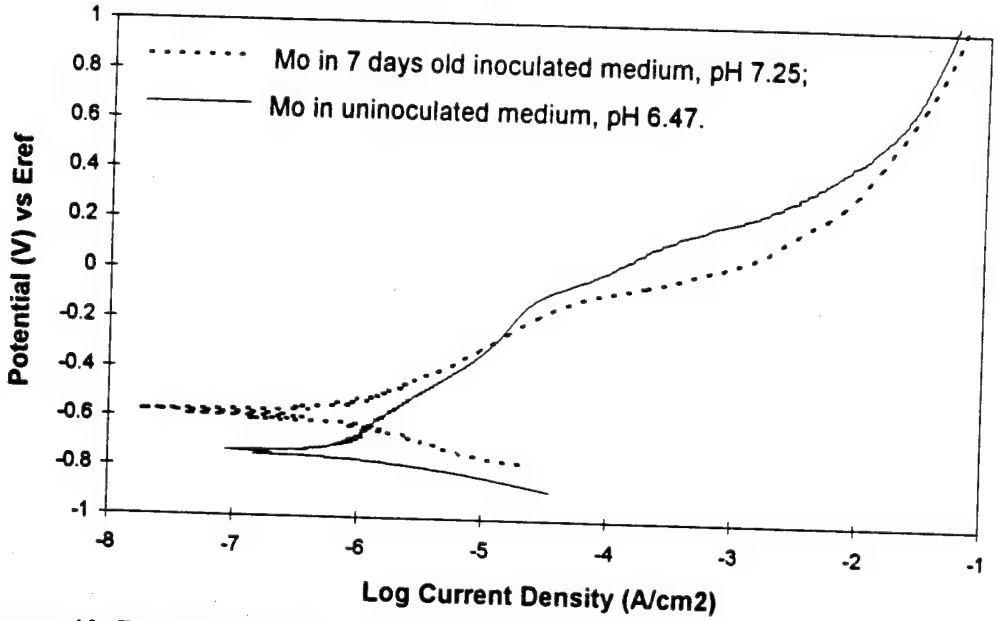

Figure 40. Potentiodynamic polarization diagram of the "as polished" Mo coupon in a 7 day old culture.

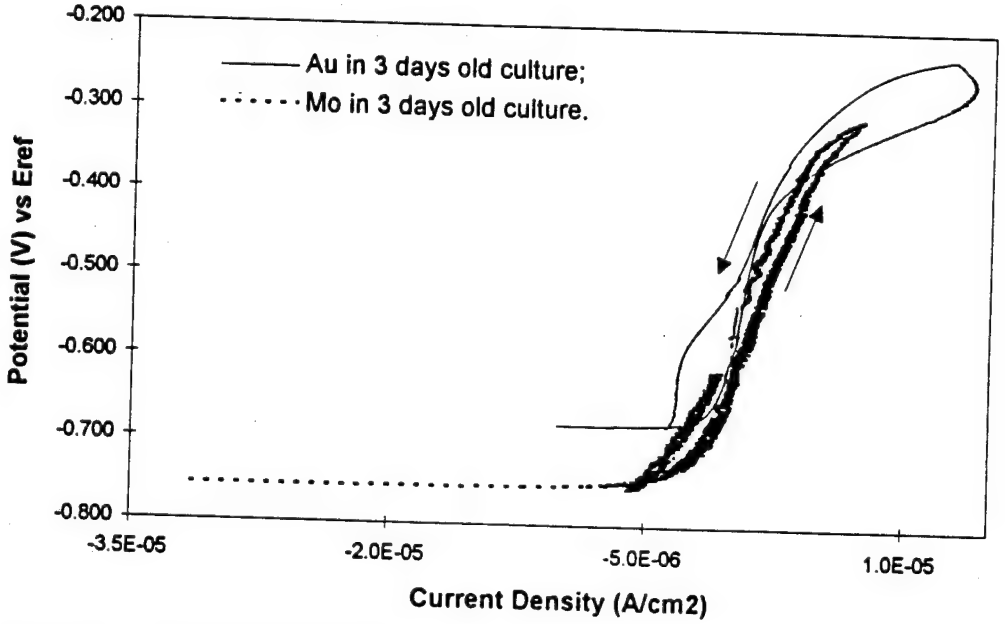

Figure 41. A comparison of the cyclic polarization diagrams of the "as polished" Mo coupon and Au in the 3 day old cultures.

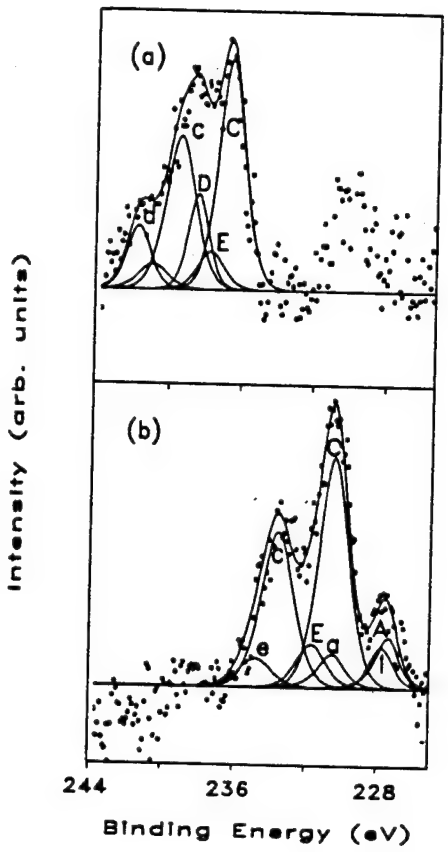

A, a: Mo°; C, c: Mo^{5+}; D, d: H_2MoO_4; E, e: MoO_4^{2-}; 1: S2s of MoS_2.

Figure 42. Mo3d spectra from the culture droplets dried on Au foil after the potentiodynamic polarization of the "as polished" Mo coupons in the 7 day old culture. (a) unfiltered; (b) filtered.

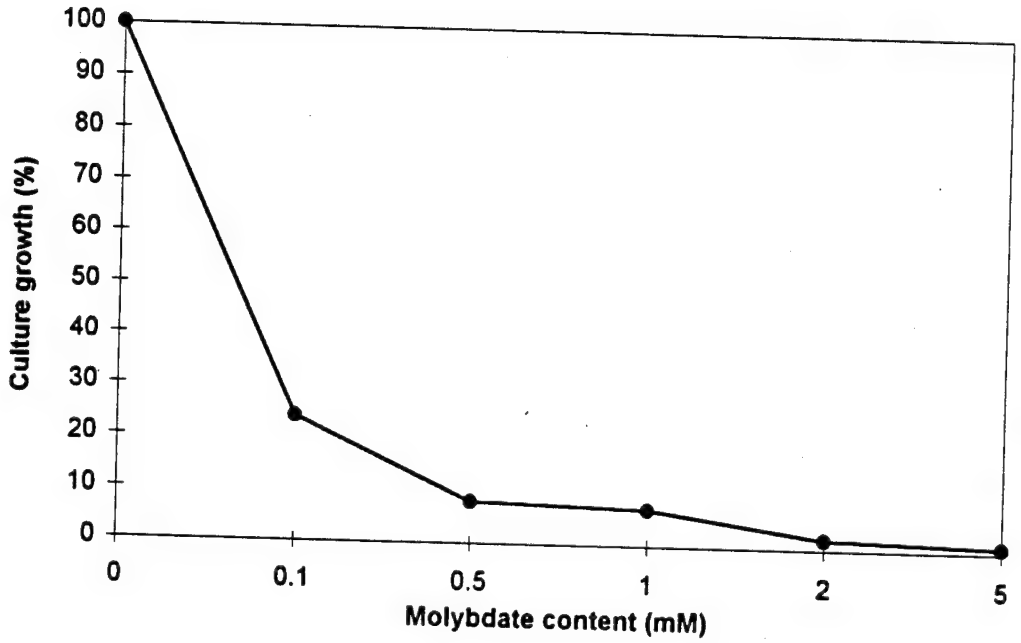

Figure 43. Inhibition of low concentrations of molybdate on the culture growth (assuming that the culture growing in the medium without molybdate reached 100% growth in 3 days, $MoO_4^{2-} + SO_4^{2-} = 20$ mM).

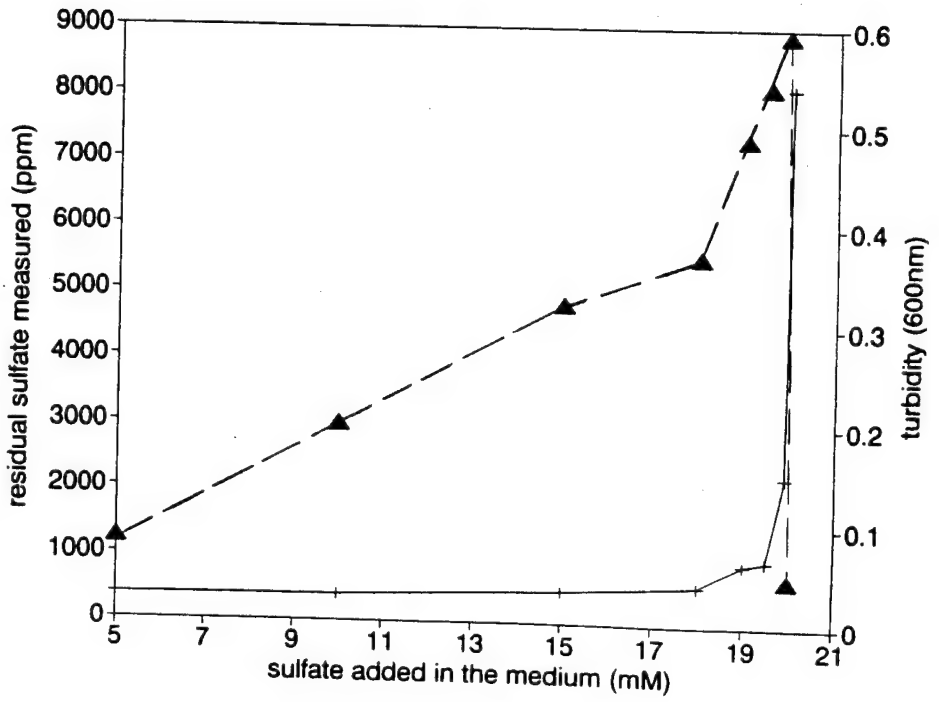

Figure 44. The relationship between the residual sulfate measured in ppm by the turbidimetric method, the culture growth (turbidity at 600 nm) and the sulfate added to the growth medium.

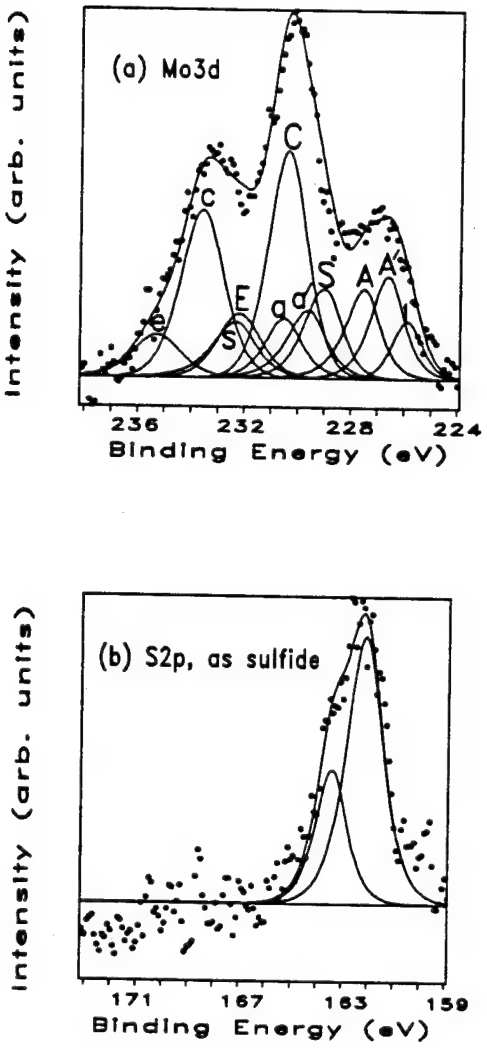

A, a: Mo^{o}; A', a': $Mo^{\prime}$; S, s: MoS_2; C, c: Mo^{5+}; E, e: MoO_4^{2-}, 1: S2s of MoS_2.

Figure 45. Mo3d (a) and S2p (b) spectra from the culture droplet after the exposure of Mo thin film for 5 days.

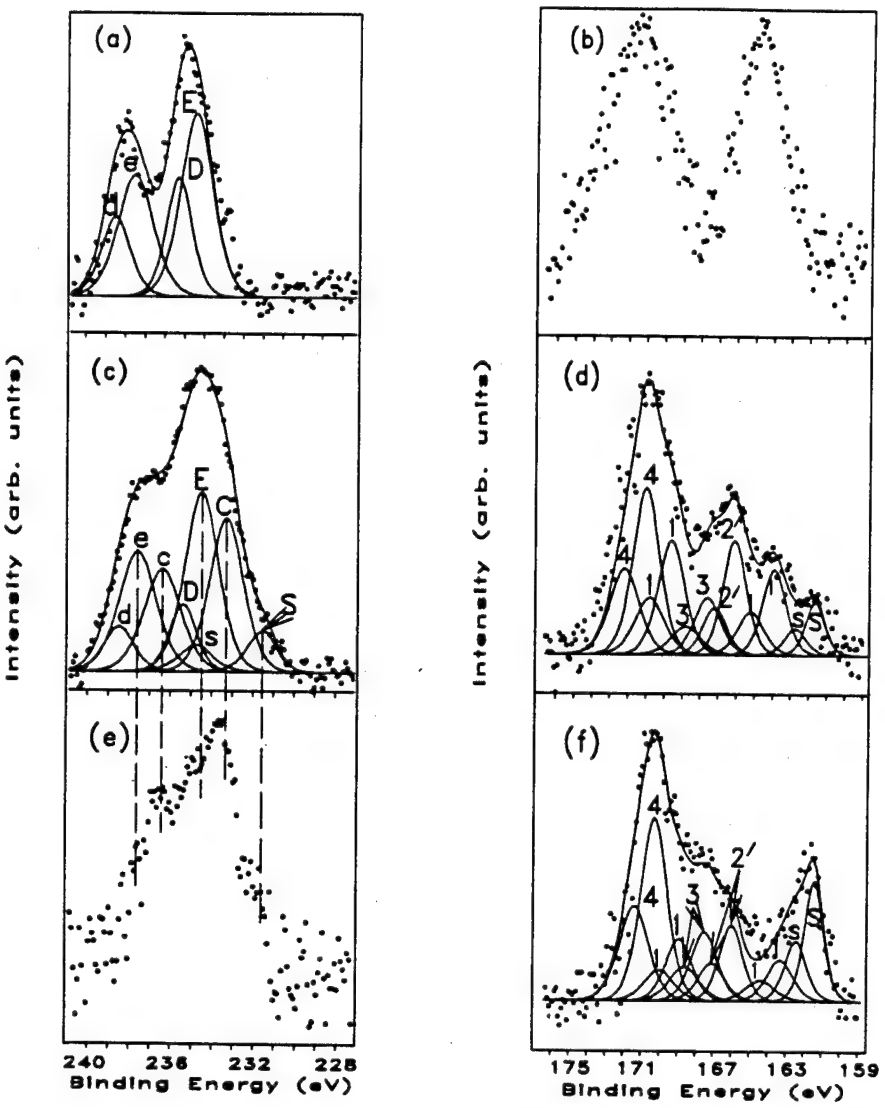

C, c: Mo^{5+}; D, d: H_2MoO_4; E, e: MoO_4^{2-}; S, s: S2s of MoS_2.

1: $S_2O_3^{2-}$; 2: organic sulfur; 3: SO_3^{2-}; 4: SO_4^{2-}; S: MoS_2.

Figure 46. Mo3d and S2p from the centrifuged biomass of the cultures growing in the media containing different concentrations of molybdate. (a) and (b), 5 mM MoO_4^{2-}; (c) and (d), 1 mM MoO_4^{2-}; (e) and (f), 0.1 mM MoO_4^{2-}.

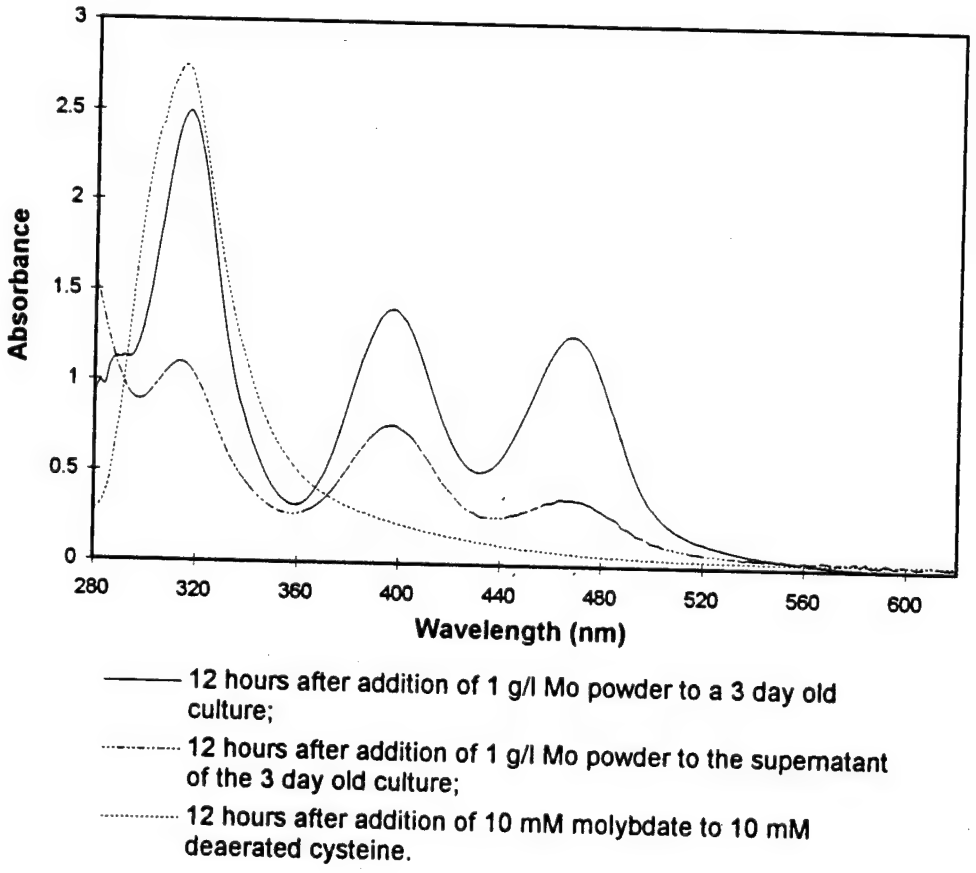

Figure 47. A comparison of the UV absorption spectra of the dissolved Mo during the 12 hour exposure of Mo powder (1 g/l) to the 3 day old culture and its supernatant.

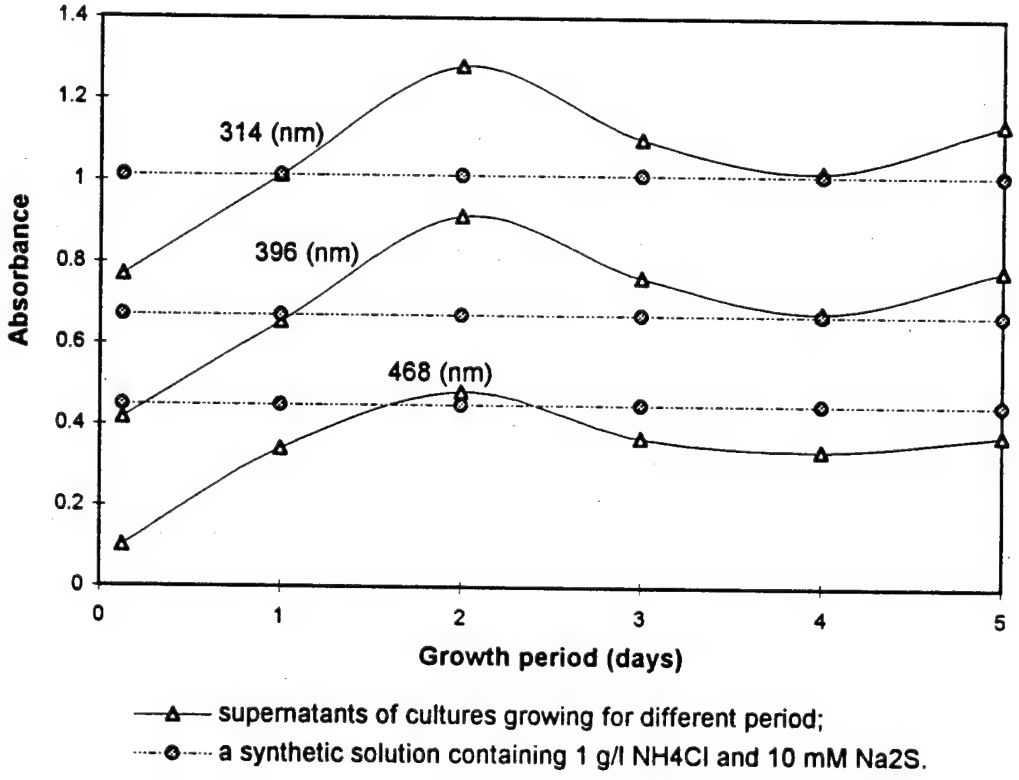

Figure 48. The UV absorbance of the dissolved Mo during the 12 hour exposure of Mo powder (1 g/l) to the supernatants of the cultures growing for different periods.

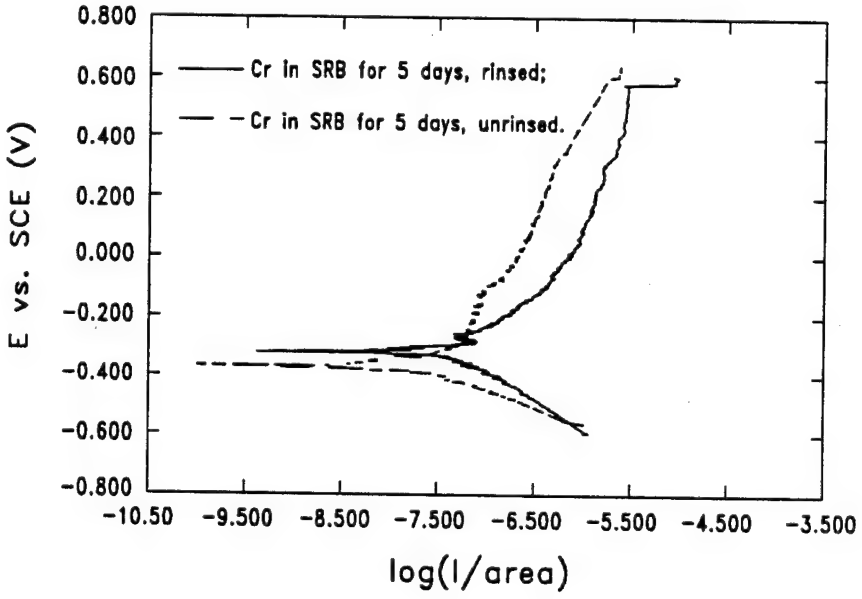

Figure 49. Potentiodynamic polarization diagrams of the SRB-exposed pure Cr coupons in deaerated 0.1 M HCl.

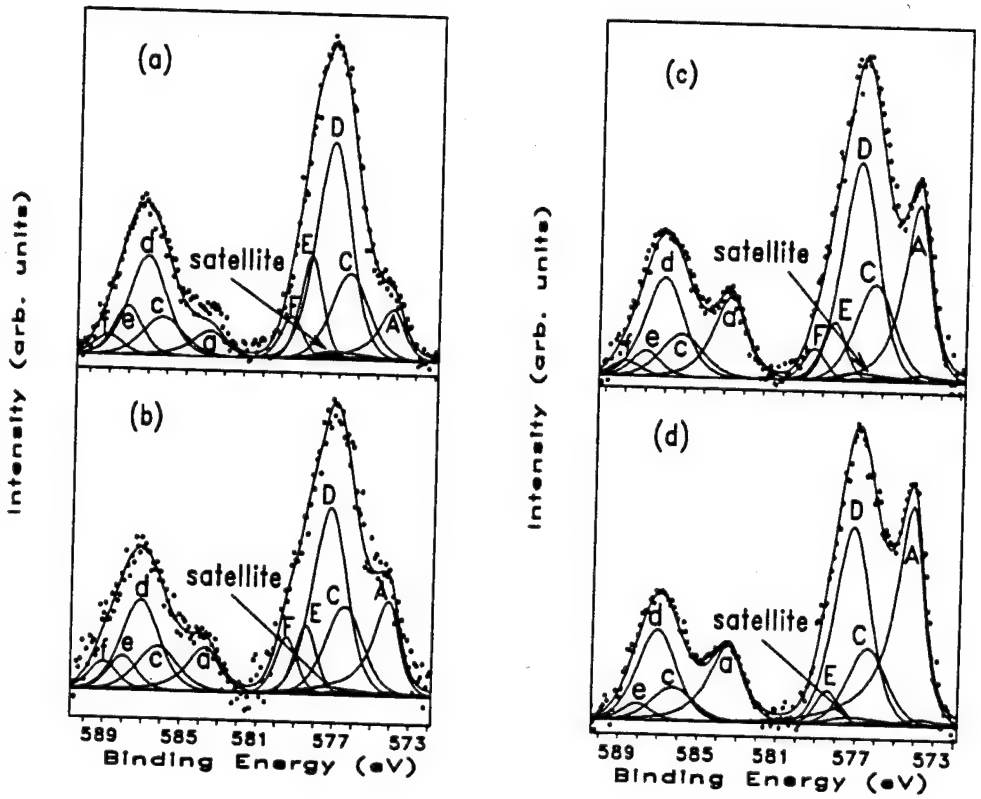

A, a: Cr; C, c: Cr_2O_3; D, d: $Cr(OH)_3$; E, e: CrO_3; F, f: CrO_4^{2-}.

Figure 50. Cr2p spectra from the surfaces of the pure Cr coupons, TOA: 20°. (a) In SRB for 5 days, rinsed; (b) In SRB for 5 days, rinsed and then polarized at -160 mV_{SCE} in deaerated 0.1 M HCl for 5 minutes; (c) A control sample corresponding to (a); (d) A control sample corresponding to (b).

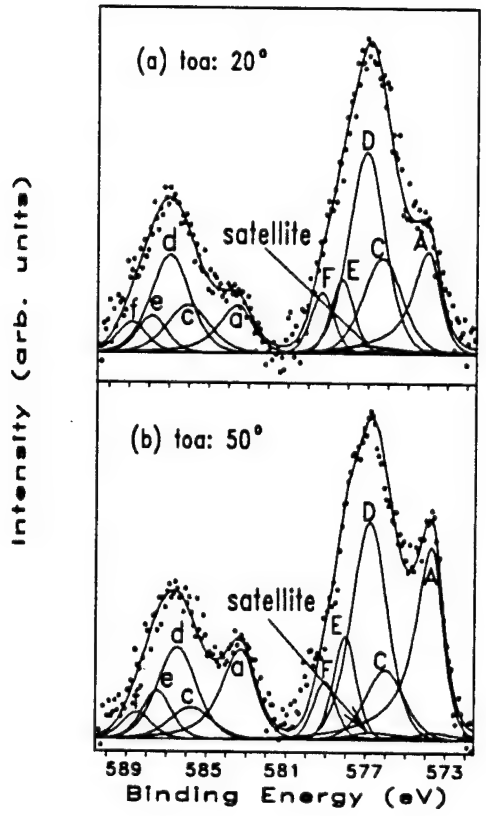

A, a: Cr; C, c: Cr_2O_3; D, d: $Cr(OH)_3$; E, e: CrO_3; F, f: CrO_4^{2-}.

Figure 51. Variable angle Cr2p spectra from the rinsed surface of the SRB-exposed Cr coupon after the subsequent potentiostatic polarization at -160 mV_{SCE} in deaerated 0.1 M HCl for 5 minutes, (a) TOA: 20°; (b) TOA: 50°.

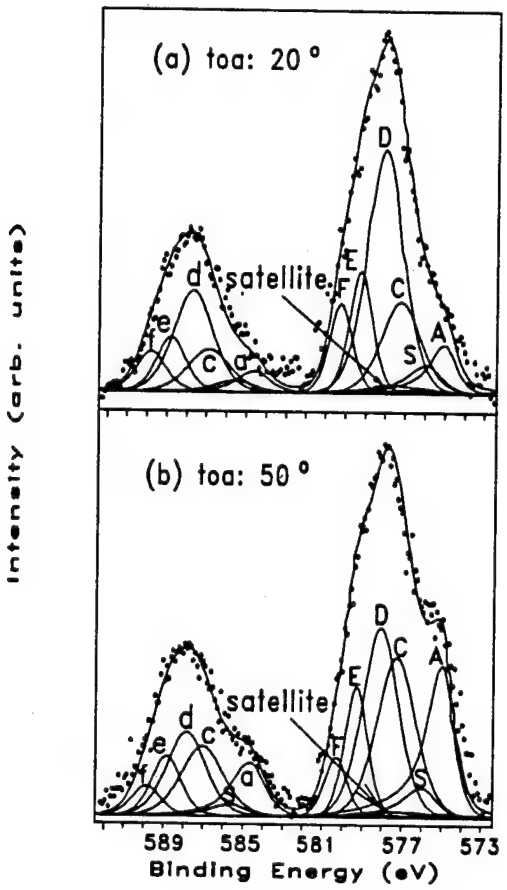

A, a: Cr; C, c: Cr_2O_3; D, d: $Cr(OH)_3$; E, e: CrO_3; F, f: CrO_4^{2-}; S, s: Cr_2S_3.

Figure 52. Variable angle Cr2p spectra from the unrinsed surface of the SRB-exposed Cr coupon after the subsequent potentiostatic polarization at -160 mV_{SCE} in deaerated 0.1 M HCl for 5 minutes, (a) TOA: 20°; (b) TOA: 50°.

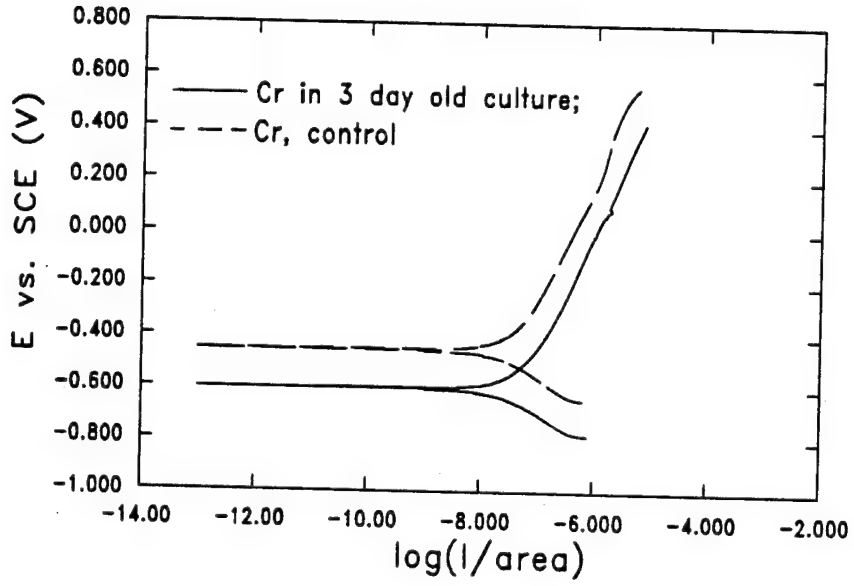

Figure 53. Potentiodynamic polarization diagrams of the "as polished" Cr coupons in the 3 day old culture and in the uninoculated medium.

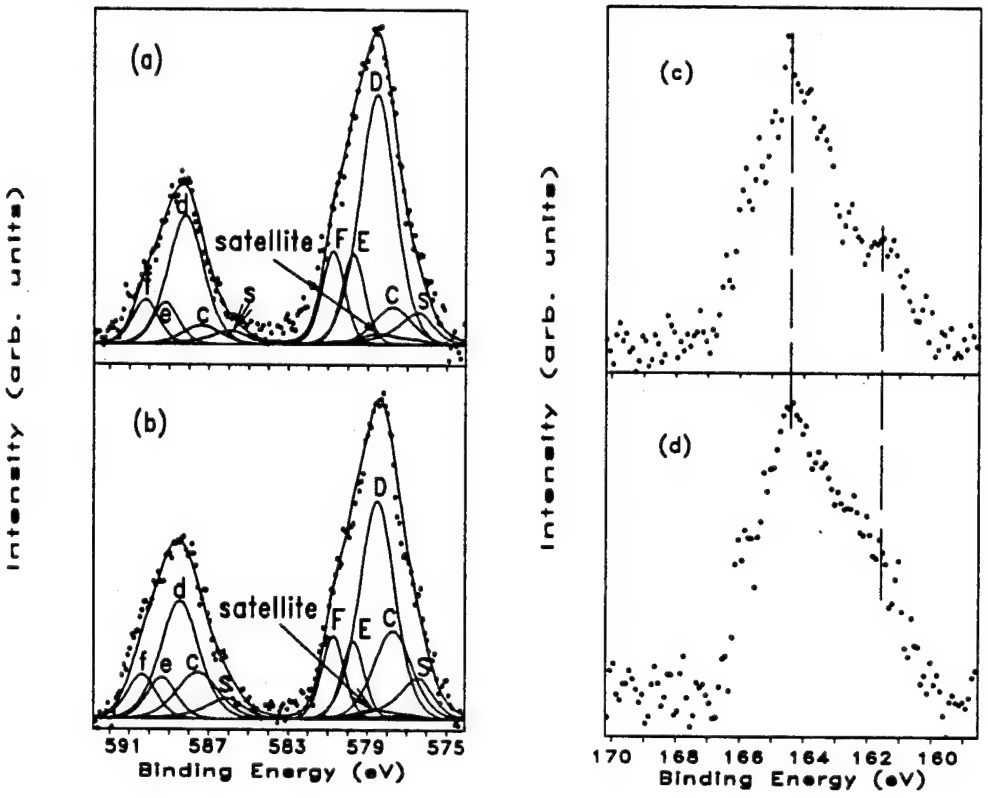

A, a: Cr; C, c: Cr_2O_3; D, d: $Cr(OH)_3$; E, e: CrO_3; F, f: CrO_4^{2-}; S, s: Cr_2S_3.

Figure 54. Cr2p from the centrifuged biomass of the cultures growing in the medium containing 0.21 g/l $Cr(OH)_3$, (a) biomass of 2 day old culture; (b) biomass of 5 day old culture; (c) S2p of biomass (a); (d) S2p of biomass (b).

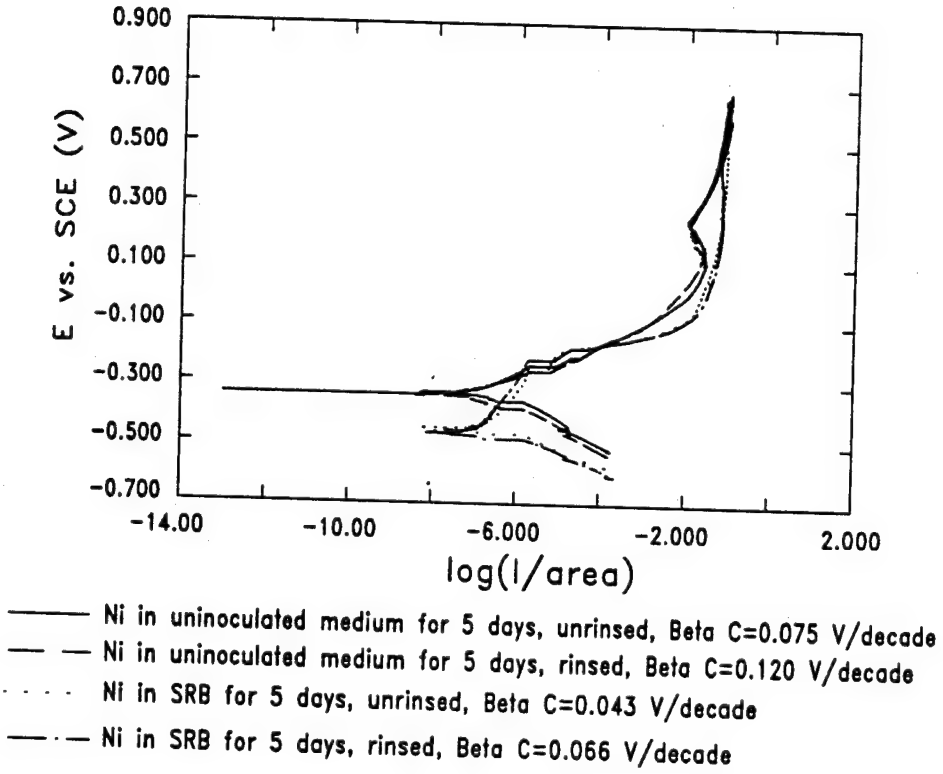

Figure 55. Potentiodynamic polarization diagrams of SRB-exposed Ni coupons in deaerated 0.1 M HCl.

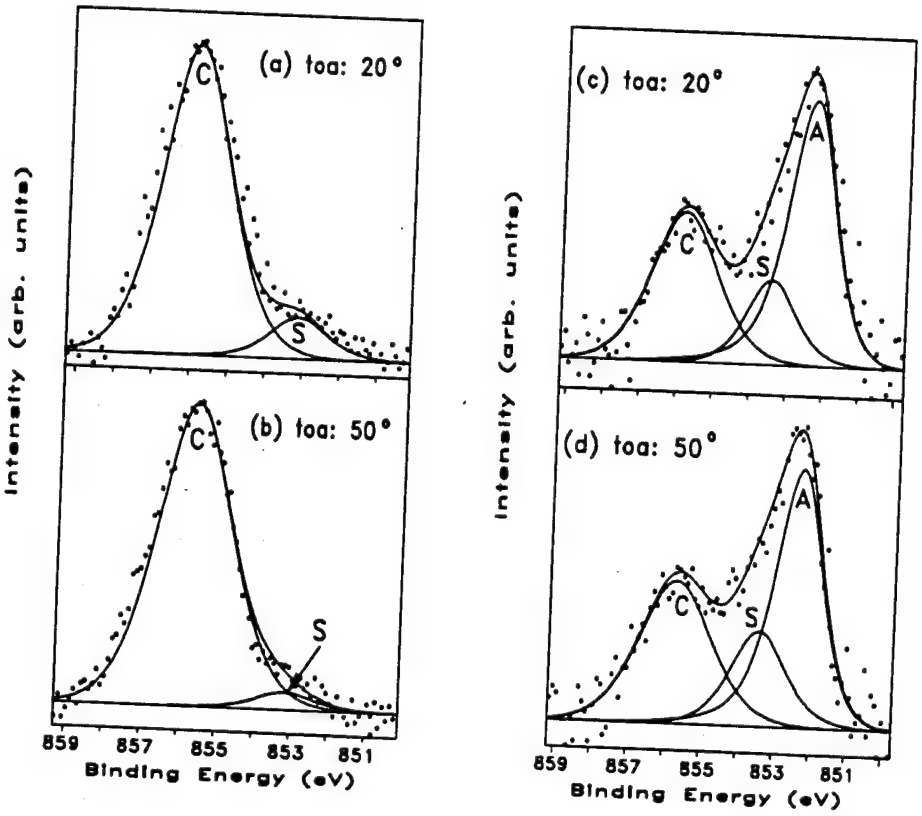

A: Ni; C: $Ni(OH)_2$; S: NiS.

Figure 56. Ni2p spectra from the SRB-exposed Ni samples. (a) In SRB for 5 days, rinsed; (b) In SRB for 5 days, rinsed and then anodically polarized at -210 mV_{SCE} in 0.1 M HCl for 5 minutes; (c) In SRB for 5 days, unrinsed; (d) In SRB for 5 days, unrinsed and then anodically polarized.

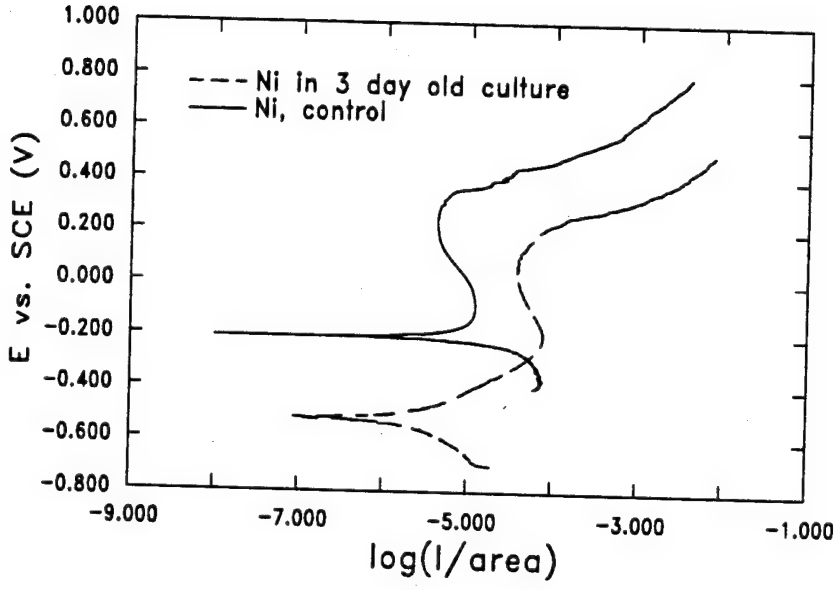

Figure 57. Potentiodynamic polarization diagrams of the "as polished" Ni coupons in the 3 day old culture.

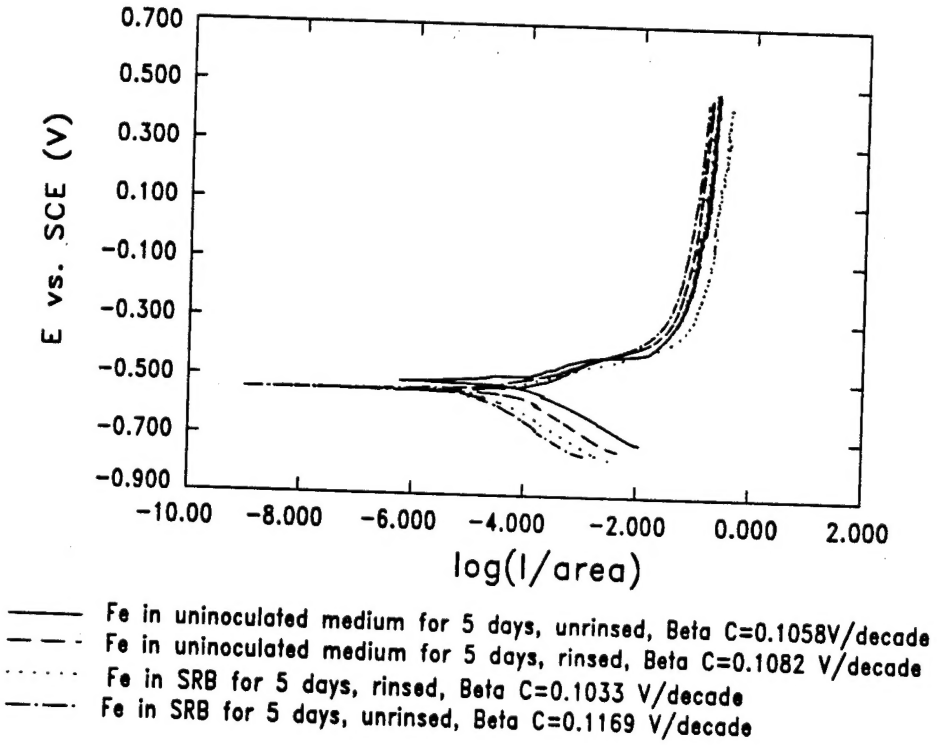

Figure 58. Potentiodynamic polarization diagrams of the SRB-exposed Fe samples in deaerated 0.1 M HCl.

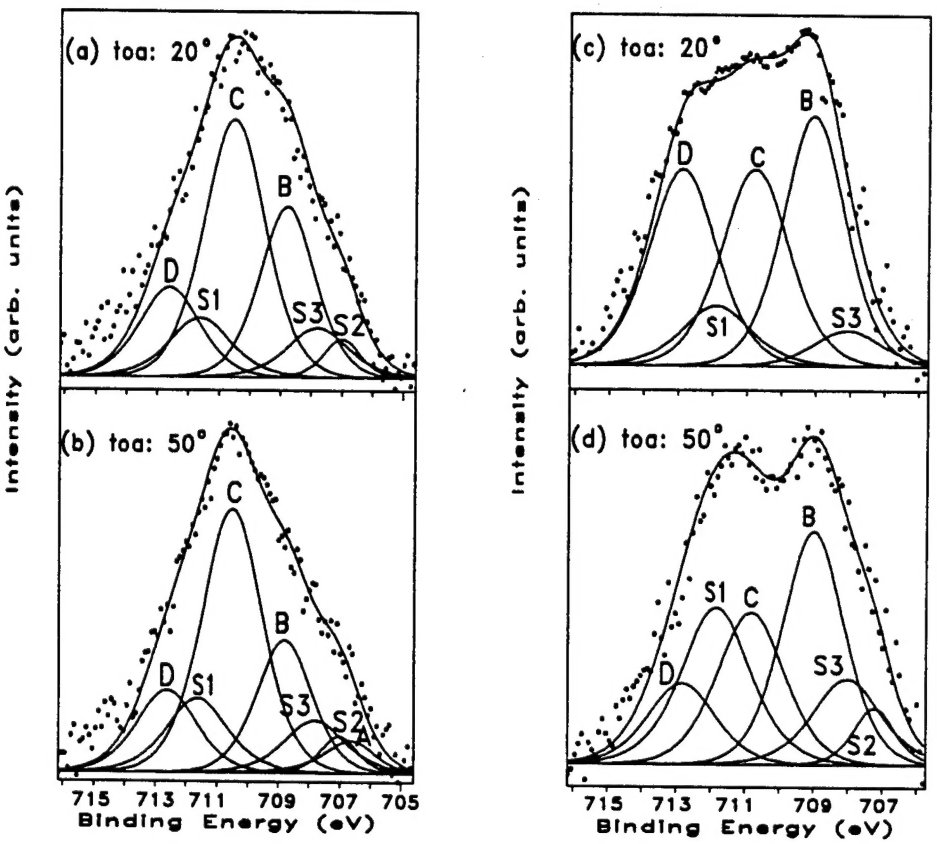

B: Fe^{2+}; C: Fe^{3+}; D: $Fe(OOH)_{\alpha}$; S1: FeS; S2: FeS_2; S3: Fe_xS.

Figure 59. Variable angle Fe2p spectra from the Fe coupons after the exposure to SRB. (a) and (b): From a rinsed sample; (c) and (d) From an unrinsed sample.

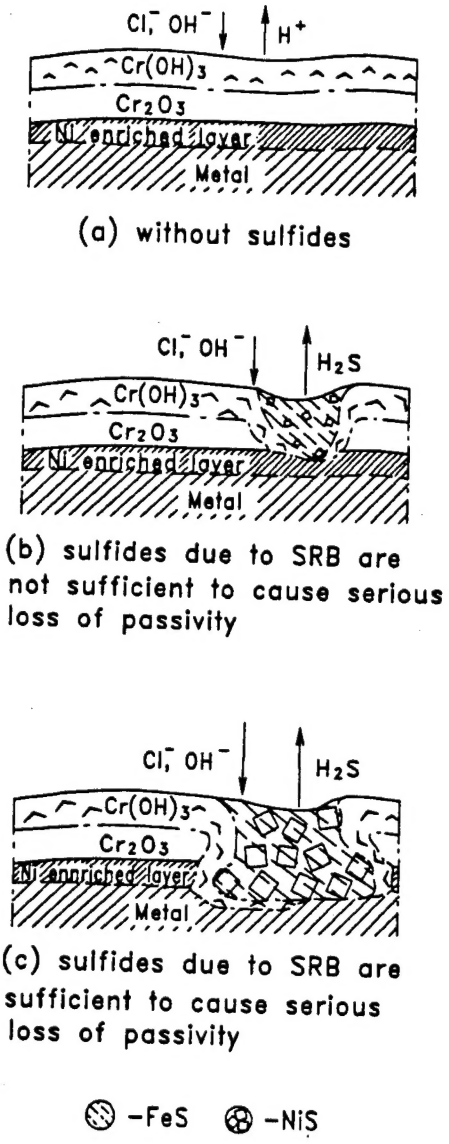

Figure 60. An illustrative schematic of the nonuniform interaction resulting from the exposure of 304 SS to SRB.

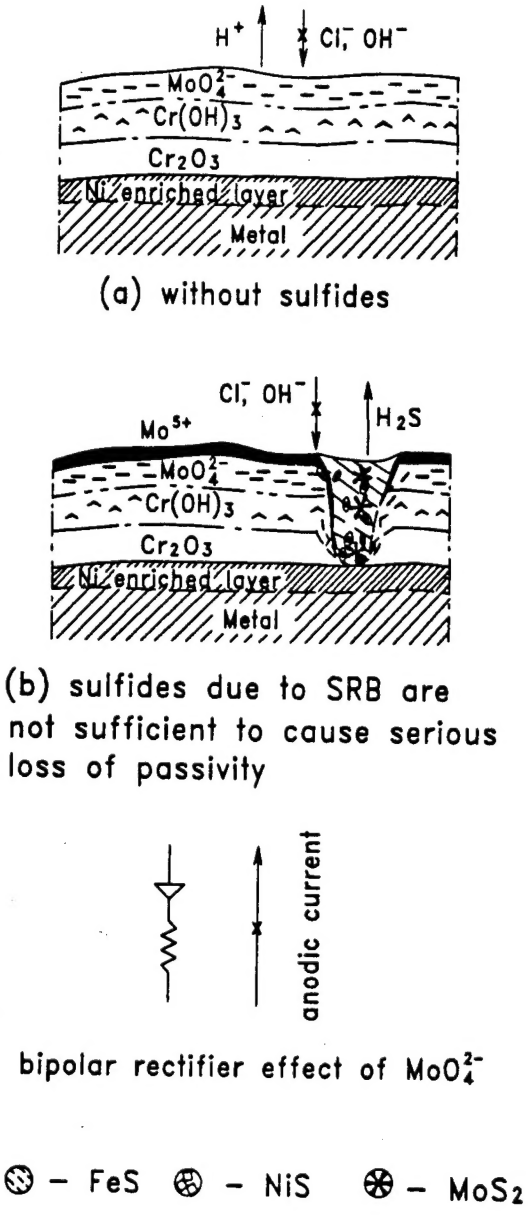

Figure 61. An illustrative schematic of the uniform interaction resulting from the exposure of 317L SS to SRB, and the protection effect of the biofilm.